NASA TM-78,427

(NASA-TM-78427) AERODYNAMIC CHARACTERISTICS OF A SMALL-SCALE STRAIGHT AND SWEPT-BACK WING WITH KNEE-BLOWN JET FLAPS (NASA) 125 p HC A06 MF A01 CSCL 01A

N78-13998

Unclas
G3/02 55507

Aerodynamic Characteristics of a Small-Scale Straight and Swept-Back Wing with Knee-Blown Jet Flaps

Gilbert G. Morehouse,
William T. Eckert and
Robert A. Boles

OCTOBER 1977

NASA

NASA TM-78,427

AERODYNAMIC CHARACTERISTICS OF A SMALL-SCALE STRAIGHT AND SWEPT-BACK WING WITH KNEE-BLOWN JET FLAPS

Gilbert G. Morehouse and William T. Eckert

Ames Research Center
and
Aeromechanics Laboratory
U.S. Army Aviation R&D Command
Ames Research Center
Moffett Field, Calif. 94035

and

Robert A. Boles

Lockheed-Georgia Company
Marietta, Georgia 30063

NOTATION

A_{noz}	blown flap slot area
b	model wing span without tip extensions
c	nominal wing chord
C_D	drag coefficient, based on S
$\tilde{C}_D$	blown flap slot discharge coefficient
C_L	lift coefficient, based on S
C_M	pitching moment coefficient about the quarter chord, based on S and C
C_P	total pressure coefficient
C_μ	momentum blowing coefficient, based on S
FRL	fuselage reference line
H	total pressure in model plenum
M	mach number
MAC	mean aerodynamic chord
P_o	static pressure at model station
q	wind tunnel test section dynamic pressure
S	model wing area
α	angle of attack
γ	ratio of specific heats of air

LIST OF FIGURES

AERODYNAMIC CHARACTERISTICS OF A SMALL-SCALE STRAIGHT AND SWEPT-BACK WING WITH KNEE-BLOWN JET FLAPS

Gilbert G. Morehouse and William T. Eckert

Ames Research Center
and
Aeromechanics Laboratory
U. S. Army Aviation R & D Command

and

Robert A. Boles

Lockheed-Georgia Company

SUMMARY

Two sting-mounted, 50.8 cm (20 in) span, knee-blown, jet-flap models were tested in a large (2.1- by 2.5-m (7- by 10-ft)) subsonic wind tunnel. A straight- and swept-wing model were tested with fixed flap deflection with various combinations of full-span leading-edge slats. The swept-wing model was also tested with wing tip extensions.

Data were taken at angles-of-attack between 0° and 40°, at dynamic pressures between 143.6 N/sq m (3 lb/sq ft) and 239.4 N/sq m (5 lb/sq ft), and at Reynolds numbers (based on wing chord) ranging from 100000 to 132000. Jet-flap momentum blowing coefficients up to 10 were used. Lift, drag, and pitching-moment coefficients, and exit flow profiles for the flap blowing are presented in graphical form without analysis.

INTRODUCTION

A series of studies, reported in references 1 through 7, demonstrated the feasibility of using a floor jet for performing ground-effect testing in wind tunnels. Part of these studies involved testing small models in relatively large wind tunnels in order to obtain "interference-free" base line data.

This report presents the base line characteristics of two, similar, knee-blown, jet-flapped, 50.80-cm (20-in) span wing models (one straight and one swept at 25 degrees) as measured in a 2.1- by 2.5-m (7- by 10-ft) wind tunnel. The straight-wing model was tested with its full-span jet flap, with and without the full-span leading-edge slat (see figure 1). The swept-wing model was tested with its full-span slat and full-span jet-flap, with and without the removable wing tip extensions (see figure 2).

These studies were conducted in support of the planned modification of the NASA Ames Research Center 40- by 80-Foot Wind Tunnel, as described in references 8 and 9.

MODELS AND APPARATUS

The wing section coordinates, basic wing span, streamwise chord length, and basic wing area were the same for the two models. The geometries of the two models are given in figures 1 through 10 and tables I and II.

Straight-Wing Model

Basic model dimensions are given in table I and figure 1. The inboard airfoil section (figure 3) was derived from a supercritical design, thickened on the lower surface to approximately 16% total thickness and modified to accommodate an internal air duct and a fixed, highly deflected flap with knee blowing. ("Knee blowing" denotes blowing through a spanwise slot, located in the trailing edge of the main wing near the flap hinge line, and blowing over the upper surface of the deflected flap.) The slot upper member was supported by posts at intervals along the span, giving a mean gap of .0415 cm (.0163 in), which increased when pressurized.

Photographs of the straight-wing model are shown in figures 4 and 5.

The rather deep fuselage fairing accommodated a strain-gauged sting balance with a bellows-type air bridge mounted above it. The data were corrected for the effects of the axial loads produced by this air bridge. Internal total pressure tubes and static orifices were used for measurement and control of slot blowing rates.

Since the slot opening enlarged with pressure, a correction was applied to the momentum data. This yielded the equation

$$\frac{A_{noz}}{S} = 0.0336 + 0.00061 \left(\frac{H}{P_o}\right)$$

where S is the reference area. This equation was used in conjunction with the conventional expression for momentum coefficient, namely

$$C_\mu = \gamma \tilde{C}_D M^2 \left(\frac{P_o}{q}\right) \left(\frac{A_{noz}}{S}\right)$$

where $\tilde{C}_D$ is a slot discharge coefficient, taken as 0.98, and Mach number is derived from

$$M^2 = \left(\frac{2}{\gamma-1}\right) \left[\left(\frac{H}{P_o}\right)^{\frac{\gamma-1}{\gamma}} - 1 \right]$$

Since the varying slot area affected the axial force tare on the air bridge and because of the impact on drag measurements, a special dynamic tare calibration rig was made. This replaced the model wing with a spanwise plenum with long carefully-aligned holes drilled at each end. Directing the air spanwise at right angles to the balance axis and in opposite directions permitted full mass flows to be passed through the air bridge without any lift, drag, or pitching moment due to jet reaction. Bellows tares were then directly measured by the balance at various exit areas depending upon the number of holes left open.

Additional details of the construction and arrangements of the model and balance are given in reference 2.

Swept-Wing Model

Detailed dimensions of the swept wing model are presented in table III and figure 2. Photographs of the assembled model in its various configurations are shown in figures 7 through 9.

The same tare and calibration procedures were used for this model as were used for the straight-wing model.

Instrumentation

The models were sting-mounted in the U. S. Army AMRDL 7- by 10-Foot Wind Tunnel. The angle-of-attack was measured by an accelerometer which was mounted on the sting. The air supply pipe was fastened to the articulated sting as shown in figure 6. The sting drive mechanism provided infinitely variable pitch and yaw capability with an approximately 40-degree cone. High-pressure air for the knee-blown flap was piped through the sting to the model air supply pipe.

The model plenum pressure was controlled from the test section by exercising direct control over the dome pressure of a large pressure regulator located in the air supply line. Model plenum and air supply pipe pressures were monitored using $\pm$ 50 psid Statham pressure transducers. Wake rake pressures were measured using six 48-port type D scannivalves fitted with Statham $\pm$ 2.5 psid pressure transducers.

The total-pressure, flap blowing-profile rake was mounted at the trailing edge above the upper surface of the deflected flap, as shown in figure 10. This mounting allowed assessment of the flap blowing effectiveness.

Test section dynamic pressure was calibrated prior to model entry using a precision pitot tube and two ± 0.3 psid Statham pressure transducers. These transducers were also used to monitor and record the tunnel contraction pressures during the test.

A twelve-channel data system was used to automatically record balance output, model internal pressures, tunnel conditions, and wake rake scannivalve information.

DATA ACQUISITION AND PROCESSING

Acquisition

The analog signals from the strain gage balance, scannivalve, and accelerometer were digitized on a multi-channel recording system and punched onto tabulation cards. All acquired data were averaged over six samples, taken at 0.25-second intervals, before being used in data reduction calculations. Final data reduction was conducted off-line.

Corrections

Due to the relative sizes of the wind tunnel test section and the models, no wall interference or blockage corrections were applied to the data. However, the data were corrected for the effects of the weight tares and pressure in the air supply and bellows arrangement, as discussed in the model description.

TEST PROCEDURE

Measurements were made at various angles-of-attack with a given configuration, flap blowing coefficient, and wind tunnel dynamic pressure. At the completion of a sweep, the configuration required for the next run (model geometry, blowing rate, and air speed) was set and the process was repeated.

RESULTS

The drag and pitching moment data were plotted against lift at constant flap blowing rates; all four parameters are presented in non-dimensional coefficient form. (Those curves presented without symbols -- those data plotted against lift coefficient — were derived from cross-plots.) The plotted data are indexed by configuration in table III.

The force and moment results for the straight-wing model without the leading-edge slat are given in figures 11 through 13. Figure 14 shows the corresponding blown-flap rake data for the variation of pressure coefficient with angle-of-attack and blowing coefficient. (Only the rake data for the tubes nearest the flap upper surface are shown -- data for the region beyond the effect of the blowing are not shown.) Figures 15 through 17 present the force and moment data for the straight-wing model with the leading-edge slat. The related blown-flap rake data are given in figure 18.

Figures 19 through 21 present the data for the swept-wing model with slats and without tip extensions. The results for the same model with added tip extensions are given in figures 22 through 24.

All data are presented without analysis.

REFERENCES

1. Hackett, J. E. and Boles, R. A.: Ground Simulation and Tunnel Blockage for a Swept, Jet-Flapped Wing Tested to Very High Lift Coefficients. NASA CR-152,032, 1977.

2. Hackett, J. E.; Boles, R. A.; and Lilley, D. E.: Ground Simulation and Tunnel Blockage for a Jet-Flapped, Basic STOL Model Tested to Very High Lift Coefficients. NASA CR-137,857, March 1976.

3. Hackett, J. E. and Boles, R. A.: High Lift Testing in Closed Wind Tunnels. AIAA Paper No. 74-641, July 1974.

4. Hackett, J. E. and Lyman, V.: The Jet Flap in Three Dimensions: Theory and Experiment. AIAA Paper No. 73-653, July 1973.

5. Hackett, J. E. and Praytor, E. B.: Ground Effect for V/STOL Aircraft Configurations and Its Simulation in the Wind Tunnel, Part I - Introduction and Theoretical Studies. NASA CR 114,495, November 1972.

6. Hackett, J. E.; Boles, R. A.; and Praytor, E. B.: Ground Effect for V/STOL Aircraft Configurations and Its Simulation in the Wind Tunnel, Part II - Experimental Studies. NASA CR 114,496, November 1972.

7. Hackett, J. E.; Praytor, E. B.; and Caldwell, E. O.: Ground Effect for V/STOL Aircraft Configurations and Its Simulation in the Wind Tunnel, Part III - Application to the NASA-Ames 40- by 80-Foot Wind Tunnel. NASA CR 114,497, November 1972.

8. Mort, Kenneth W.; Kelly, Mark W.; and Hickey, David H.: The Rationale and Design Features for the 40- by 80-Foot Wind Tunnel. Paper 9, AGARD Conference Proceedings 174 on Windtunnel Design and Testing Techniques, AGARD-CP-174, October 6-8, 1975.

9. Mort, Kenneth W.; Soderman, Paul T.; and Eckert, William T.: Improving Large-Scale Testing Capability by Modifying the 40- by 80-Foot Wind Tunnel. AIAA Paper 77-587, AIAA/NASA Ames V/STOL Conference, June 6-8, 1977.

TABLE I

DIMENSIONS OF STRAIGHT WING MODEL

Fuselage:		
length	31.55 cm	(12.42 in)
maximum width	4.46 cm	(1.76 in)
maximum height	7.76 cm	(3.06 in)
maximum cross section area	30.30 cm^2	(4.70 in^2)
equivalent diameter	6.21 cm	(2.44 in)
fineness ratio	5.08	
Wing:		
span	50.80 cm	(1.667 ft)
reference chord	10.16 cm	(0.333 ft)
area	516.13 cm^2	(0.556 ft^2)
aspect ratio	5.00	
twist	0 deg	
sweep	0 deg	
taper ratio	1.0	
quarter chord MAC location	1.27 cm aft of fuselage station 0.0	(0.50 in)
Leading edge slat -- full span:		
chord (maximum)	2.03 cm	(0.80 in)
area (projected onto maximum chord)	103.12 cm^2	(0.111 ft^2)
slot width	0.127 cm	(0.050 in)
deflection (fixed)	80.0 deg	
Trailing edge flap -- full span:		
chord (maximum)	4.60 cm	(1.81 in)
area (projected onto maximum chord)	233.68 cm^2	(0.252 ft^2)
blowing slot width	0.041 cm	(0.016 in)
deflection (wing chord line to upper surface)	76.0 deg	

ORIGINAL PAGE IS OF POOR QUALITY

TABLE II

DIMENSIONS OF SWEPT WING MODEL

Both models used the same fuselage.

Wing:

Span	50.80 cm	(1.667 ft)
reference chord (streamwise)	10.16 cm	(0.333 ft)
area	516.13 cm^2	(0.556 ft^2)
aspect ratio	5.00	
twist	0 deg	
sweep	25.0 deg	
quarter chord MAC location	6.64 cm aft of fuselage station 0.0	(2.71 in)

Wing with tip extension:

span	76.20 cm	(2.50 ft)
reference chord of tip extension	12.70 cm	(0.417 ft)
area	967.74 cm^2	(1.042 ft^2)
aspect ratio	6.00	

Leading edge slat -- full span:

chord (maximum, streamwise)	2.03 cm	(0.80 in)
area (projected onto maximum chord)		
for span of 50.80 cm (1.667 ft)	103.12 cm^2	(0.111 ft^2)
for span of 76.20 cm (2.50 ft)	154.69 cm^2	(0.167 ft^2)
slot width (streamwise)	0.127 cm	(0.050 in)
deflection (fixed)	80.0 deg	

Trailing edge flap:

chord (maximum, streamwise)	4.60 cm	(1.81 in)
span	50.80 cm	(1.667 ft)
area (projected onto maximum chord)	233.68 cm^2	(0.252 ft^2)
blowing slot width	0.041 cm	(0.016 in)
deflection (wing chord line to flap upper surface)	60.0 deg	

TABLE III

INDEX OF DATA PLOTS ACCORDING TO MODEL CONFIGURATION

Model Configuration	Variables	Figure	Page
Straight wing; full span knee blown flaps	C_L vs α	11	24
	C_D vs C_L	12	31
	C_M vs C_L	13	38
	C_P vs α	14	45
Straight wing; full span leading edge slats: full span knee blown flaps	C_L vs α	15	51
	C_D vs C_L	16	58
	C_M vs C_L	17	65
	C_P vs α	18	72
Swept wing; full span leading edge slats; full span knee blown flaps	C_L vs α	19	78
	C_D vs C_L	20	85
	C_M vs C_L	21	92
Swept wing; full span leading edge slats; partial span knee blown flaps	C_L vs α	22	99
	C_D vs C_L	23	106
	C_M vs C_L	24	113

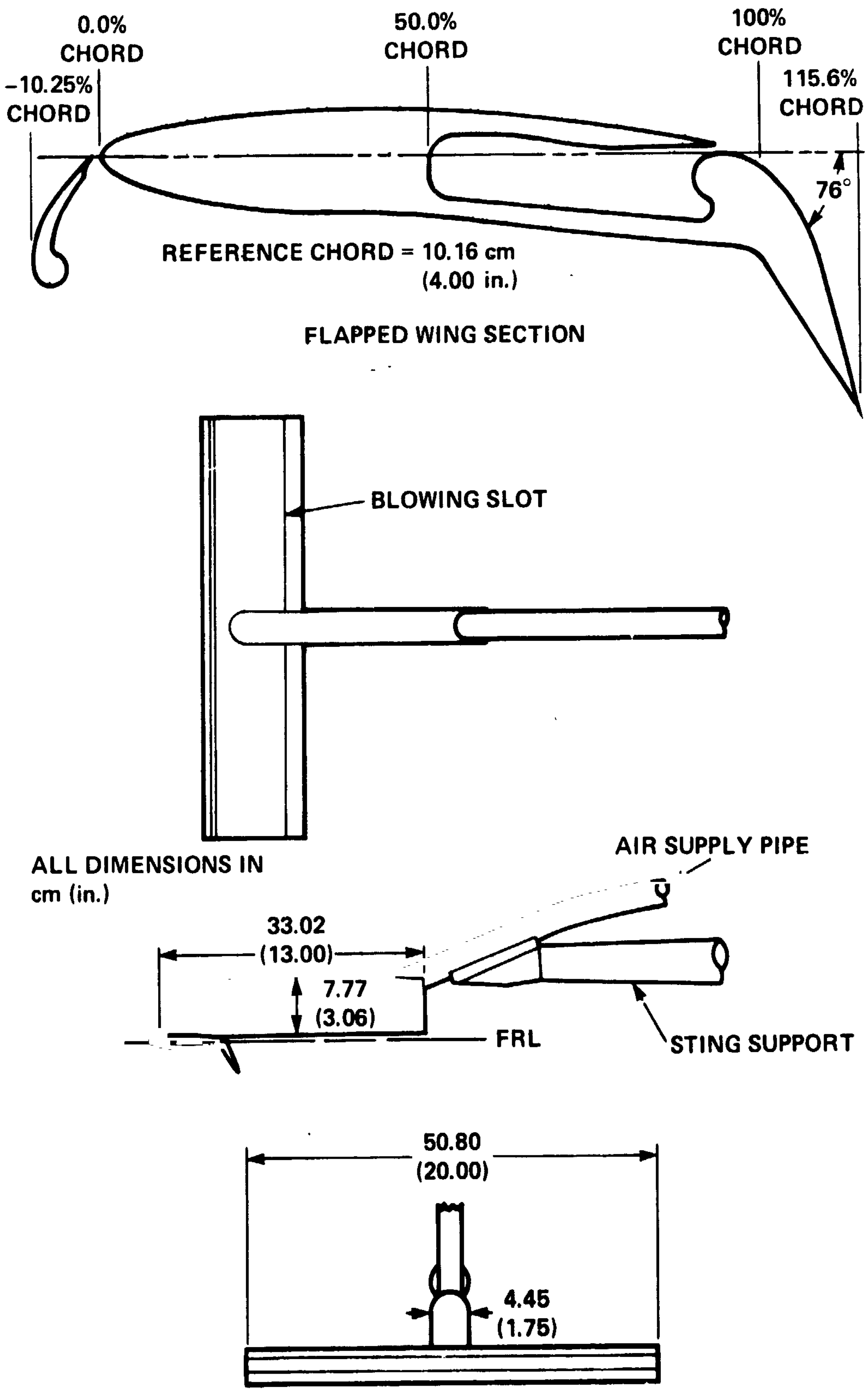

Figure 1.- Straight-wing model geometry.

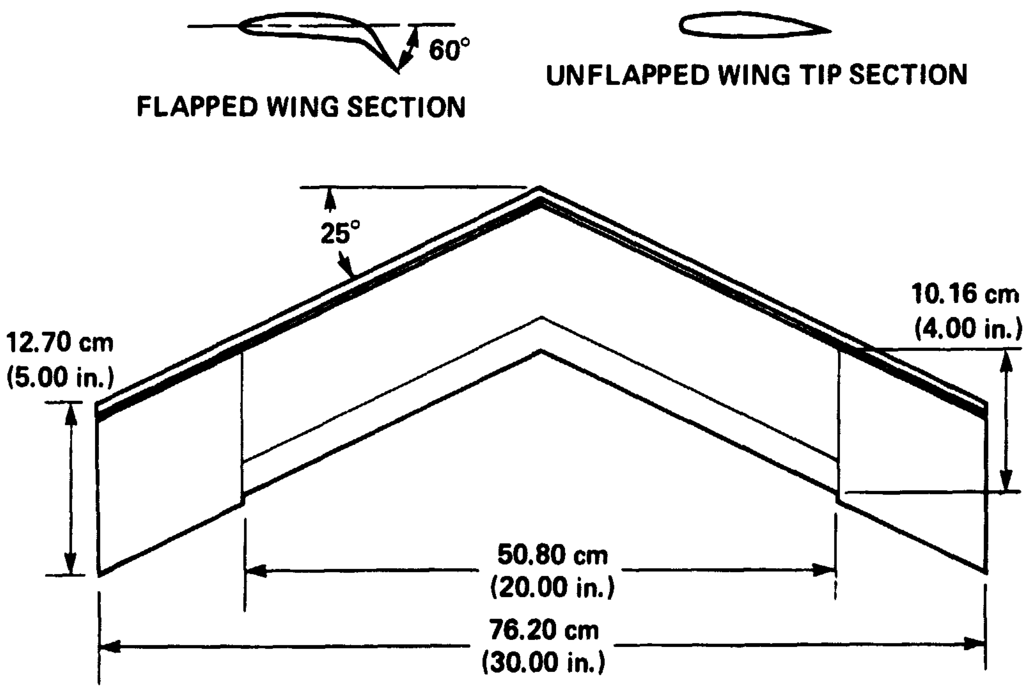

Figure 2.- Swept-wing model geometry.

ORIGINAL PAGE IS
OF POOR QUALITY

ORDINATES OF UNFLAPPED WING TIP SECTION		
X/C	YU/C	YL/C
0	0	0
0.010	0.015	-0.015
0.020	0.020	-0.020
0.049	0.032	-0.033
0.099	0.045	-0.045
0.148	0.056	-0.050
0.198	0.064	-0.053
0.247	0.071	-0.055
0.296	0.077	-0.056
0.395	0.082	-0.056
0.494	0.083	-0.053
0.593	0.079	-0.049
0.692	0.069	-0.042
0.791	0.051	-0.032
0.889	0.028	-0.019
0.988	0.002	-0.003
1.000	0	0

ORDINATES OF FLAPPED WING SECTION				
	STRAIGHT WING		SWEPT WING	
X/C	YU/C	YL/C	YU/C	YL/C
0	0	0	0	0
0.017	0.019	-0.019	0.019	-0.019
0.038	0.028	–	0.028	–
0.067	0.038	-0.044	0.038	-0.044
0.103	0.045	–	0.045	–
0.147	0.053	–	0.053	–
0.250	0.062	-0.076	0.062	-0.076
0.414	0.069	-0.081	0.069	-0.081
0.585	0.063	-0.096	0.063	-0.096
0.750	0.047	-0.114	0.047	-0.114
0.913	0.020	–	0.020	–
0.936	-0.001	–	-0.001	–
0.965	–	-0.138	–	-0.138
0.968	-0.003	–	-0.003	–
0.990	-0.010	–	-0.010	–
1.015	-0.021	-0.170	-0.020	-0.145
1.025	–	–	–	-0.151
1.037	-0.037	–	-0.036	–
1.074	-0.080	–	-0.078	–
1.082	-0.096	–	–	–
1.156	-0.389	-0.391	–	–
1.214	–	–	-0.324	-0.324

Figure 3.- Model wing section ordinates.

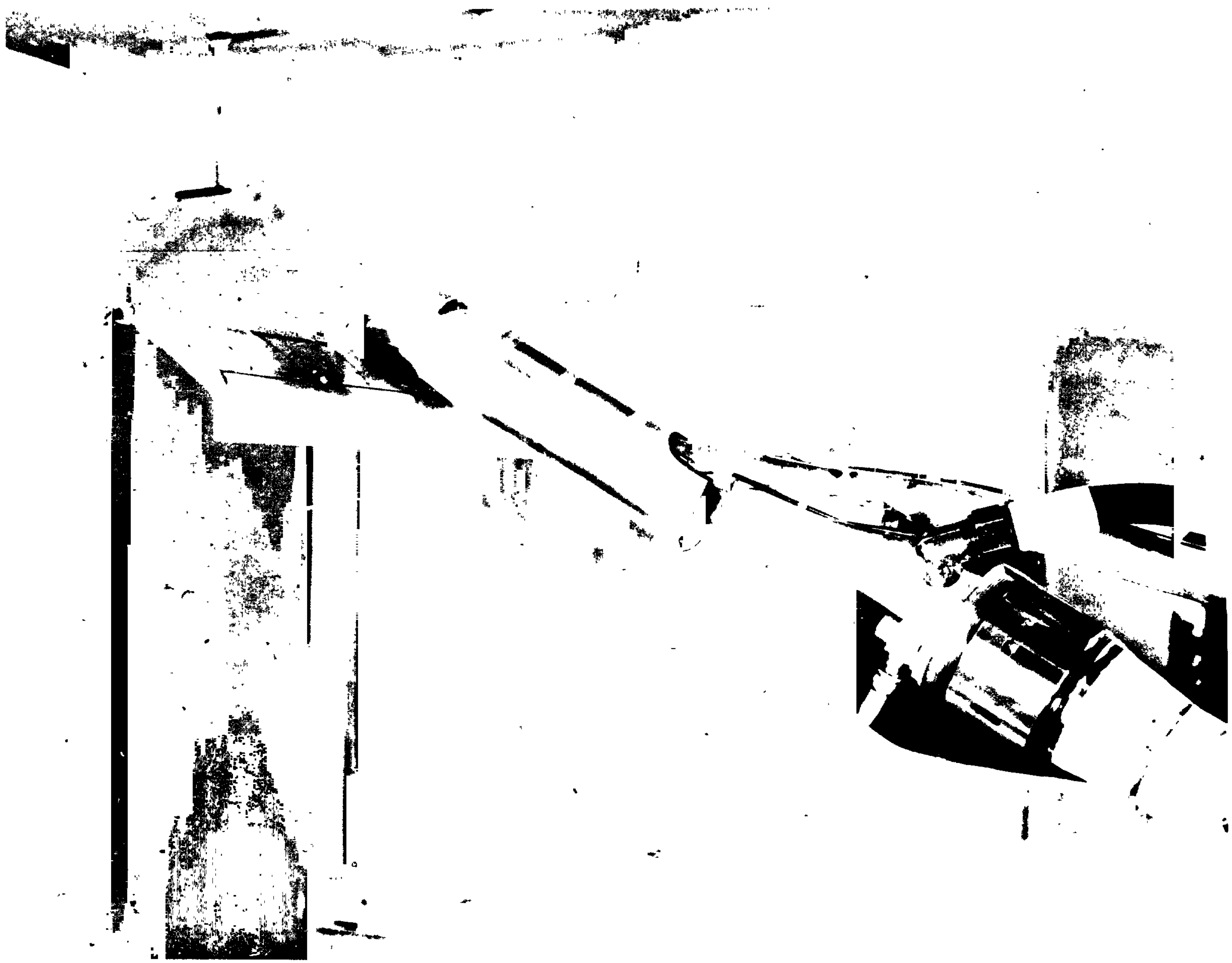

Figure 4.- Rear quarter view of straight-wing model.

ORIGINAL PAGE IS
OF POOR QUALITY

Figure 5.- Front quarter view of straight-wing model.

Figure 6.- Adaptation of model mounting and air supply to articulated sting.

ORIGINAL PAGE IS
OF POOR QUALITY

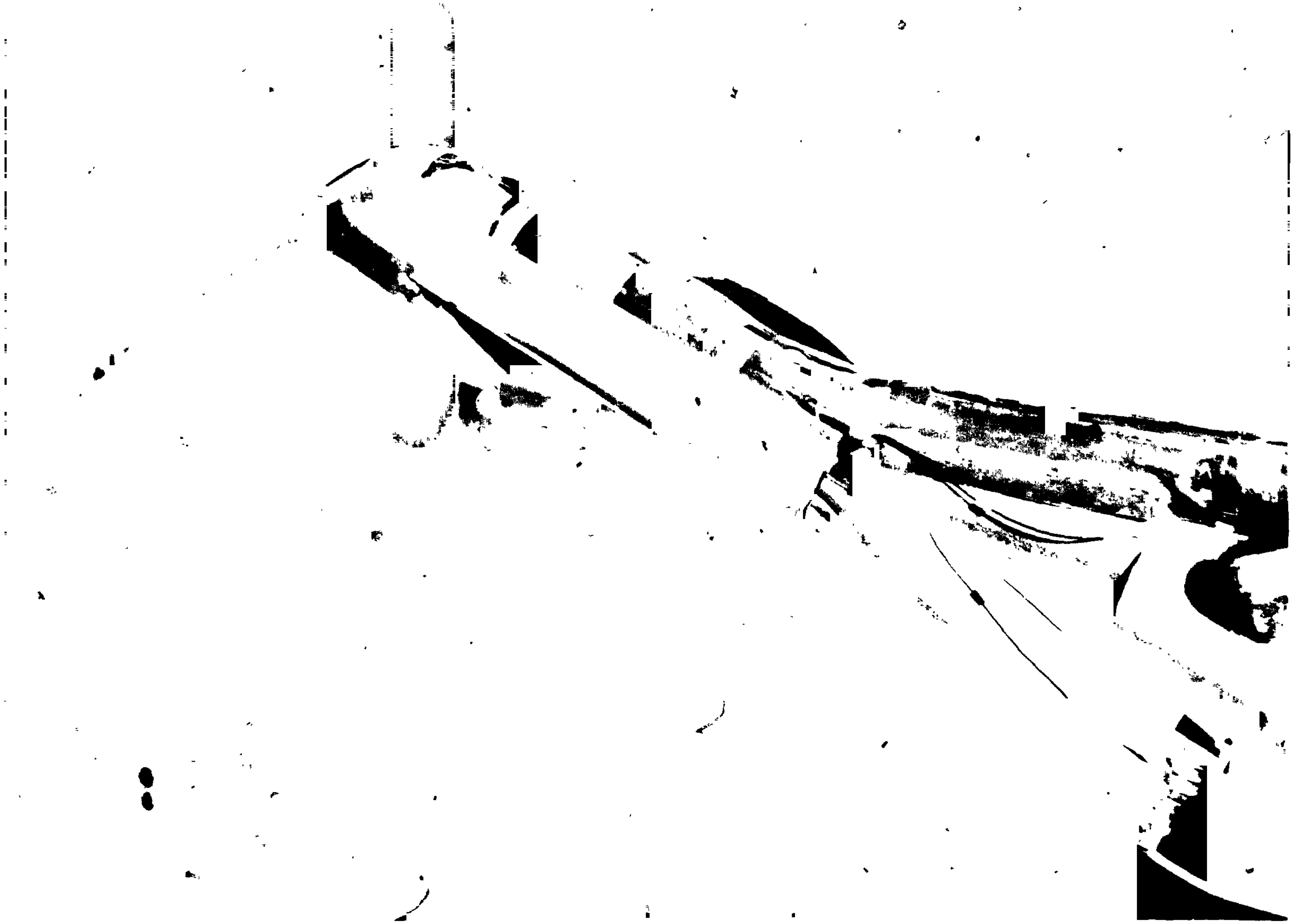

Figure 7.- Rear quarter view of swept-wing model with full-span leading-edge slats and full-span knee-blown flaps.

Figure 8.- Rear quarter view of swept-wing model with tip extensions, full-span leading-edge slats and partial-span knee-blown flaps.

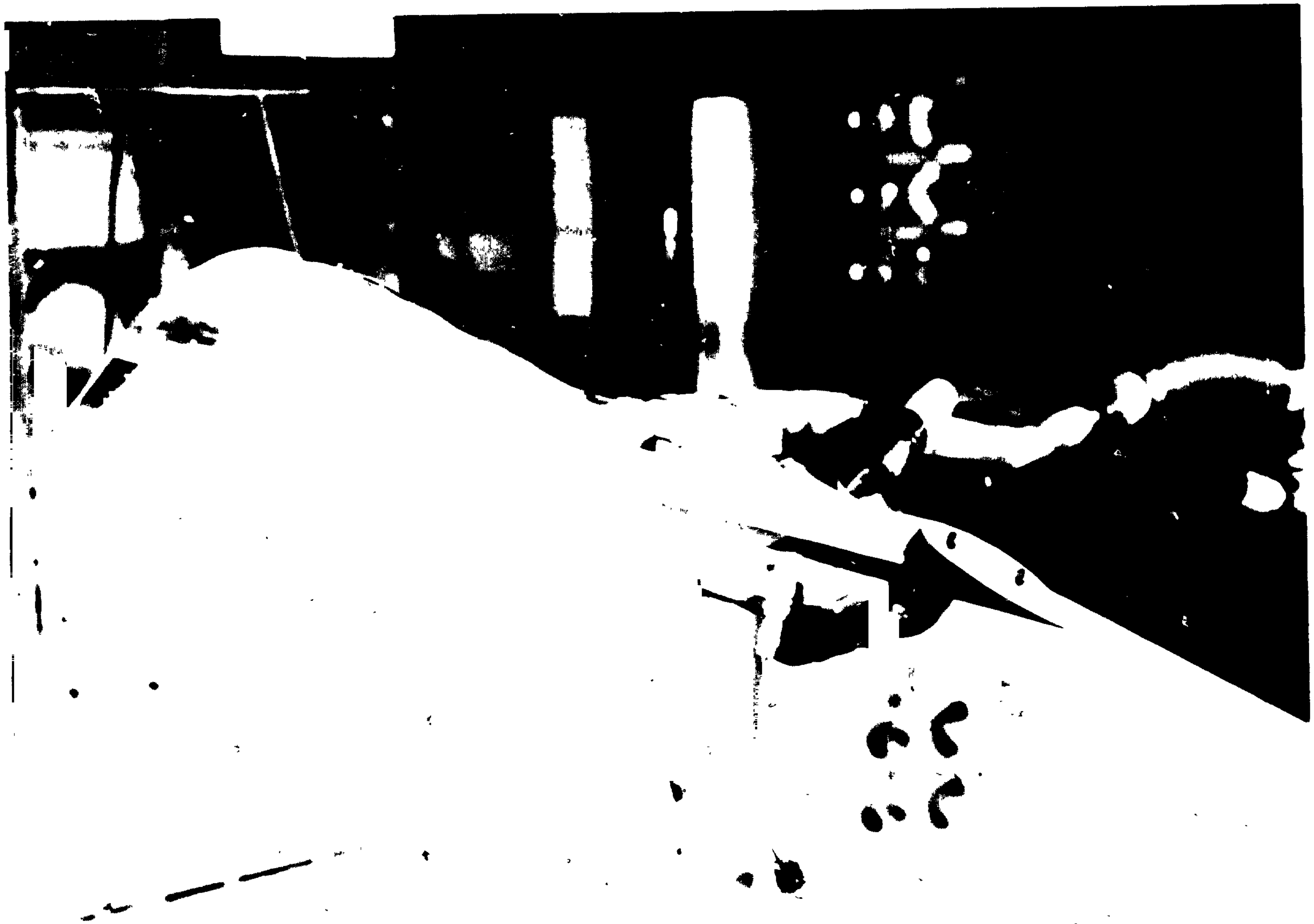

Figure 9.- Front quarter view of swept-wing model with tip extensions, full-span leading-edge slats, and partial knee-blown flaps.

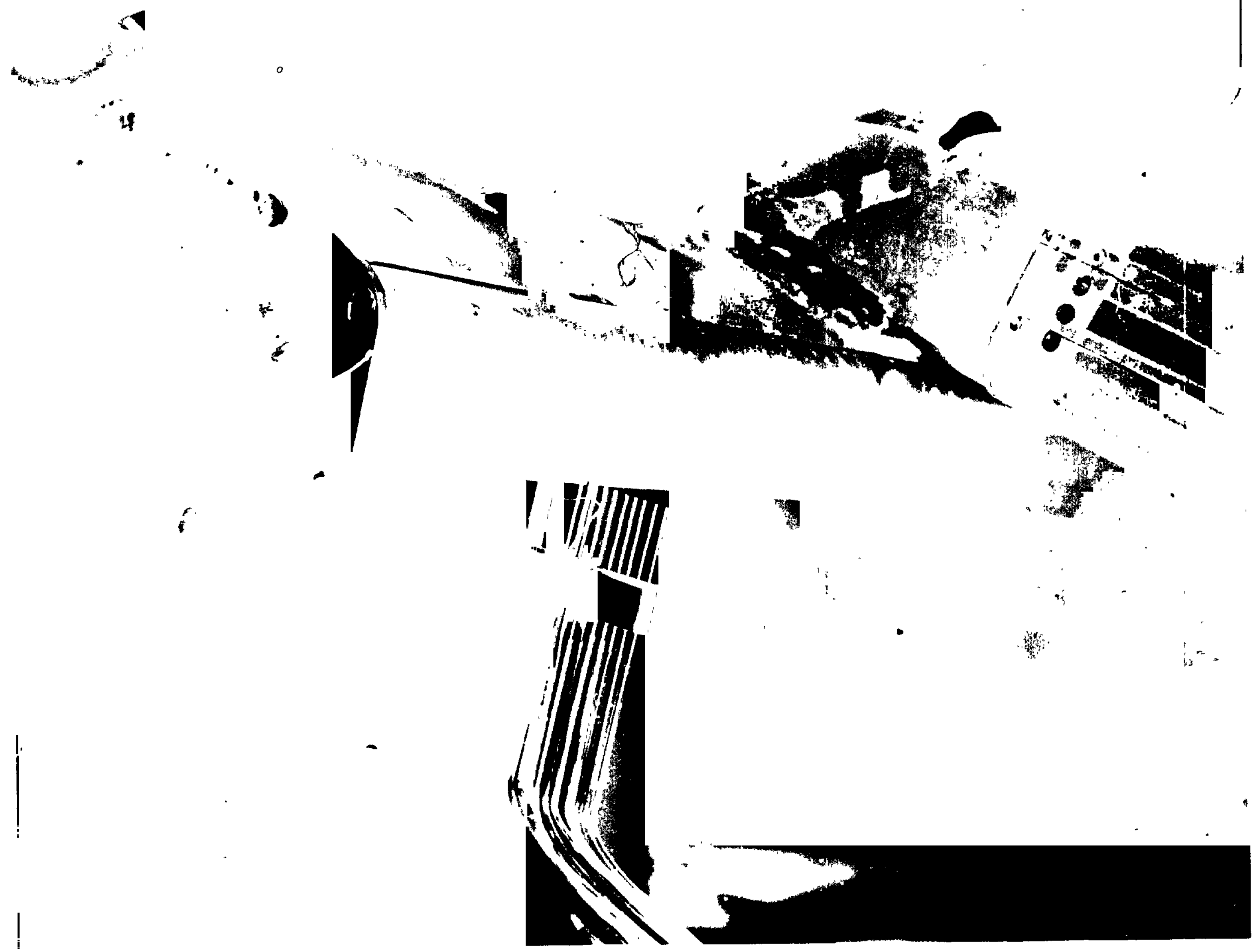

Figure 10.- Straight-wing model with flap rake.

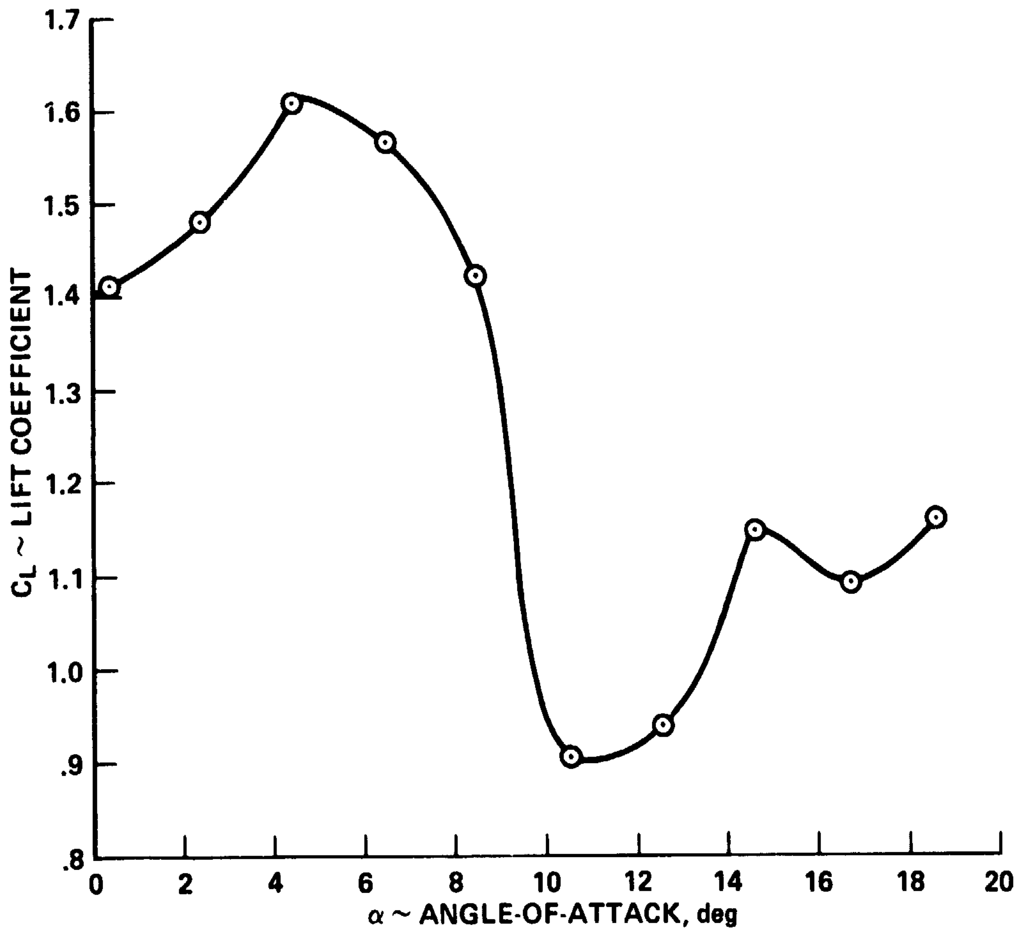

(a) $C_\mu = 0$

Figure 11.- Variation of lift with angle-of-attack for the straight-wing model with full-span knee-blown flaps at various blowing rates.

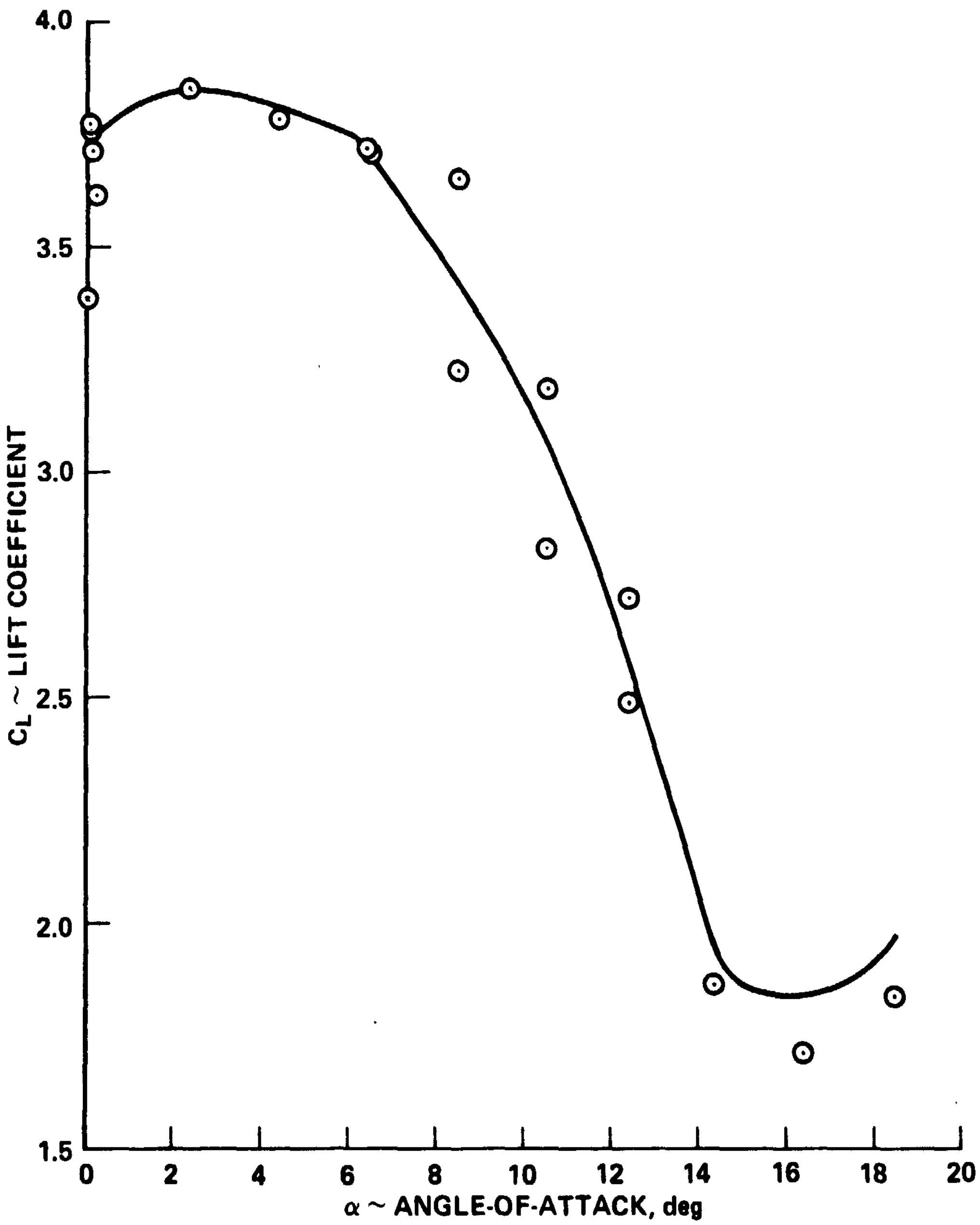

(b) $C_\mu = 0.4$

Figure 11.- Continued.

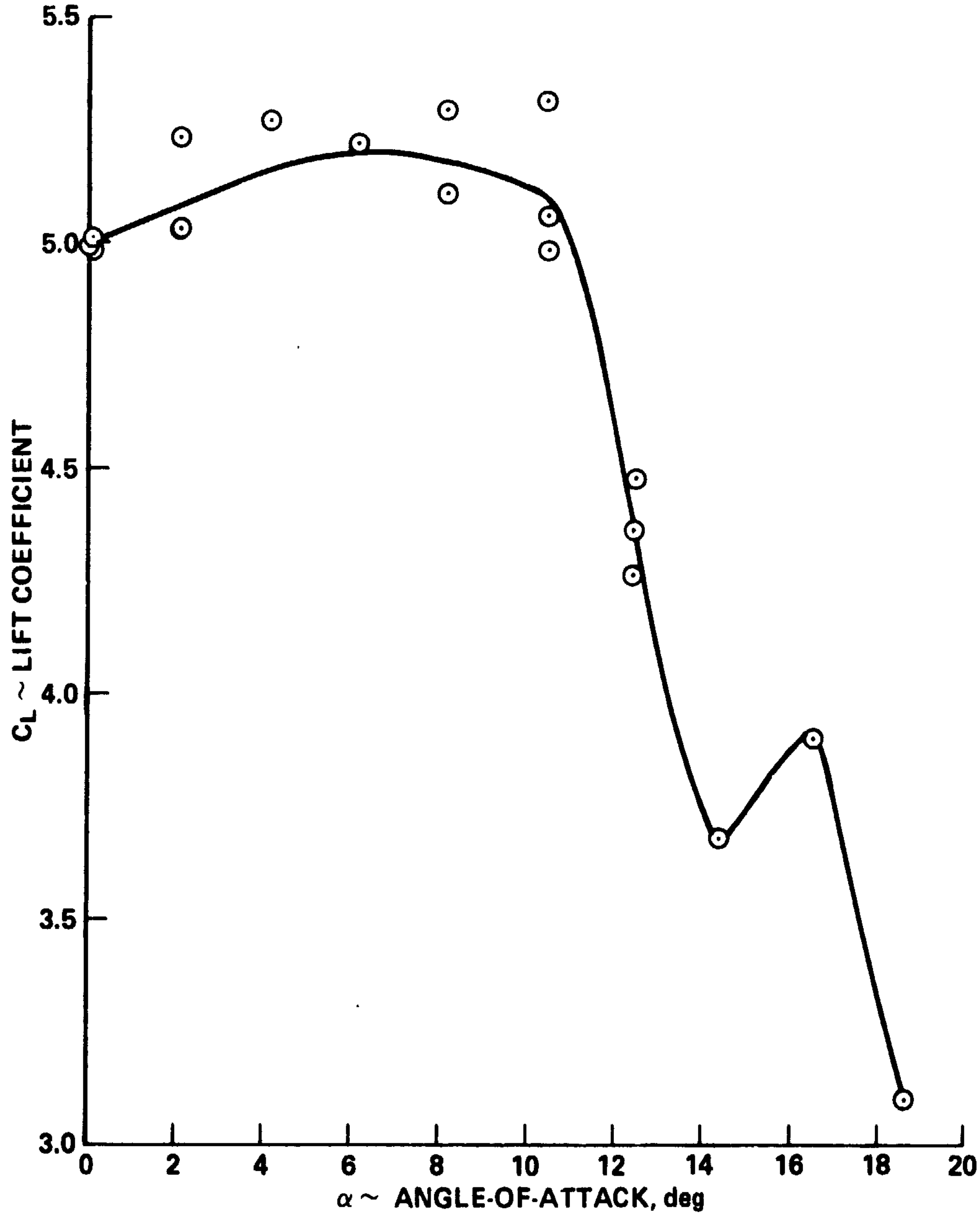

(c) C_μ = 1.0

Figure 11.- Continued

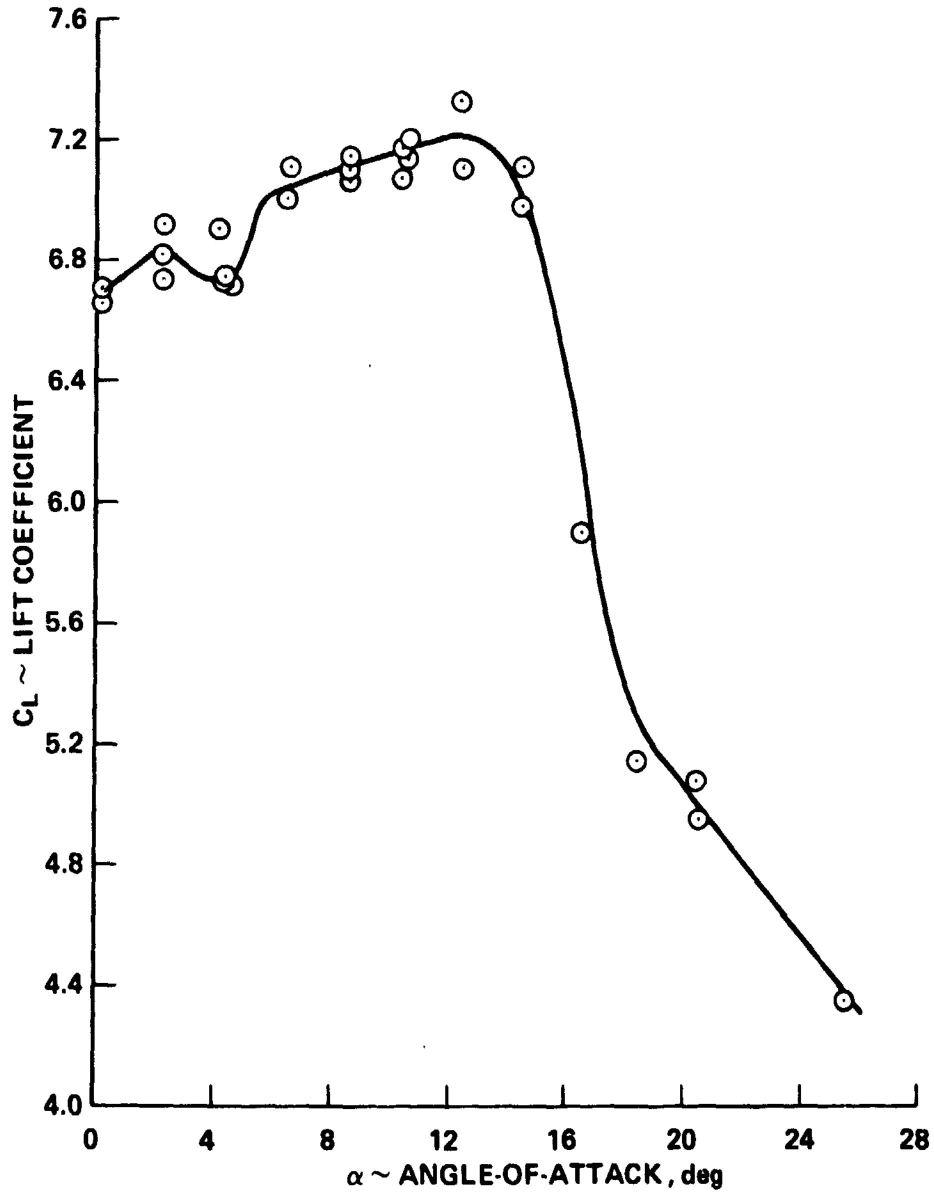

(d) $C_\mu = 2.0$

Figure 11.- Continued.

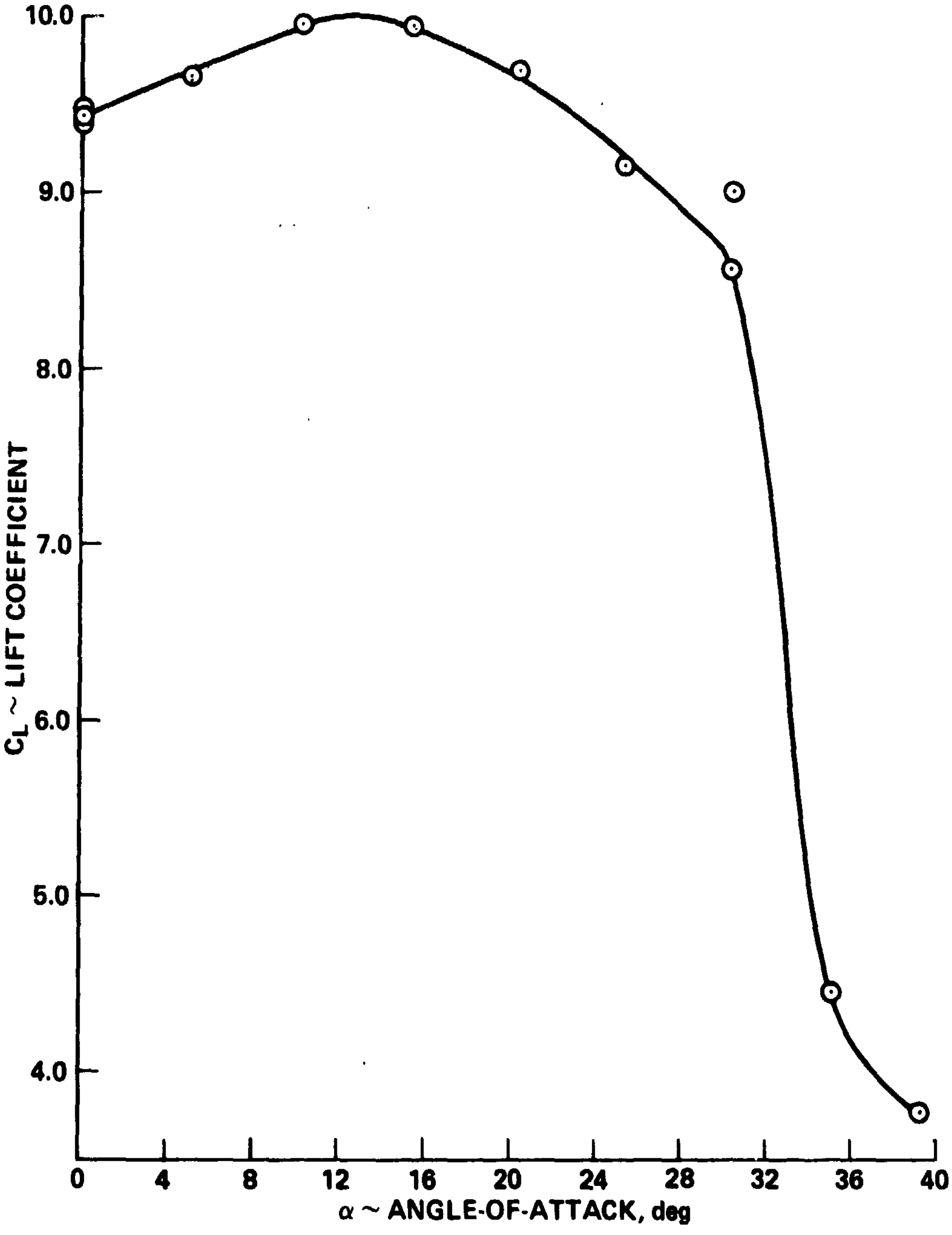

(e) $C_\mu = 4.0$

Figure 11.- Continued.

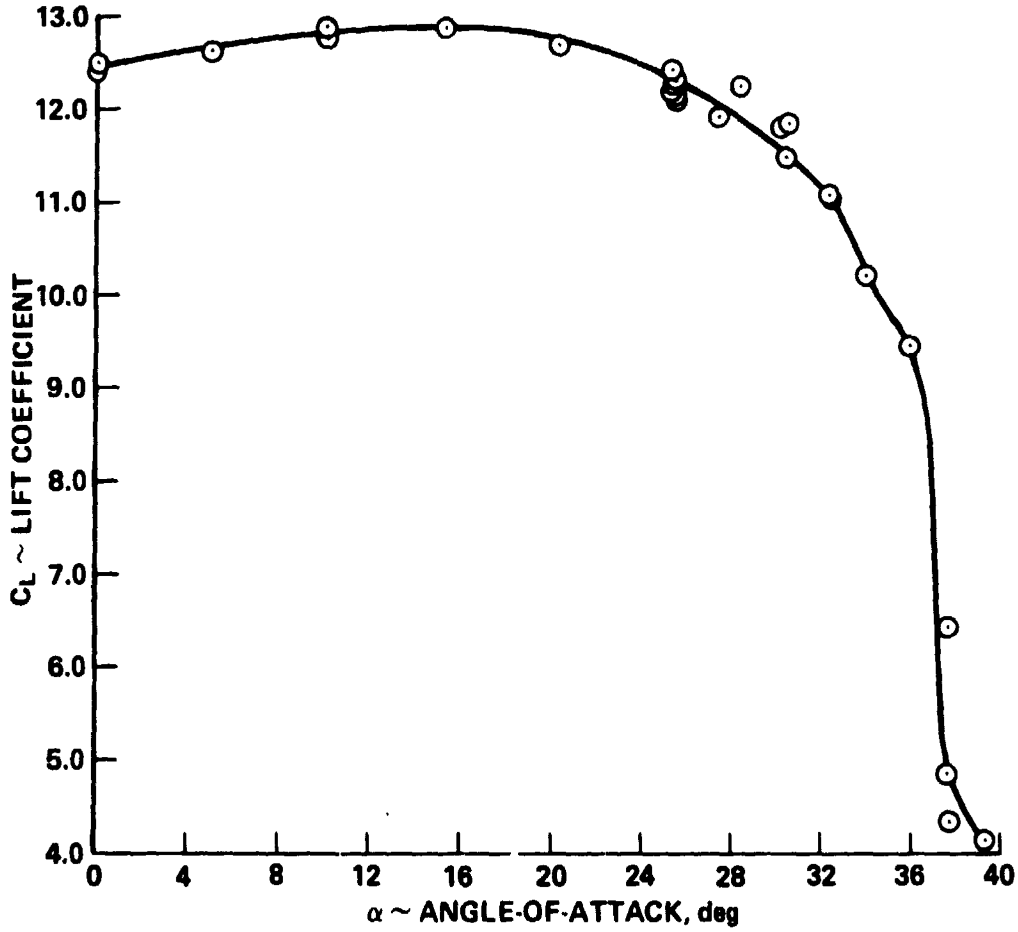

(f) $C_\mu = 6.0$

ORIGINAL PAGE IS
OF POOR QUALITY

Figure 11.- Continued.

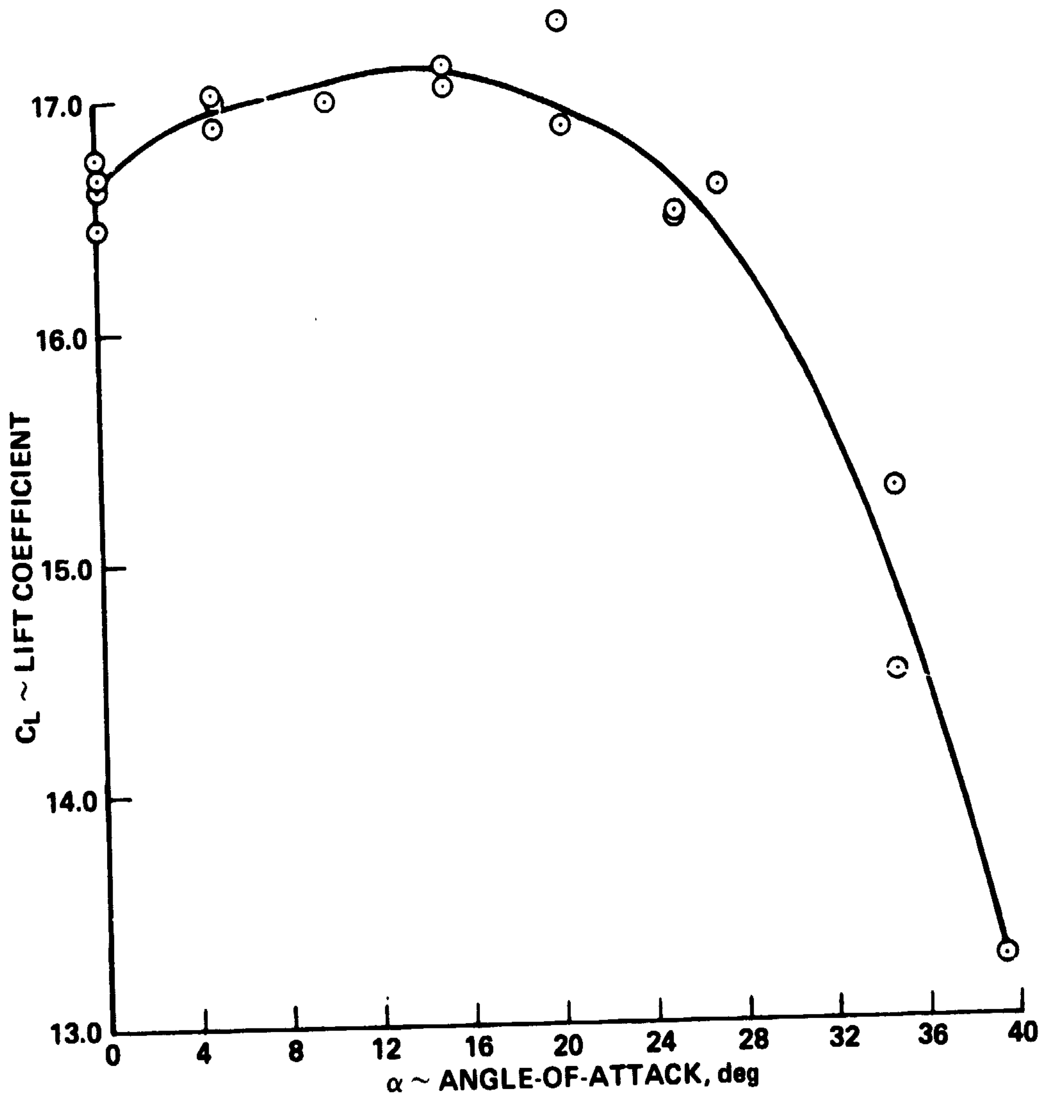

(g) C_μ = 10.0

Figure 11.- Concluded.

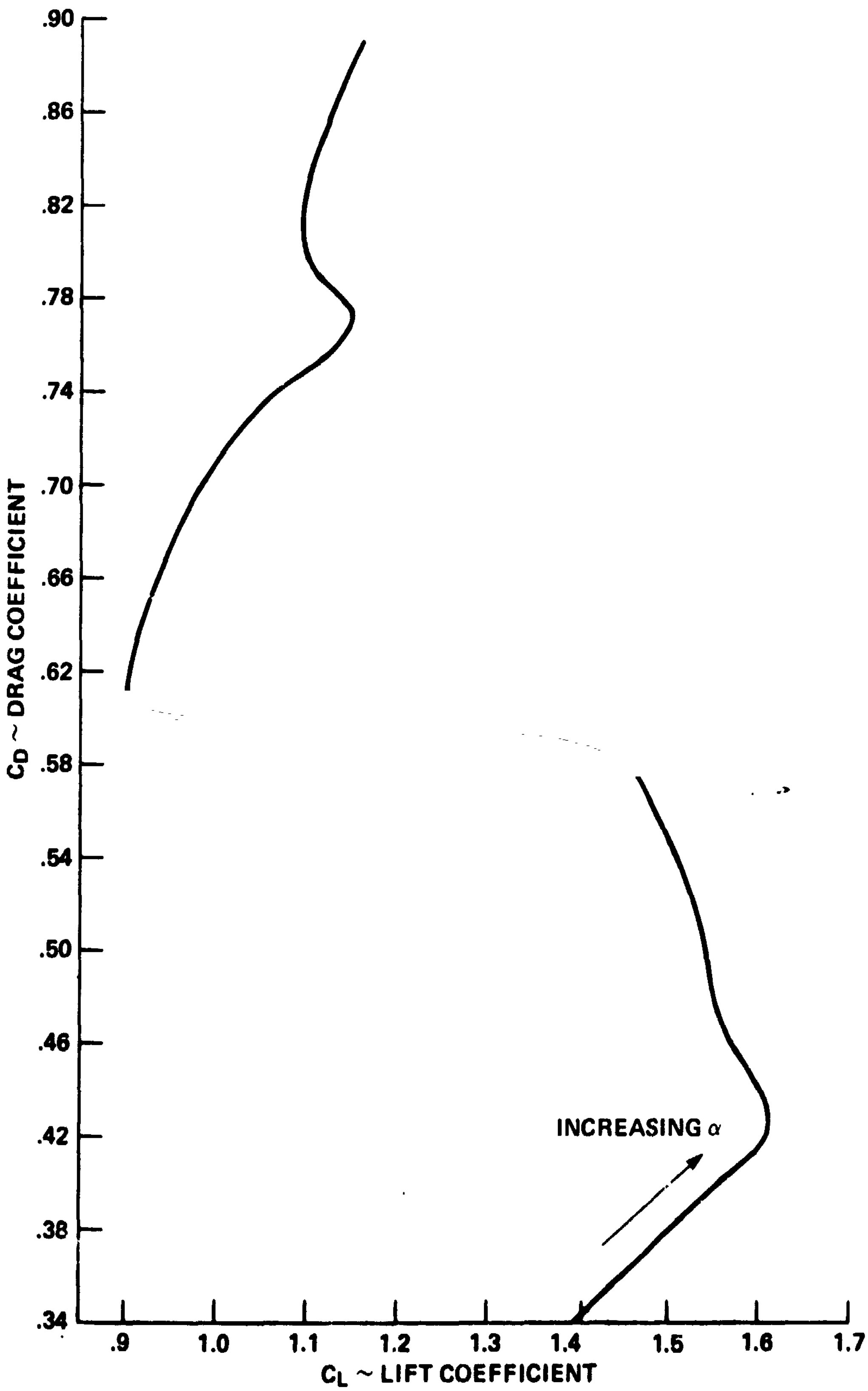

(a) $C_\mu = 0$

Figure 12.- Variation of drag with lift for the straight-wing model with full-span knee-blown flaps at various blowing rates.

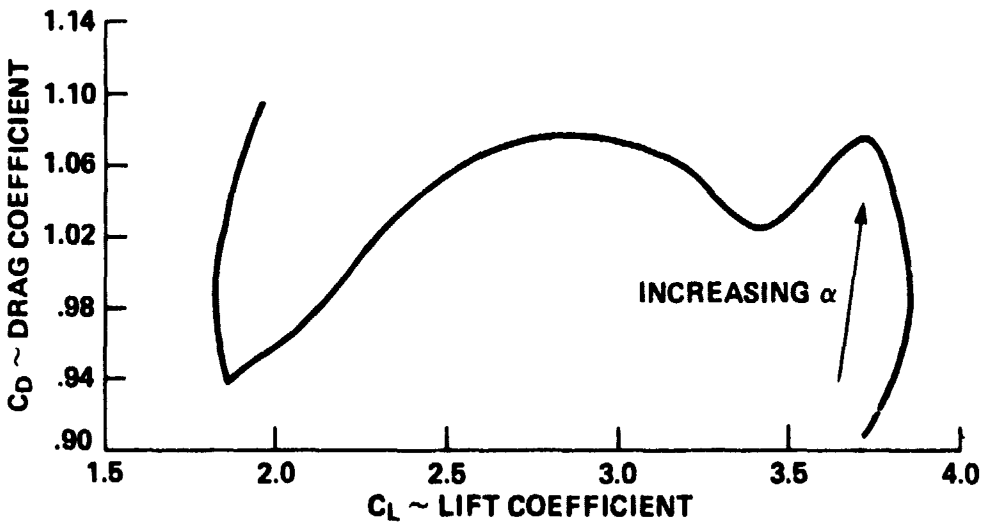

(b) $C_\mu = 0.4$

Figure 12.- Continued.

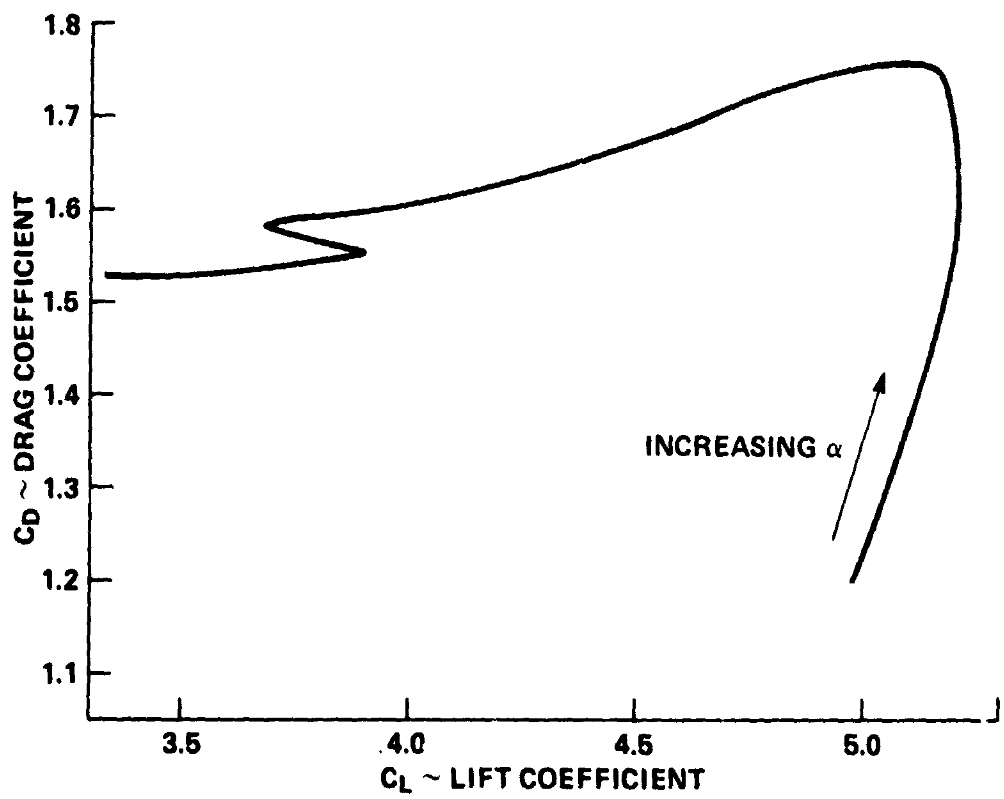

(c) $C_\mu = 1.0$

Figure 12.- Continued.

ORIGINAL PAGE IS
OF POOR QUALITY

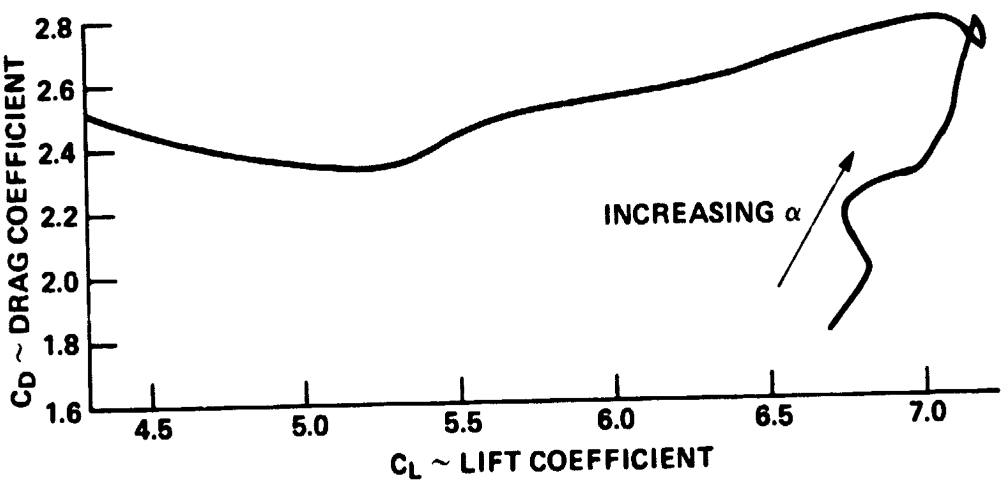

(d) $C_\mu = 2.0$

Figure 12.- Continued.

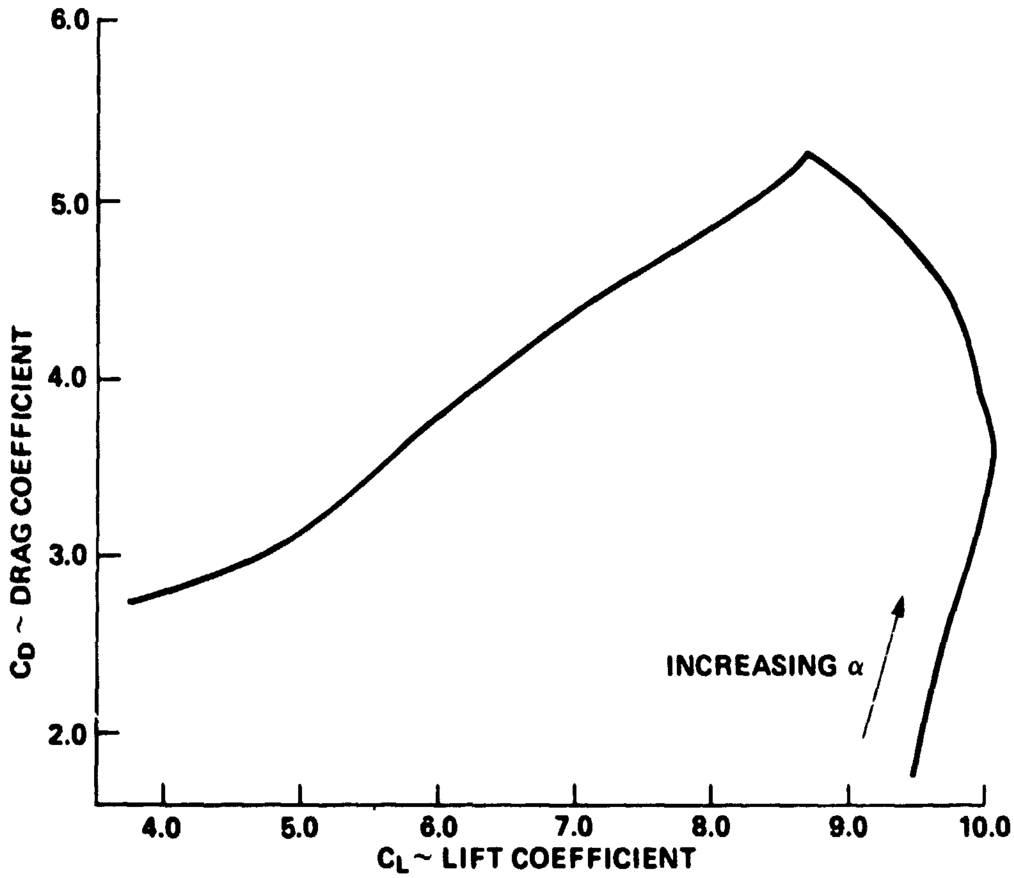

(e) $C_\mu = 4.0$

Figure 12.- Continued.

ORIGINAL PAGE IS
OF POOR QUALITY

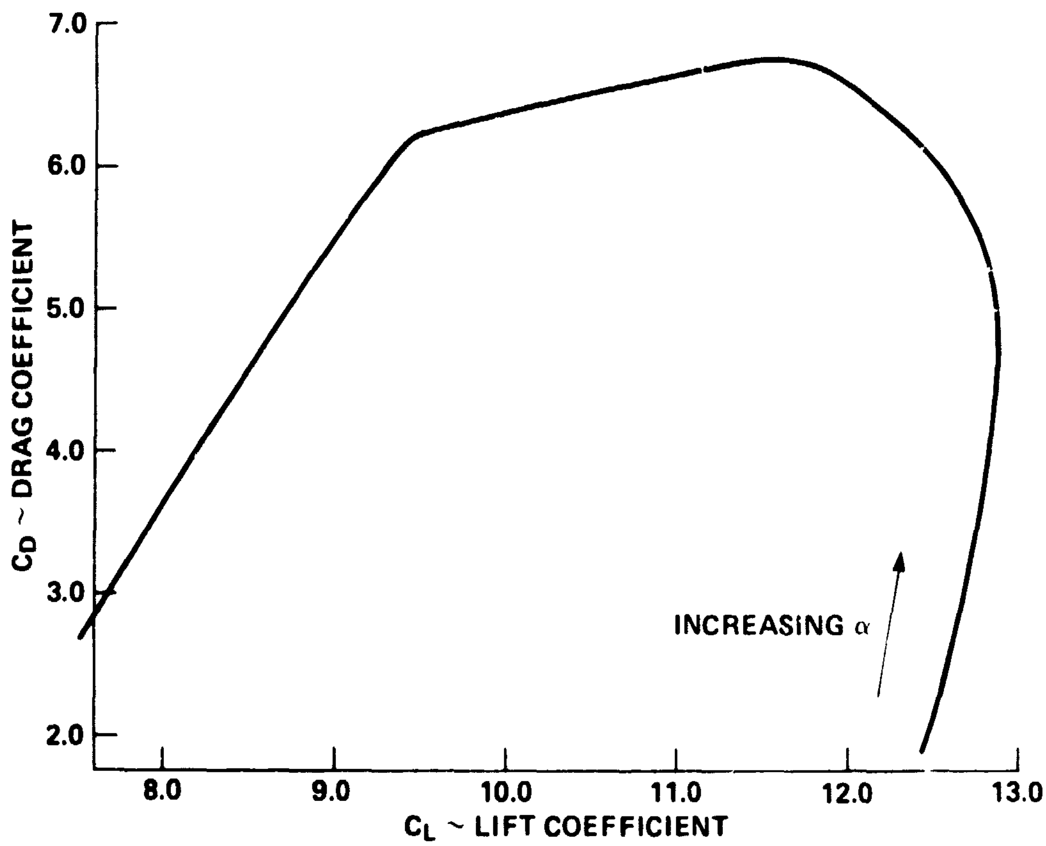

(f) $C_\mu = 6.0$

Figure 12.- Continued.

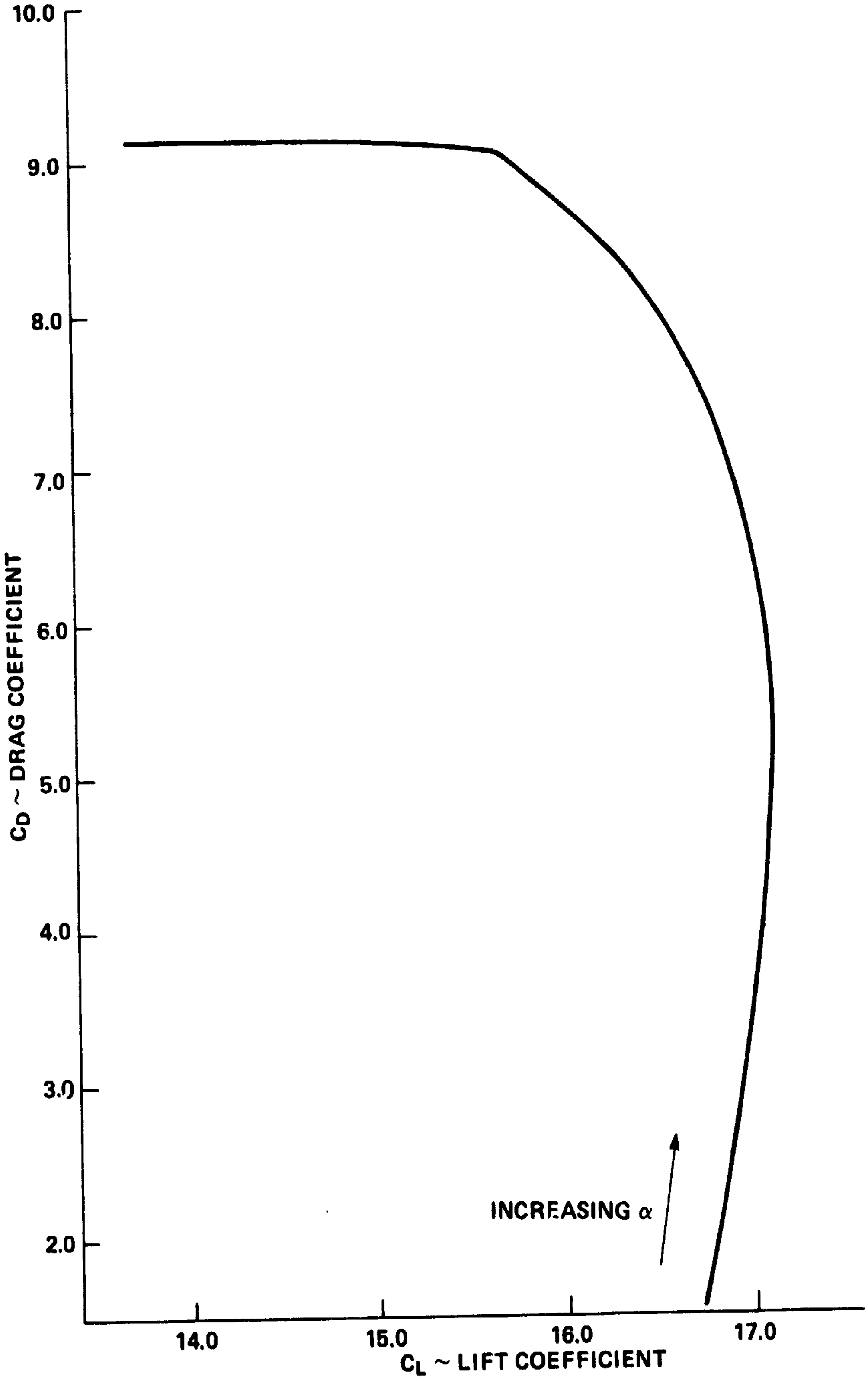

(g) $C_\mu = 10.0$

Figure 12.- Concluded.

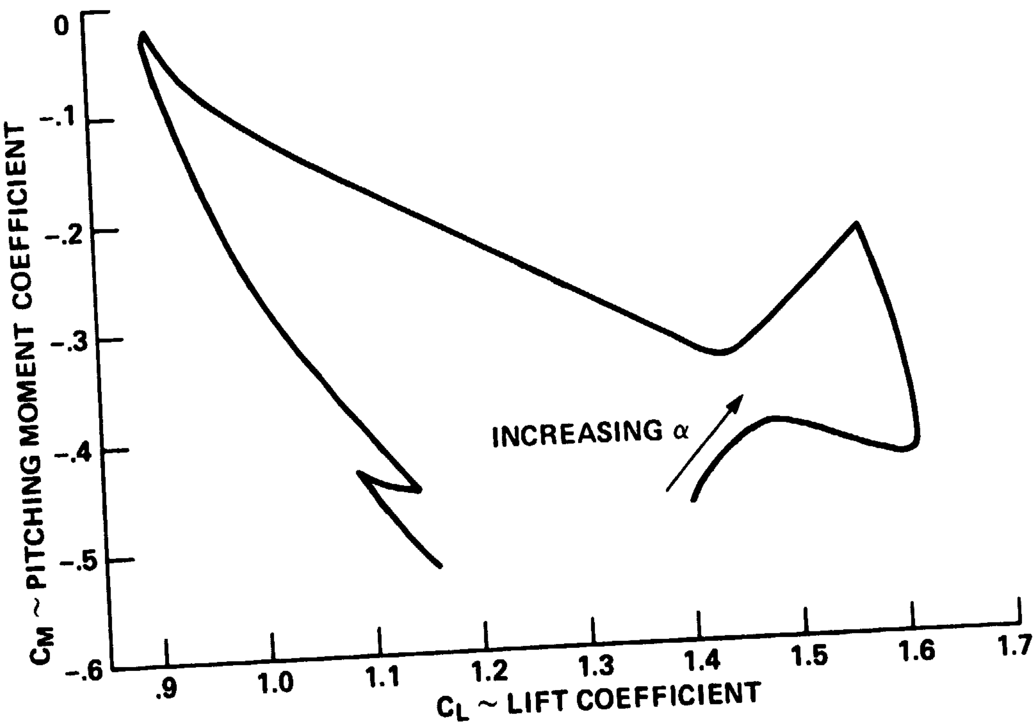

(a) $C_\mu = 0$

Figure 13.- Variation of pitching moment with lift for the straight-wing mode with full-span knee-blown flaps at various blowing rates.

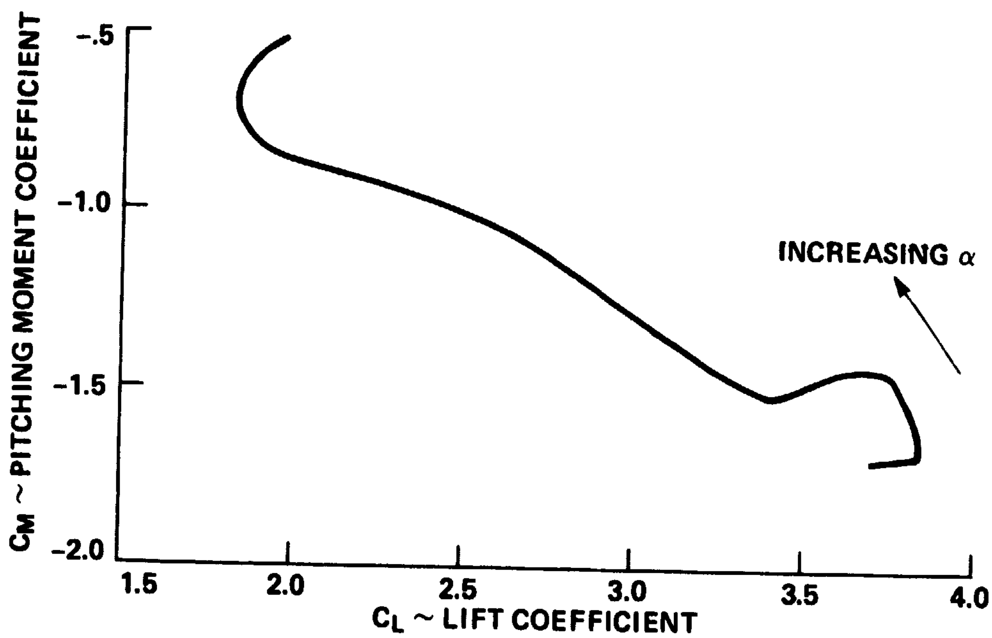

(b) $C_\mu = 0.4$

Figure 13.- Continued.

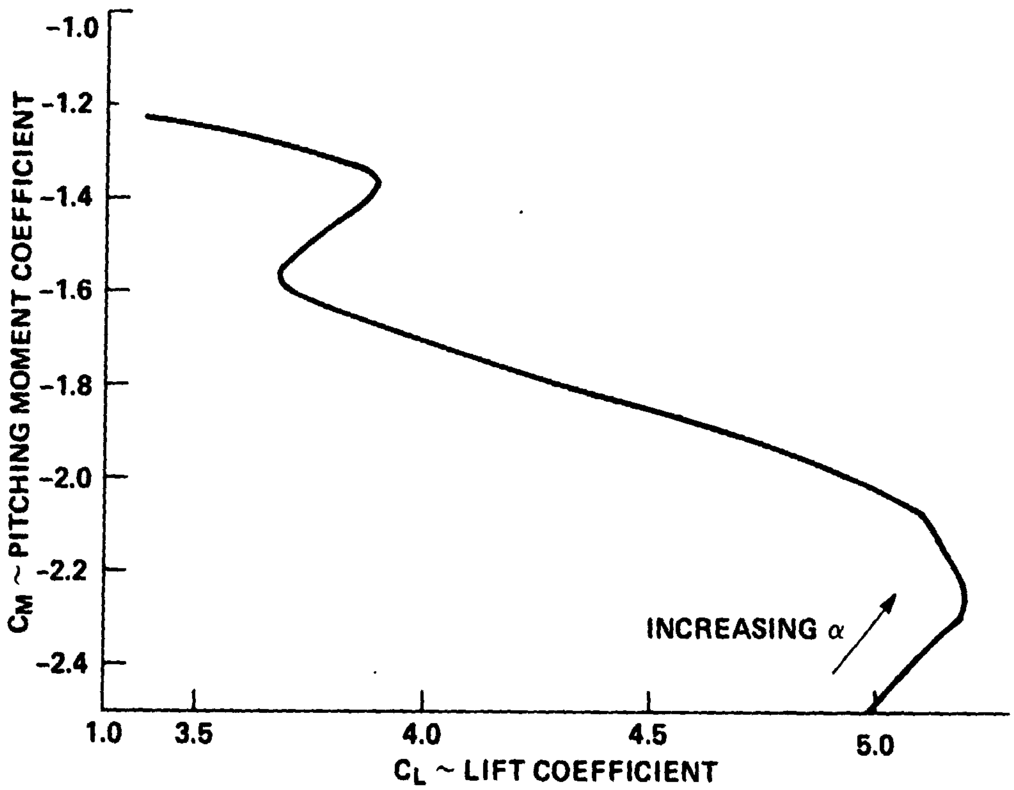

(c) C_μ = 1.0

Figure 13.- Continued.

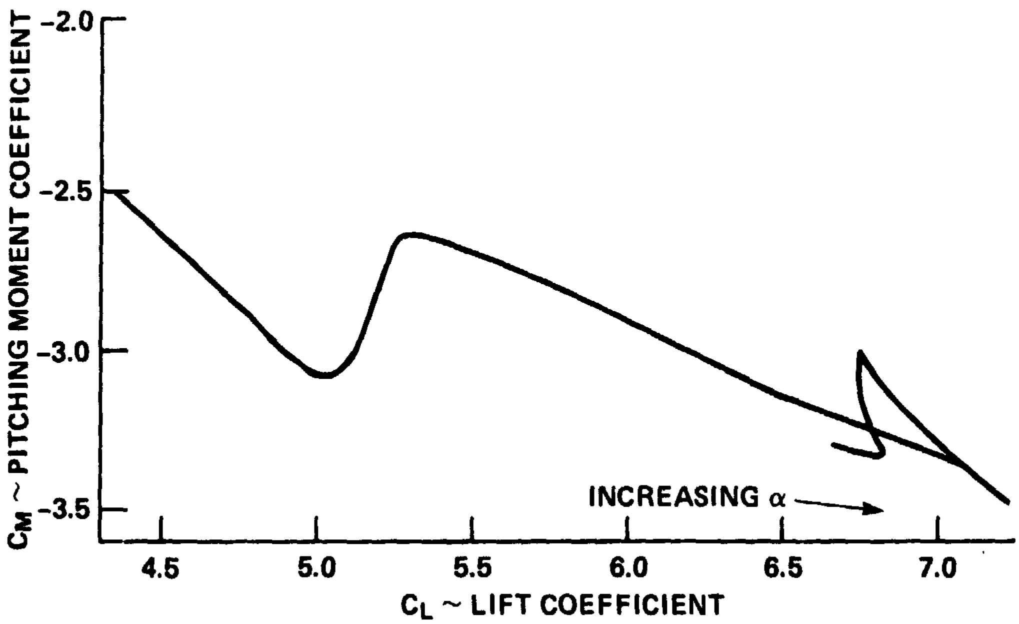

(d) $C_\mu = 2.0$

Figure 13.- Continued.

ORIGINAL PAGE IS
OF POOR QUALITY

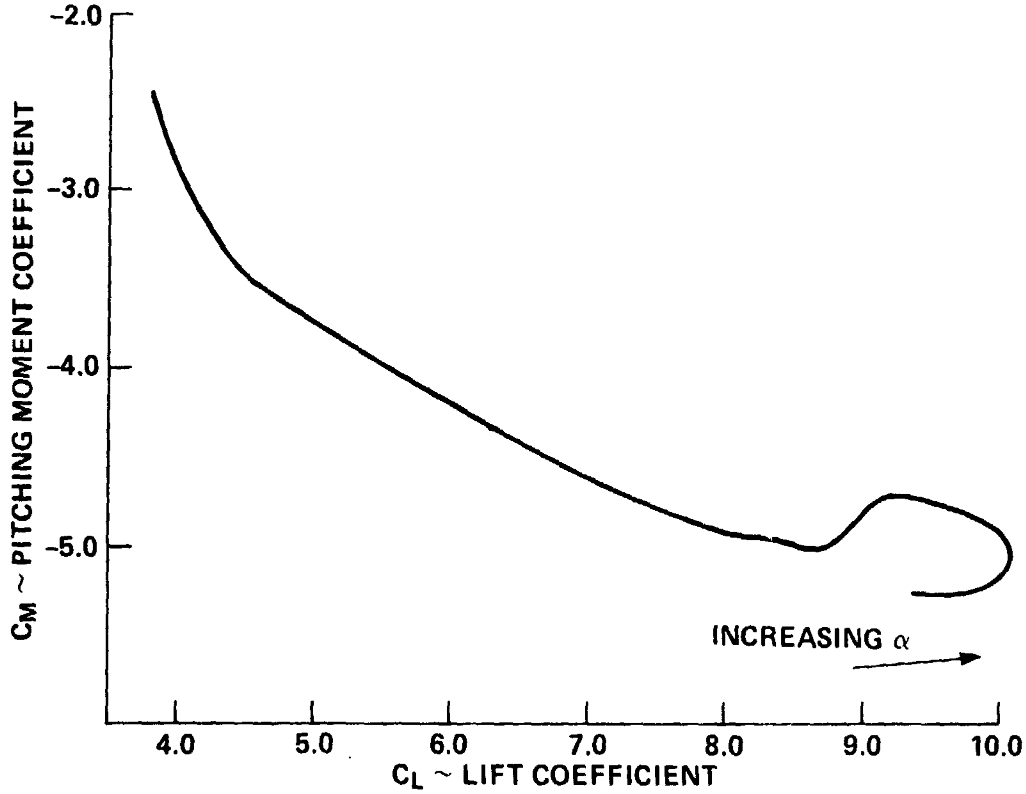

(e) $C_\mu = 4.0$

Figure 13.- Continued.

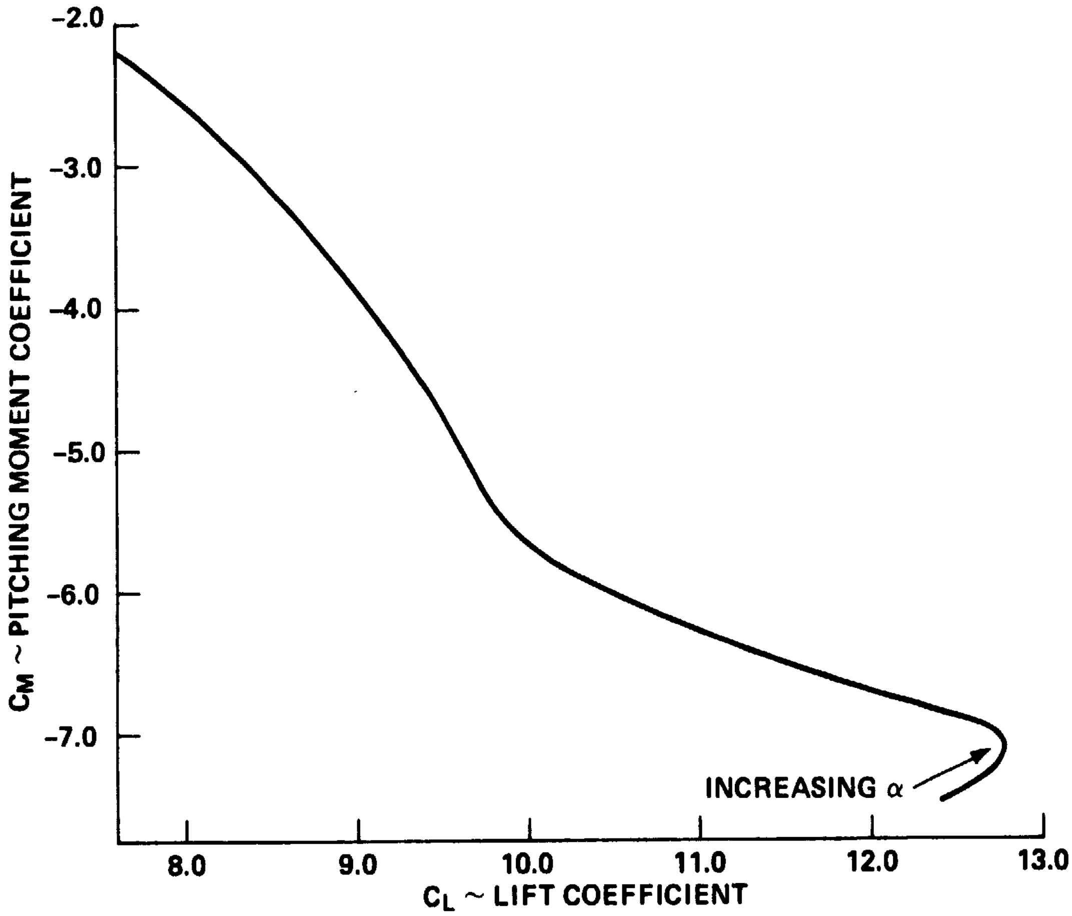

(f) $C_\mu = 6.0$

Figure 13.- Continued.

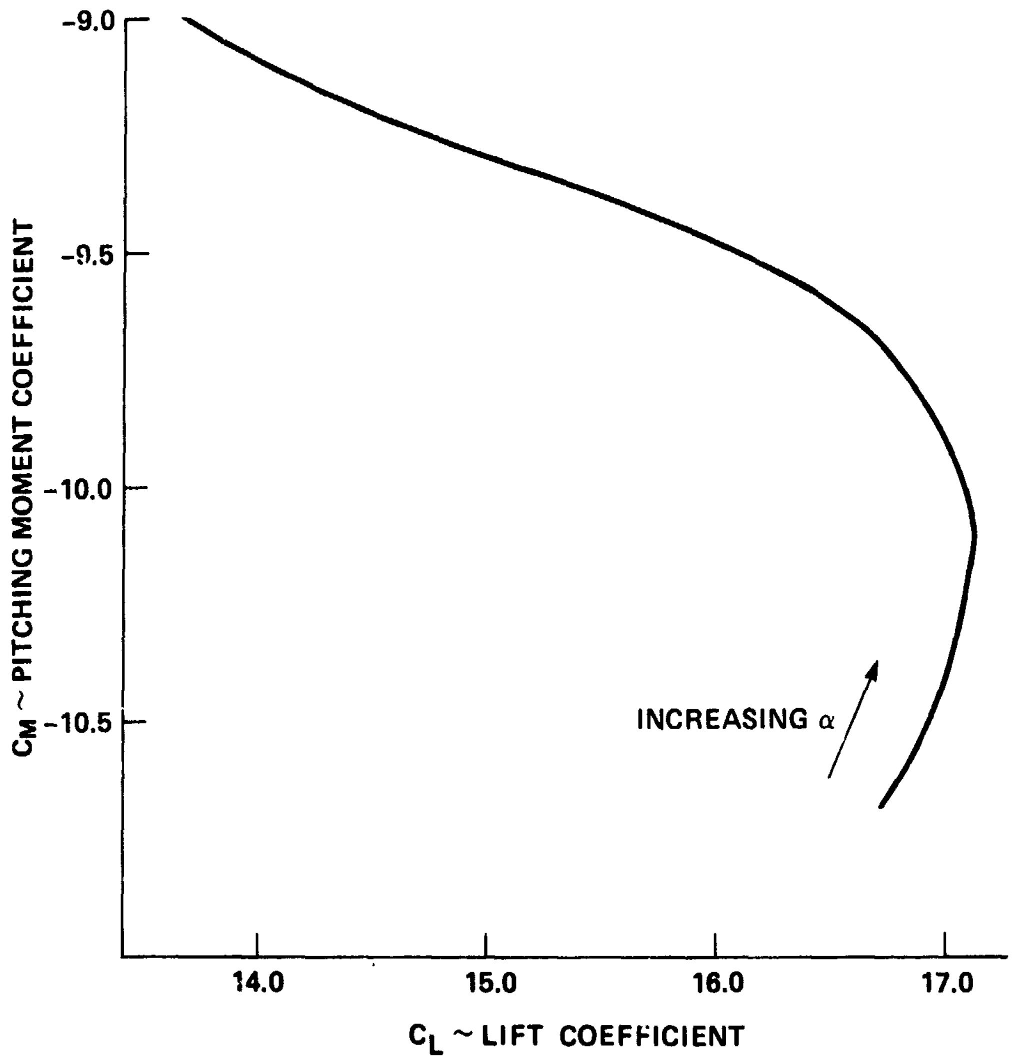

(g) C_μ = 10.0

Figure 13.- Concluded.

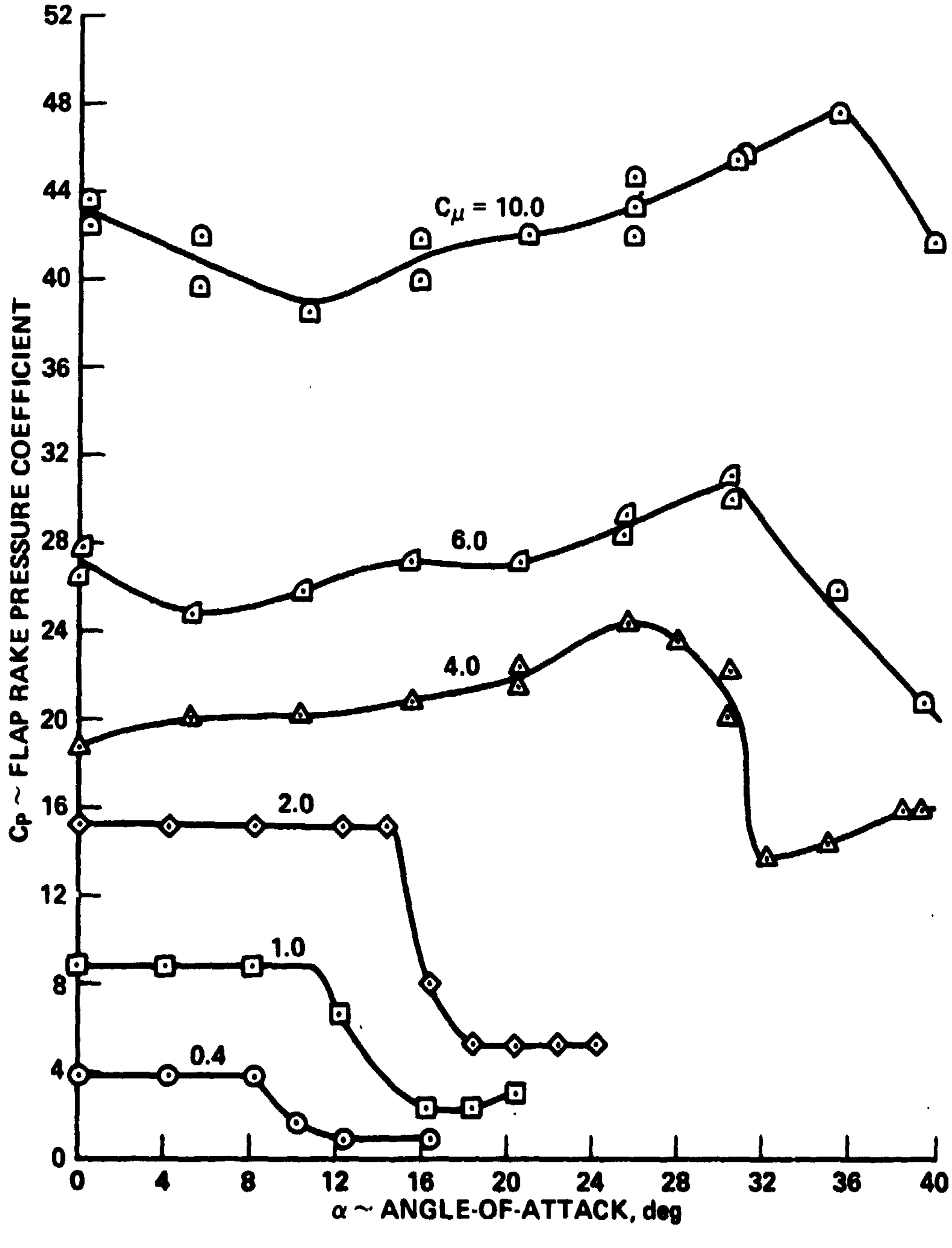

(a) Tube 1: 0.46 mm (0.018 in.) above flap upper surface.

Figure 14.- Variation of flap rake pressure coefficients with angle-of-attack for the straight-wing model with full-span knee-blown flaps at various blowing rates.

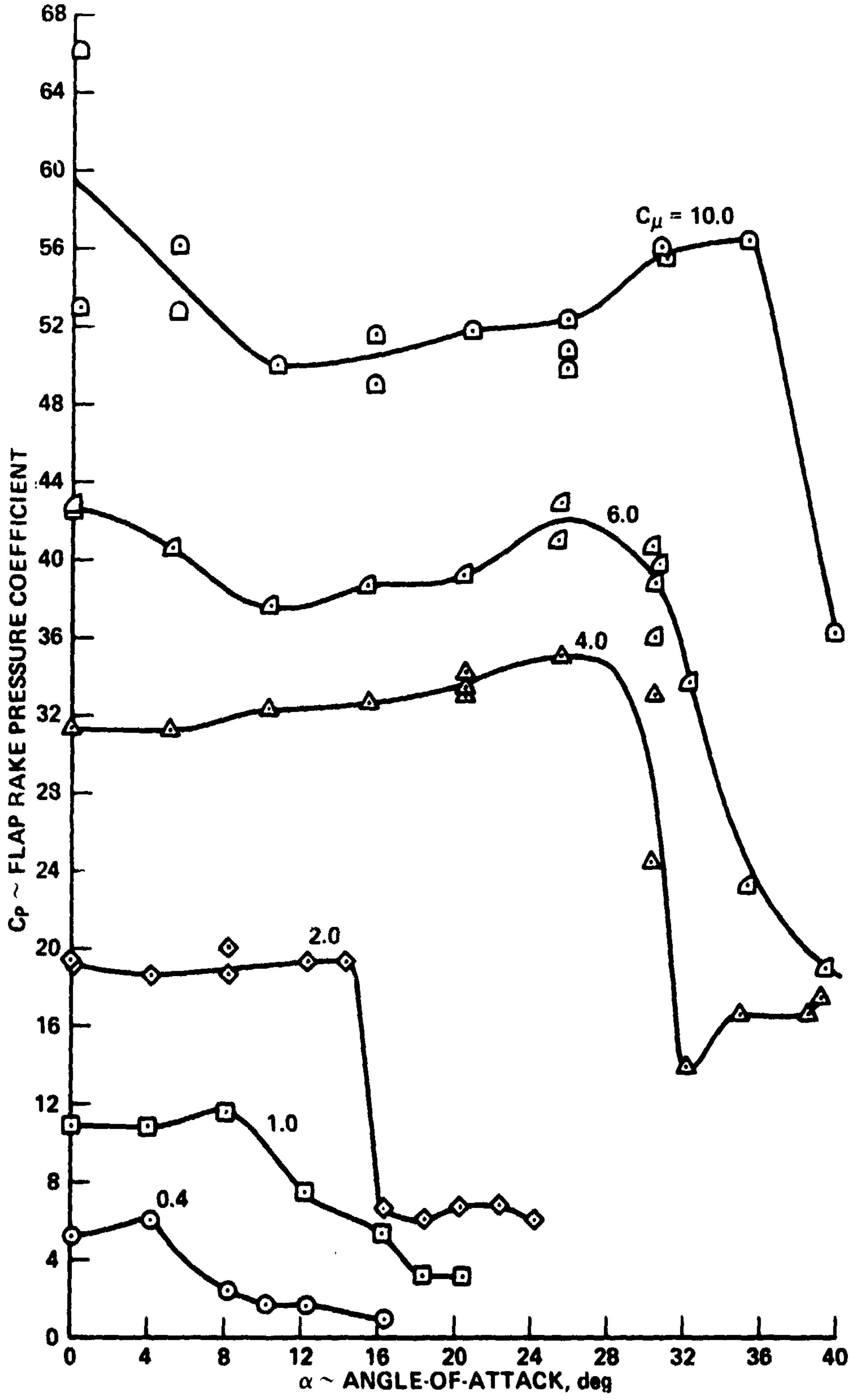

(b) Tube 2: 2.36 mm (0.093 in.) above flap upper surface.

Figure 14.- Continued.

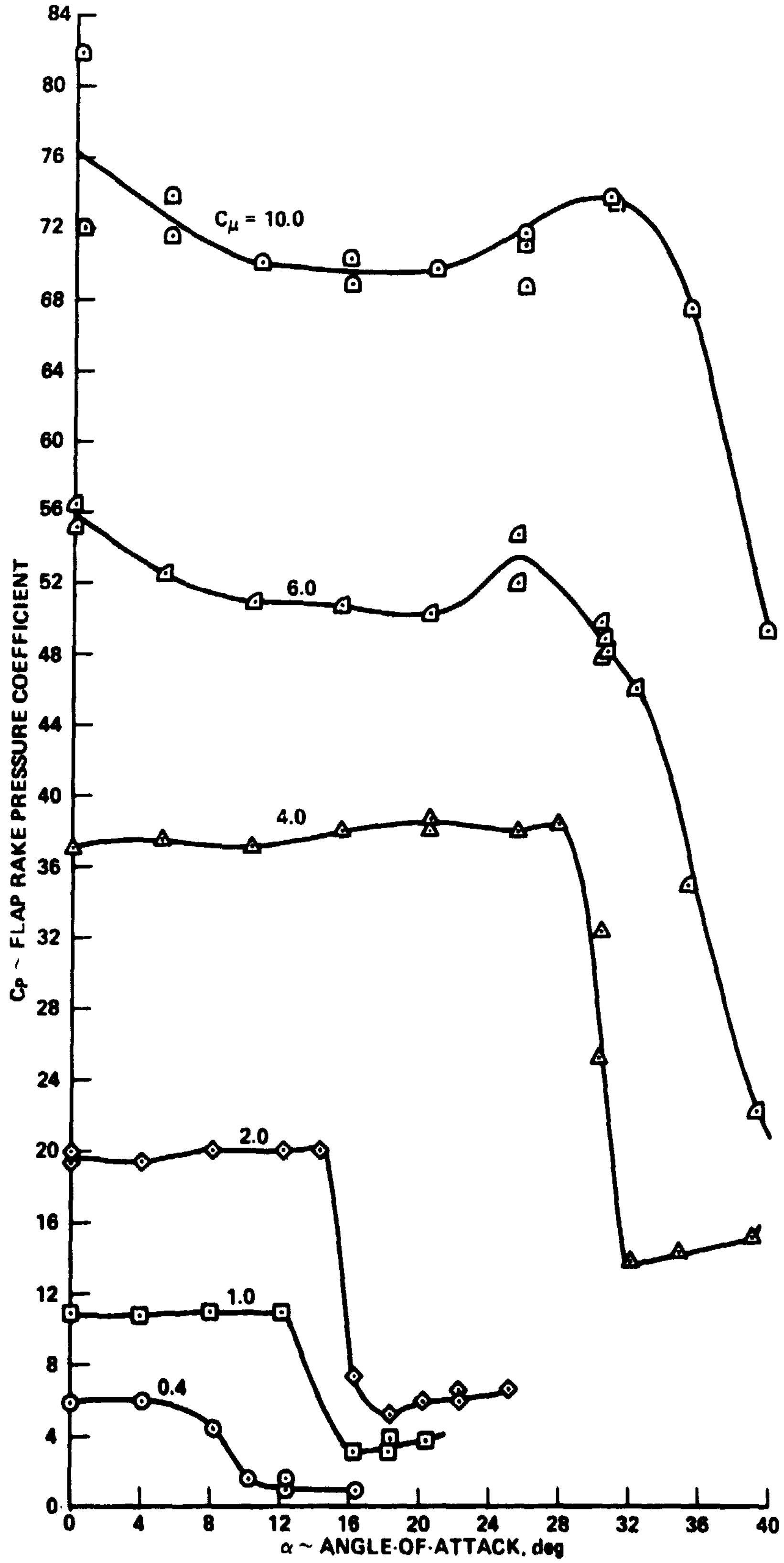

(c) Tube 3: 3.43 mm (0.135 in.) above flap upper surface.

Figure 14.- Continued.

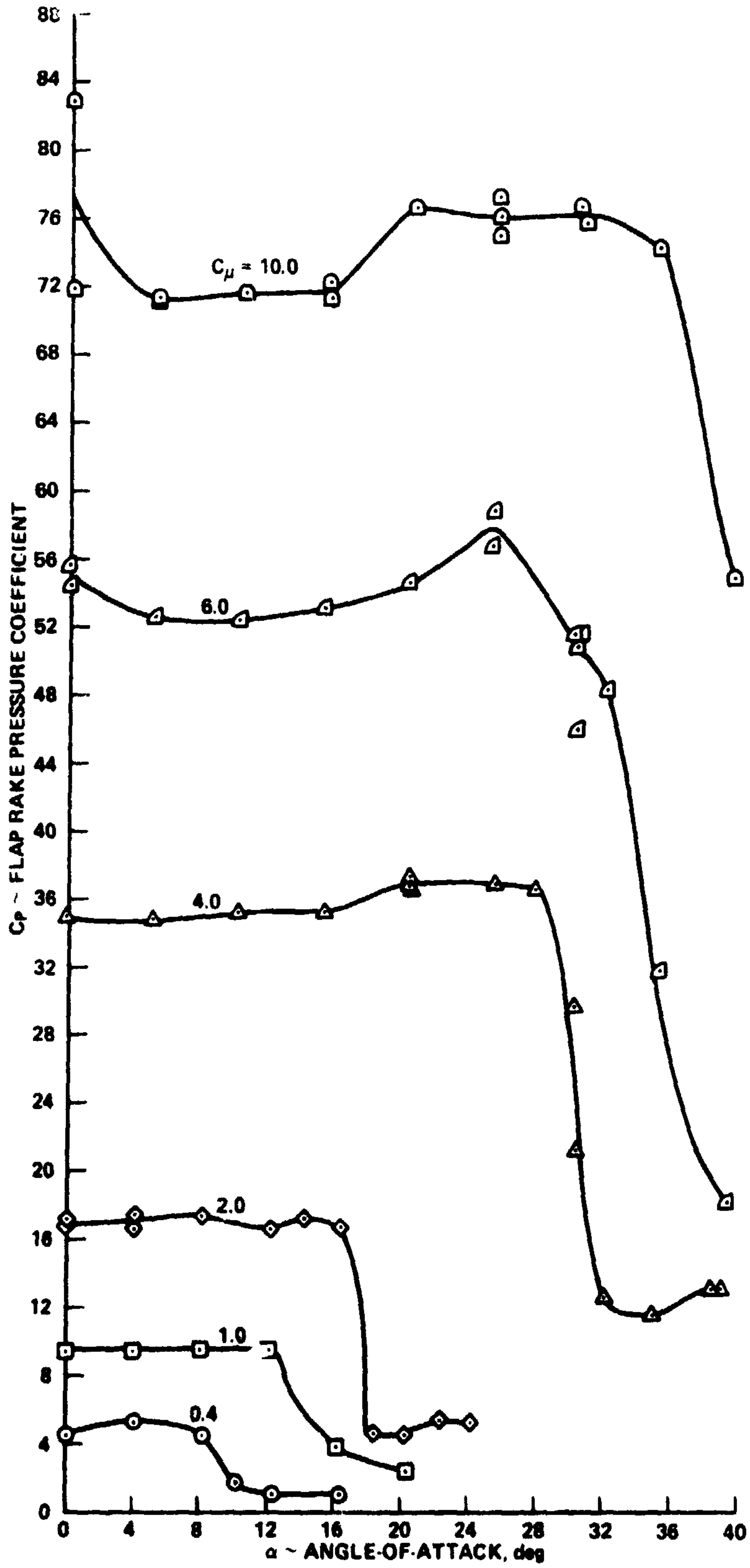

(d) Tube 4: 4.75 mm (0.187 in.) above flap upper surface

Figure 14.- Continued.

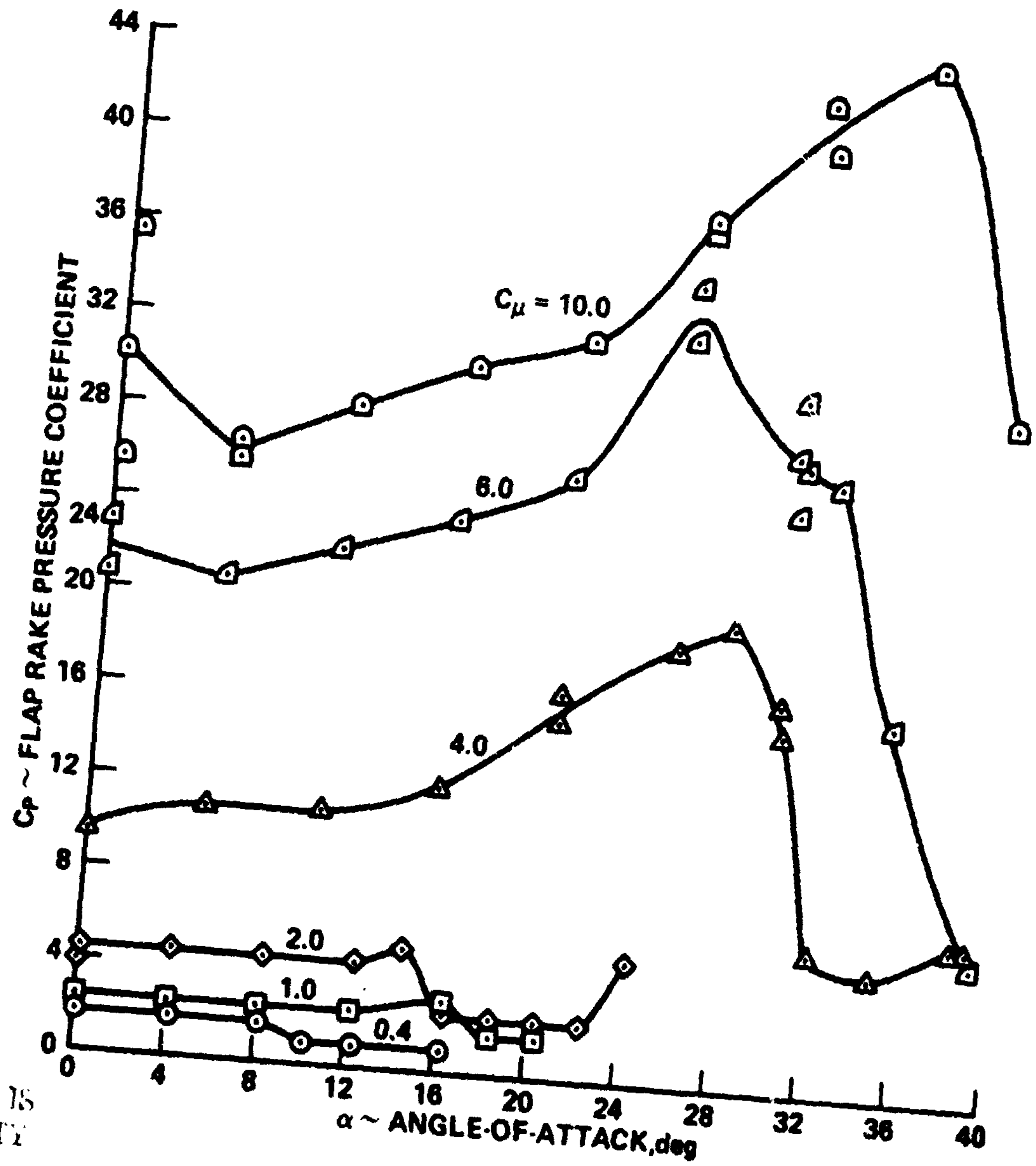

(e) Tube 5: 8.18 mm (0.322 in.) above flap upper surface.

Figure 14.- Continued.

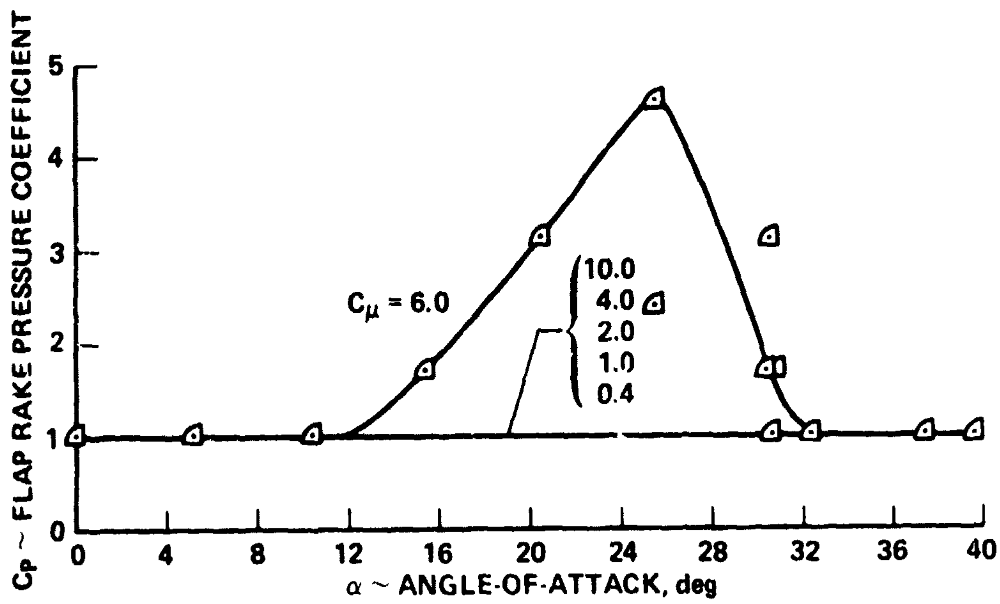

(f) Tube 6: 11.40 mm (0.449 in.) above flap upper surface.

Figure 14.- Concluded.

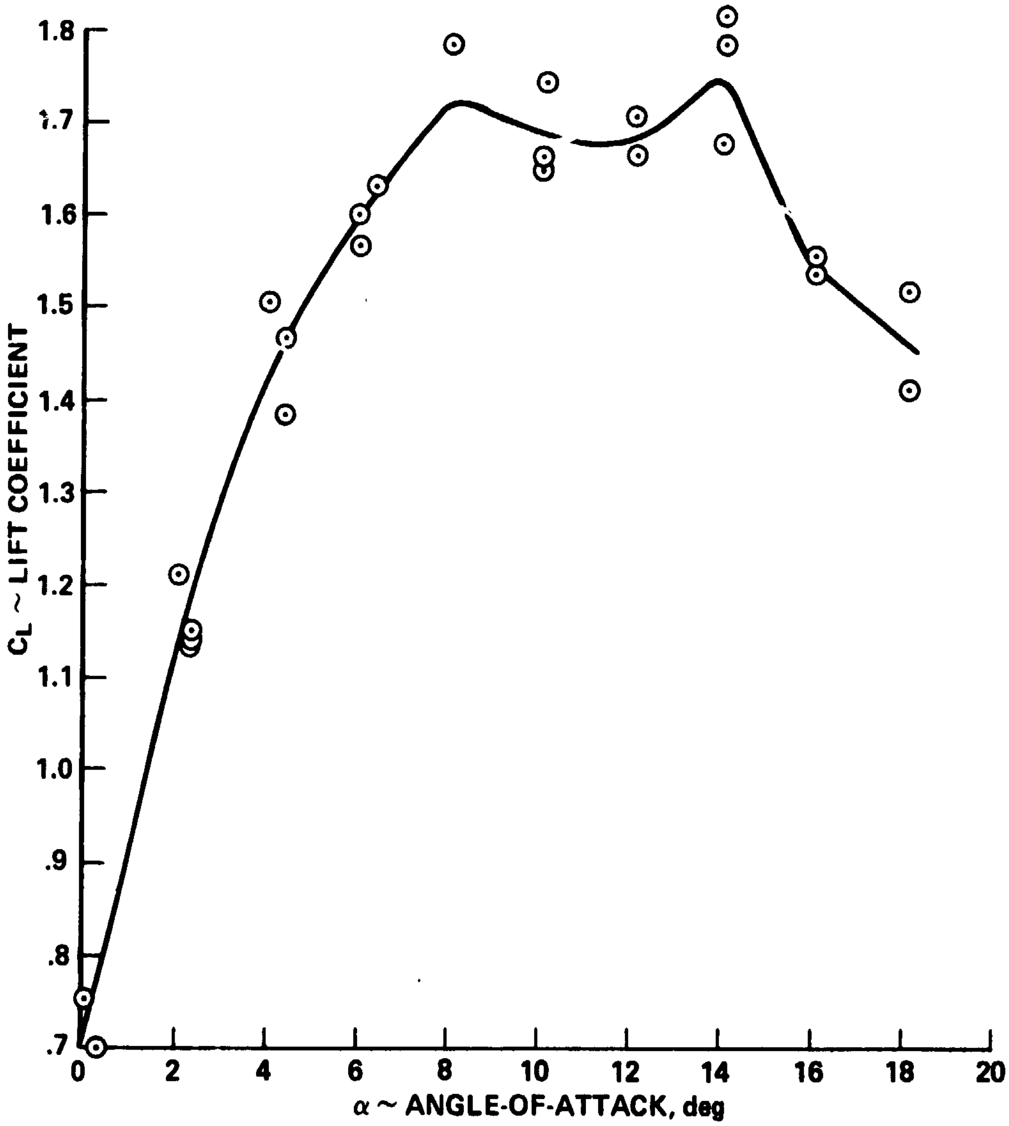

(a) $C_\mu = 0$

Figure 15.- Variation of lift with angle-of-attack for the straight-wing model with full-span leading-edge slats and full-span knee-blown flaps at various blowing rates.

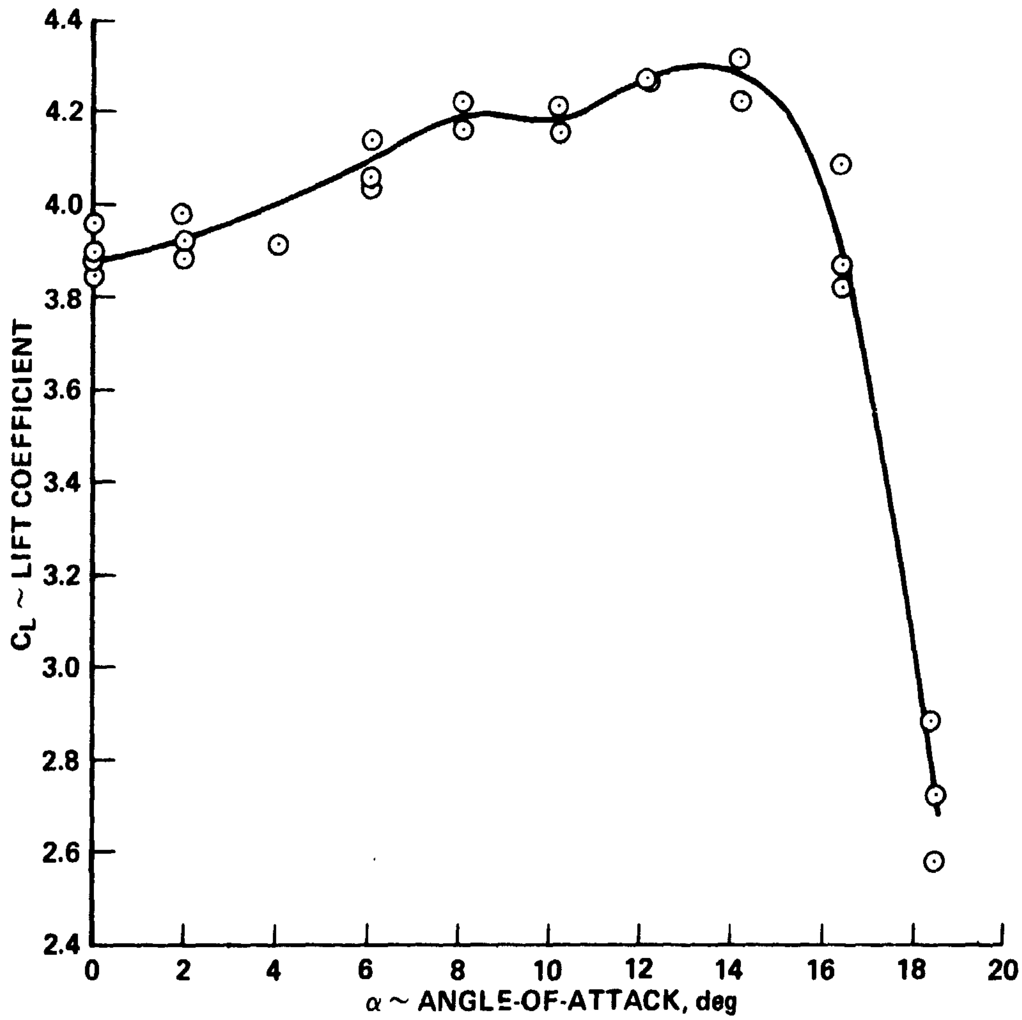

(b) C_μ = 0.4

Figure 15.- Continued.

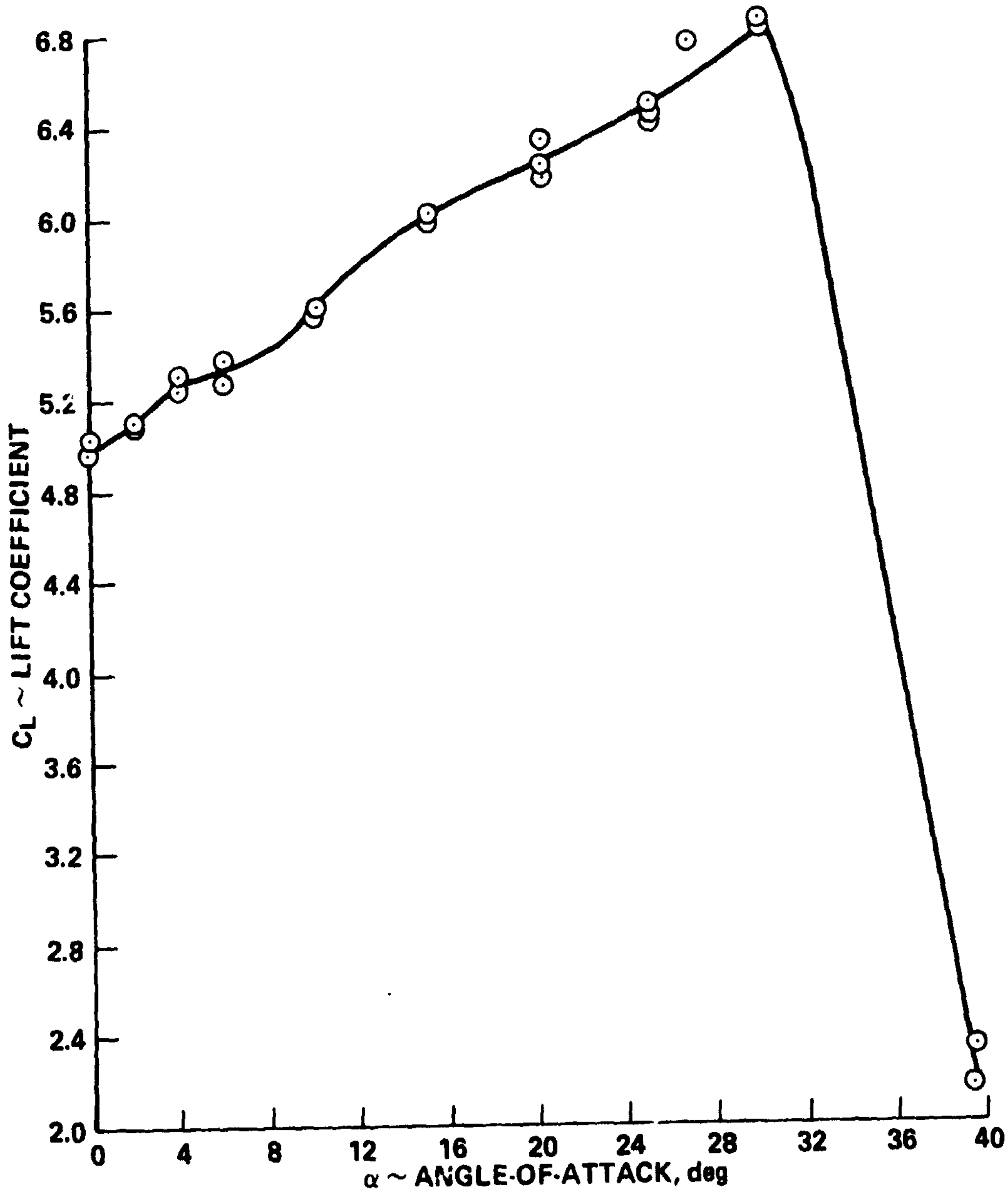

(c) $C_\mu = 1.0$

Figure 15.- Continued.

ORIGINAL PAGE IS
OF POOR QUALITY

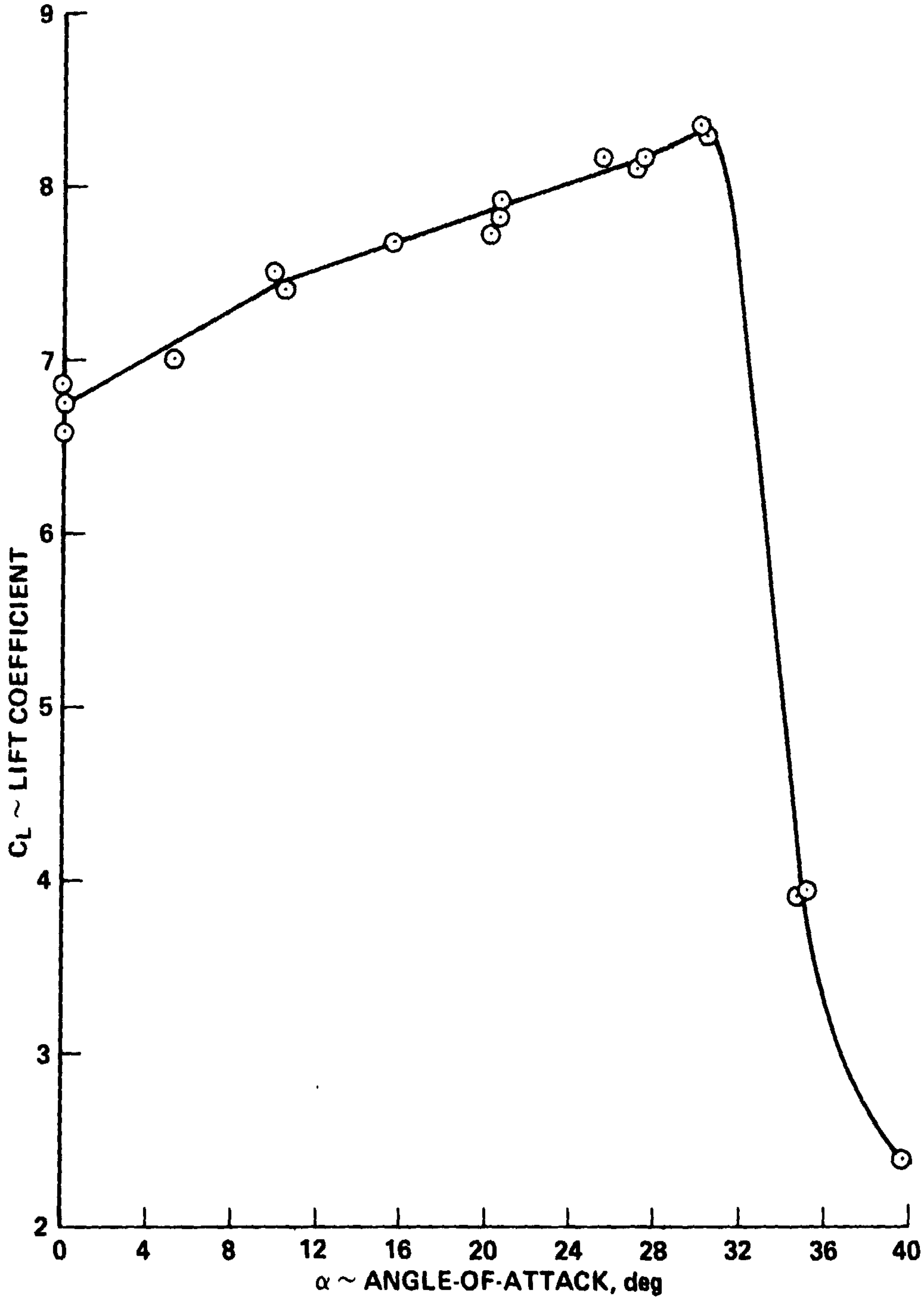

(d) $C_\mu = 2.0$

Figure 15.- Continued.

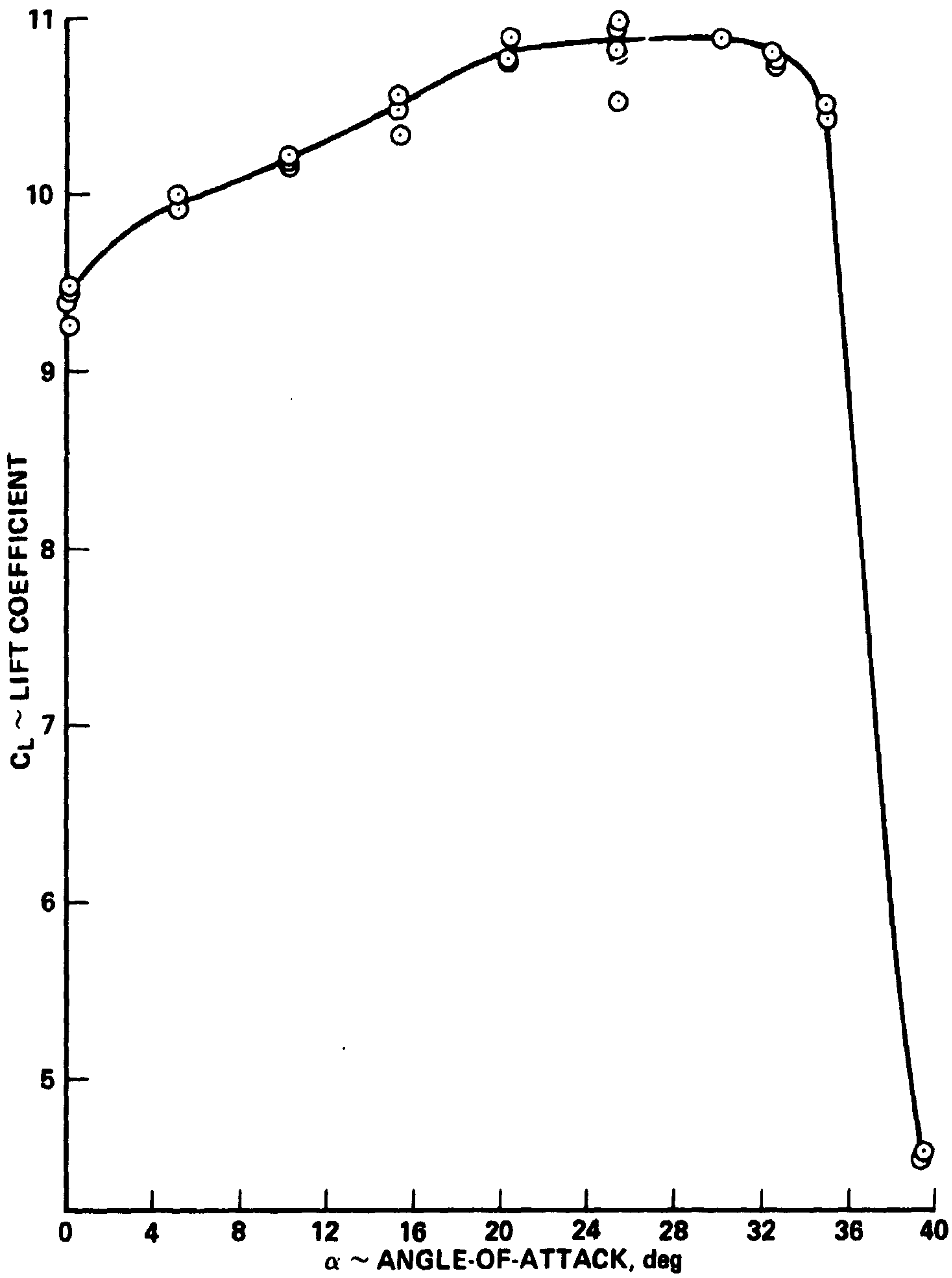

(e) C_μ = 4.0

Figure 15.- Continued.

ORIGINAL PAGE IS OF POOR QUALITY

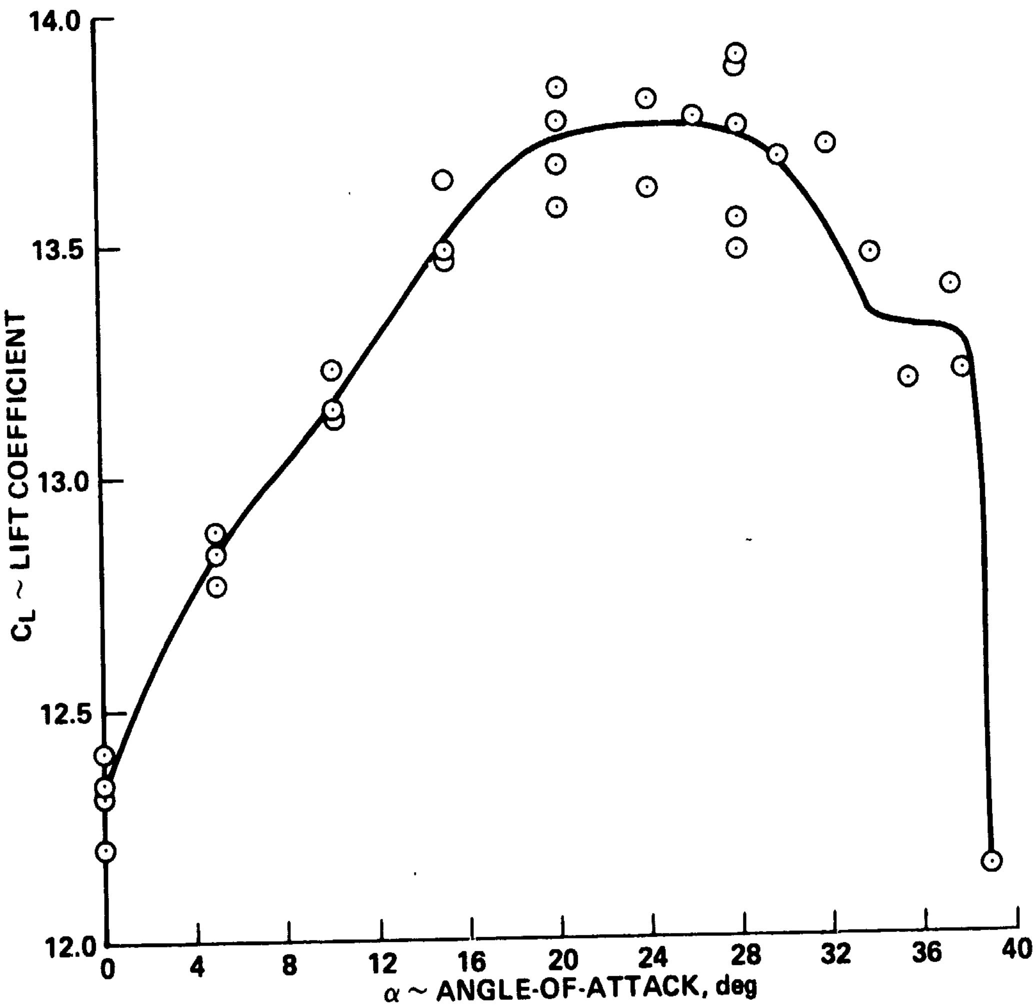

(f) C_μ = 6.0

Figure 15.- Continued.

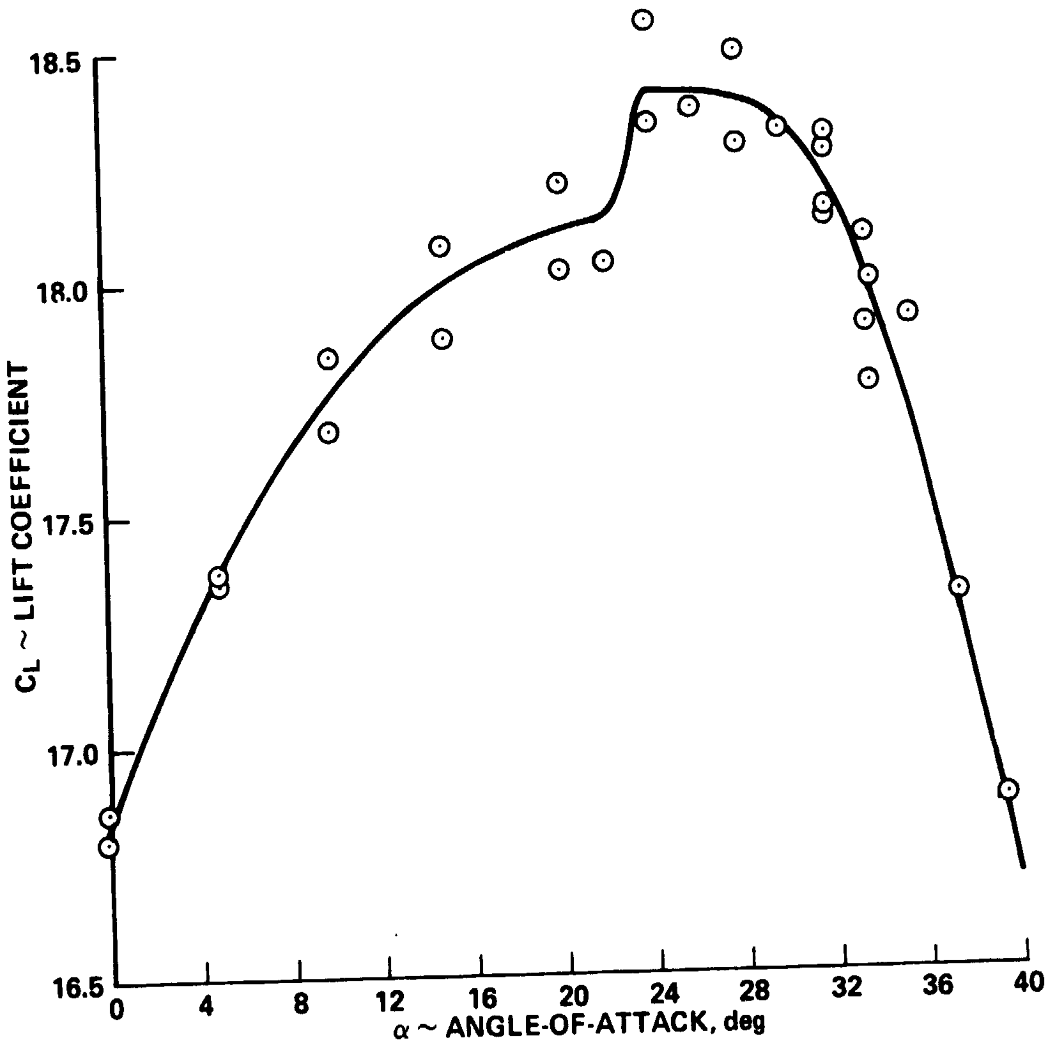

(g) C_μ = 10.0

Figure 15.- Concluded.

ORIGINAL PAGE IS
OF POOR QUALITY

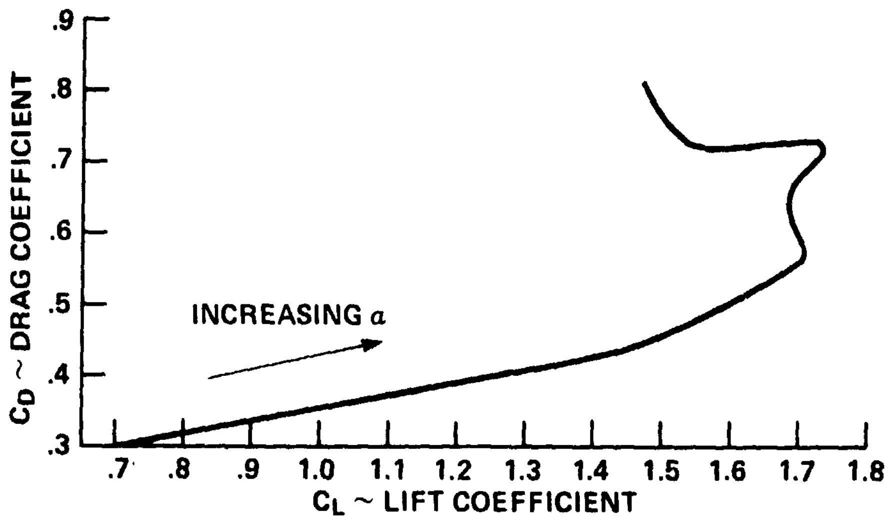

(a) $C_\mu = 0$

Figure 16.- Variation of drag with lift for the straight-wing model with full-span leading-edge slats and full-span knee-blown flaps at various blowing rates.

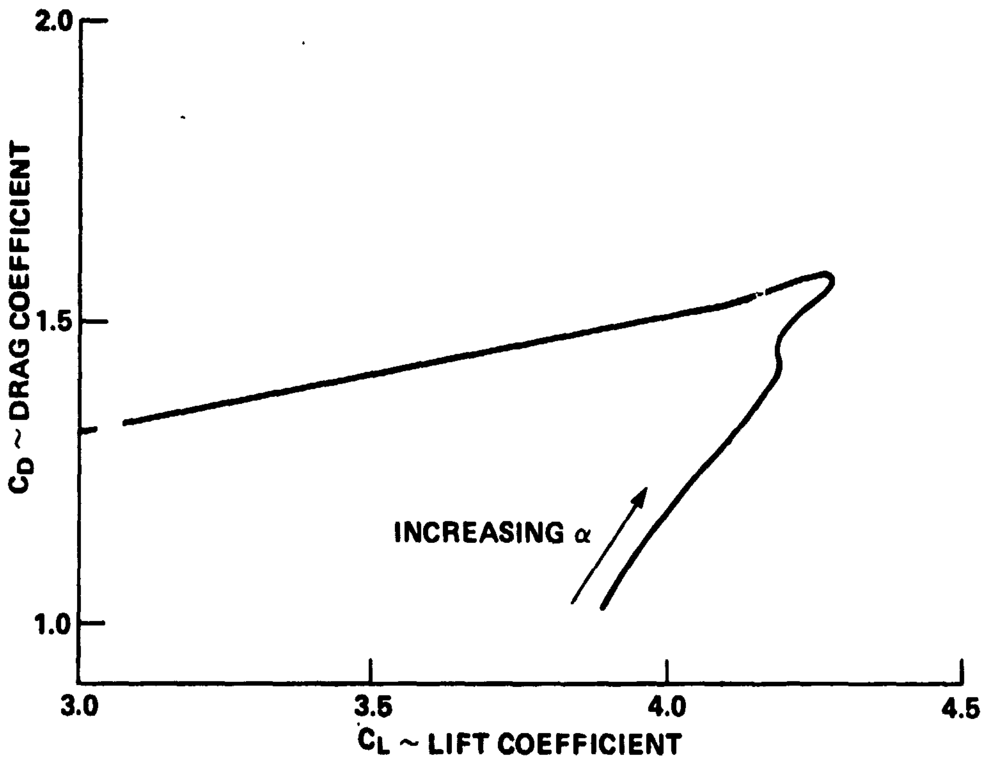

(b) C_μ = 0.4

Figure 16.- Continued.

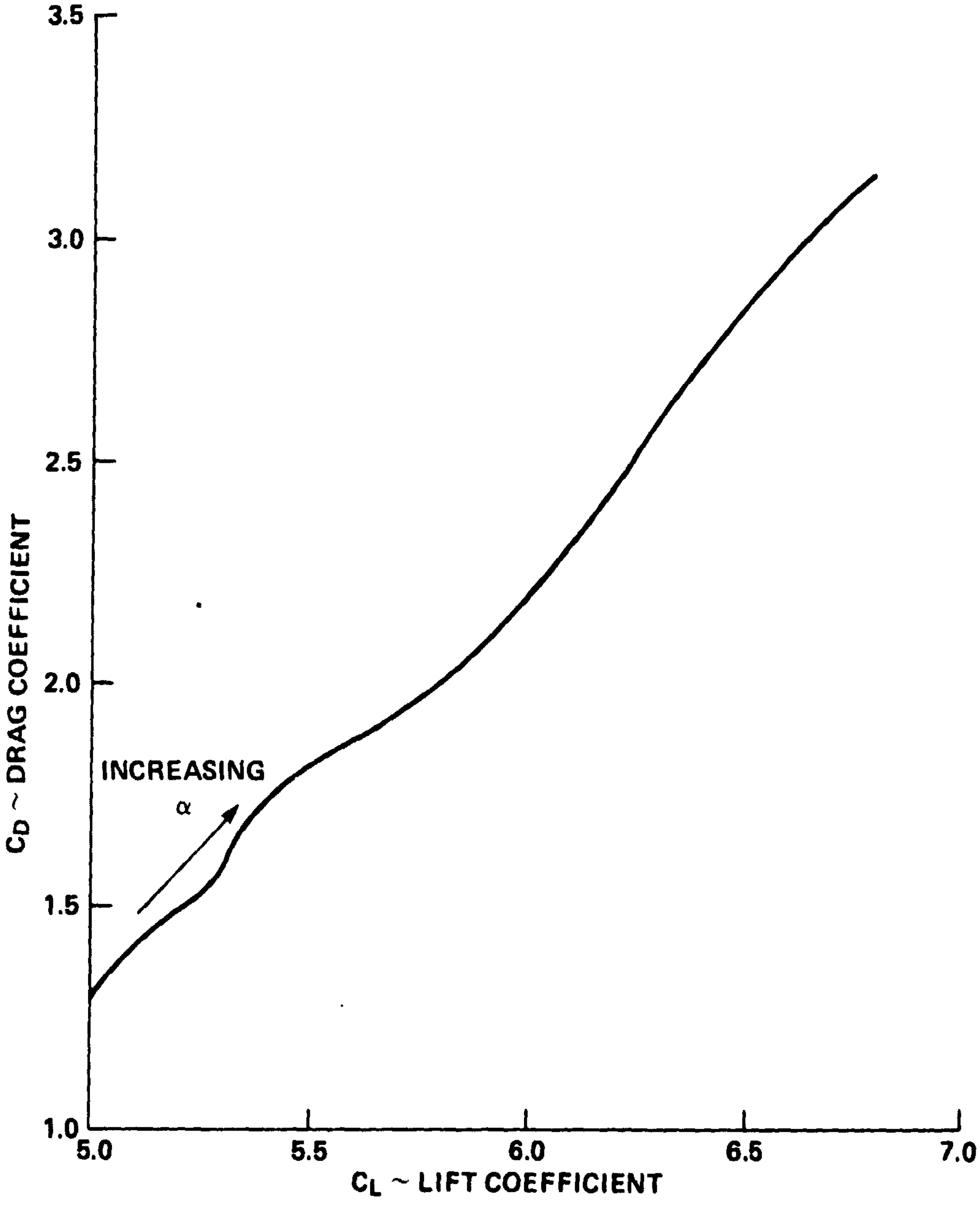

(c) $C_\mu = 1.0$

Figure 16.- Continued.

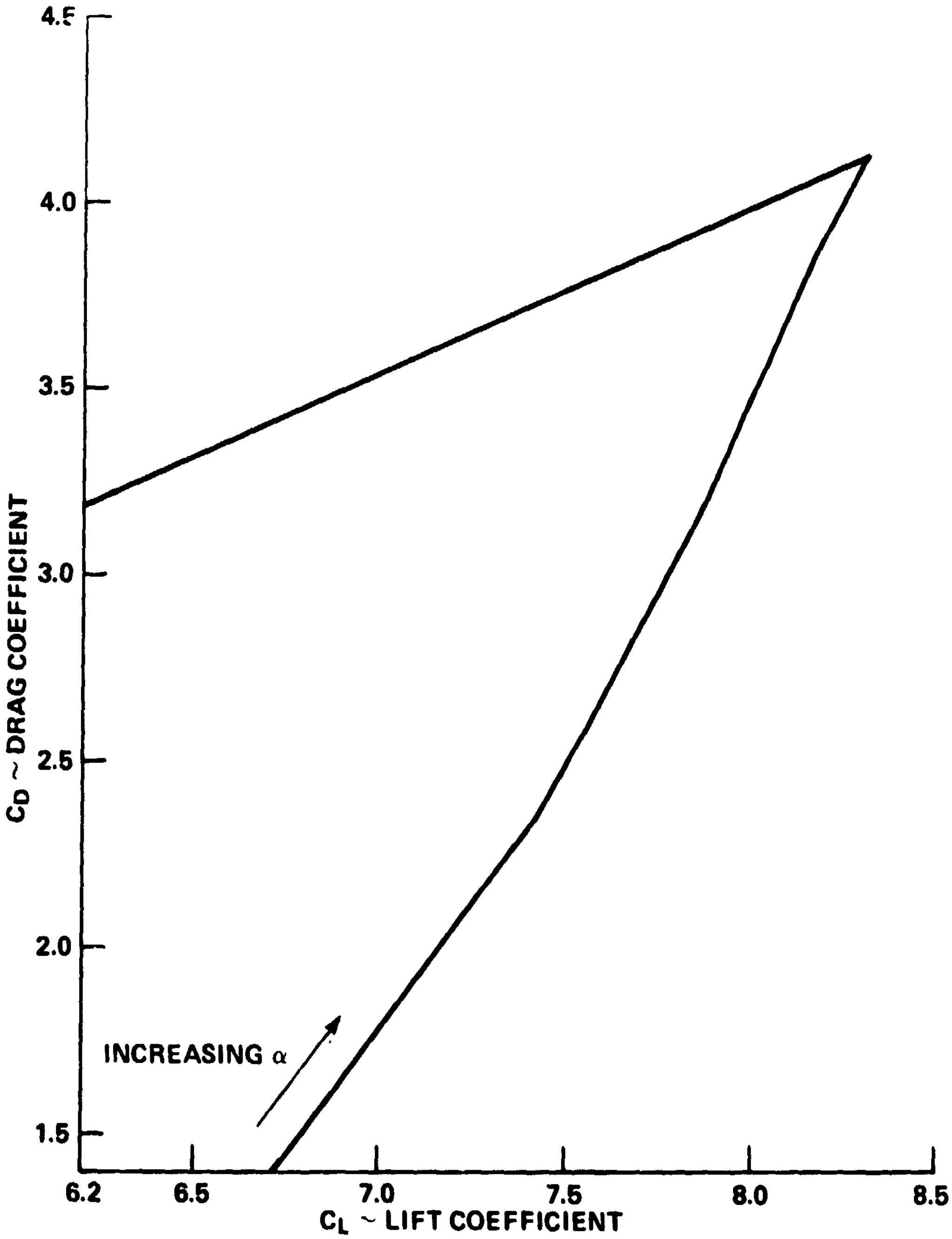

(d) C_μ = 2.0

Figure 16.- Continued.

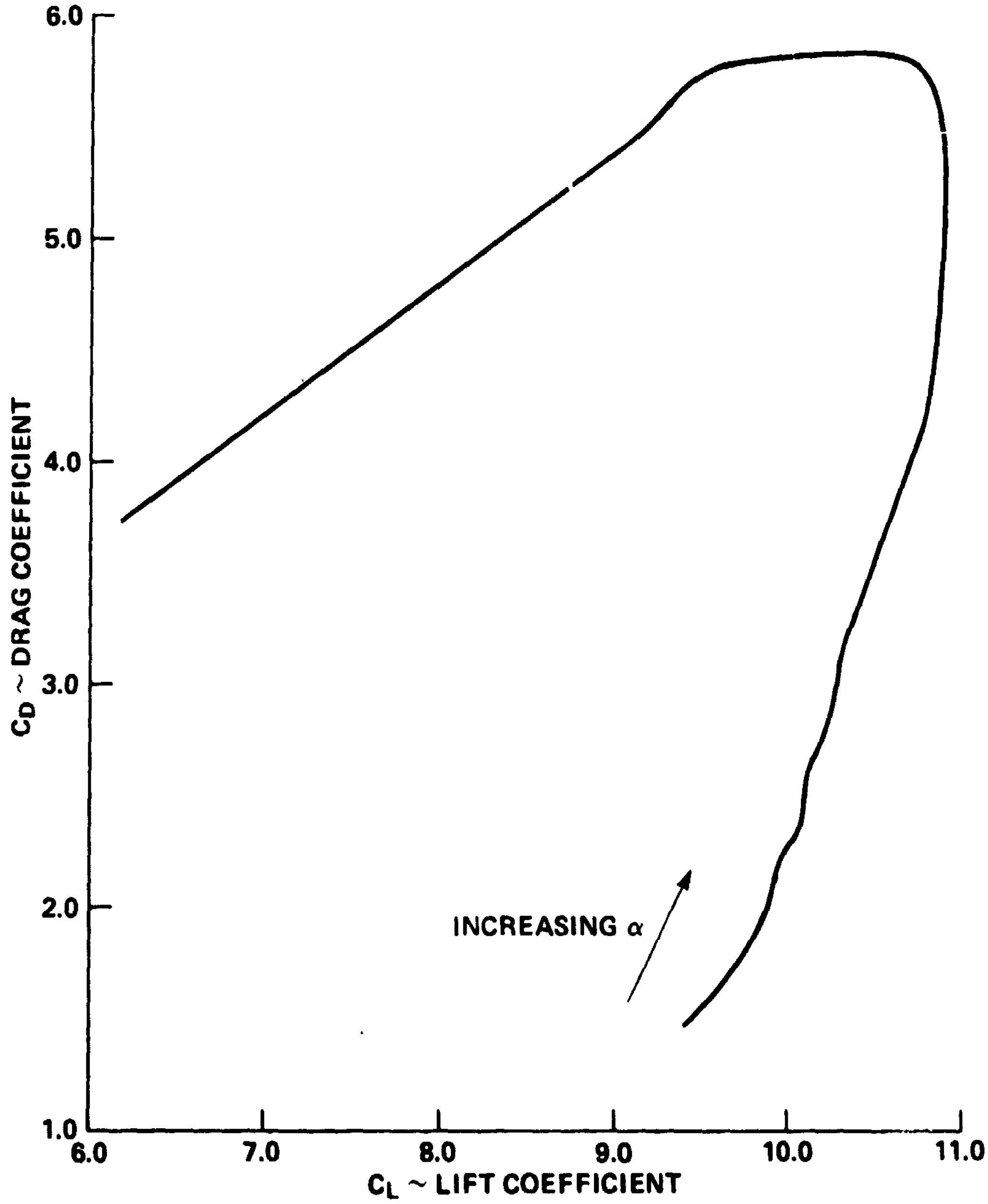

(e) C_μ = 4.0

Figure 16.- Continued.

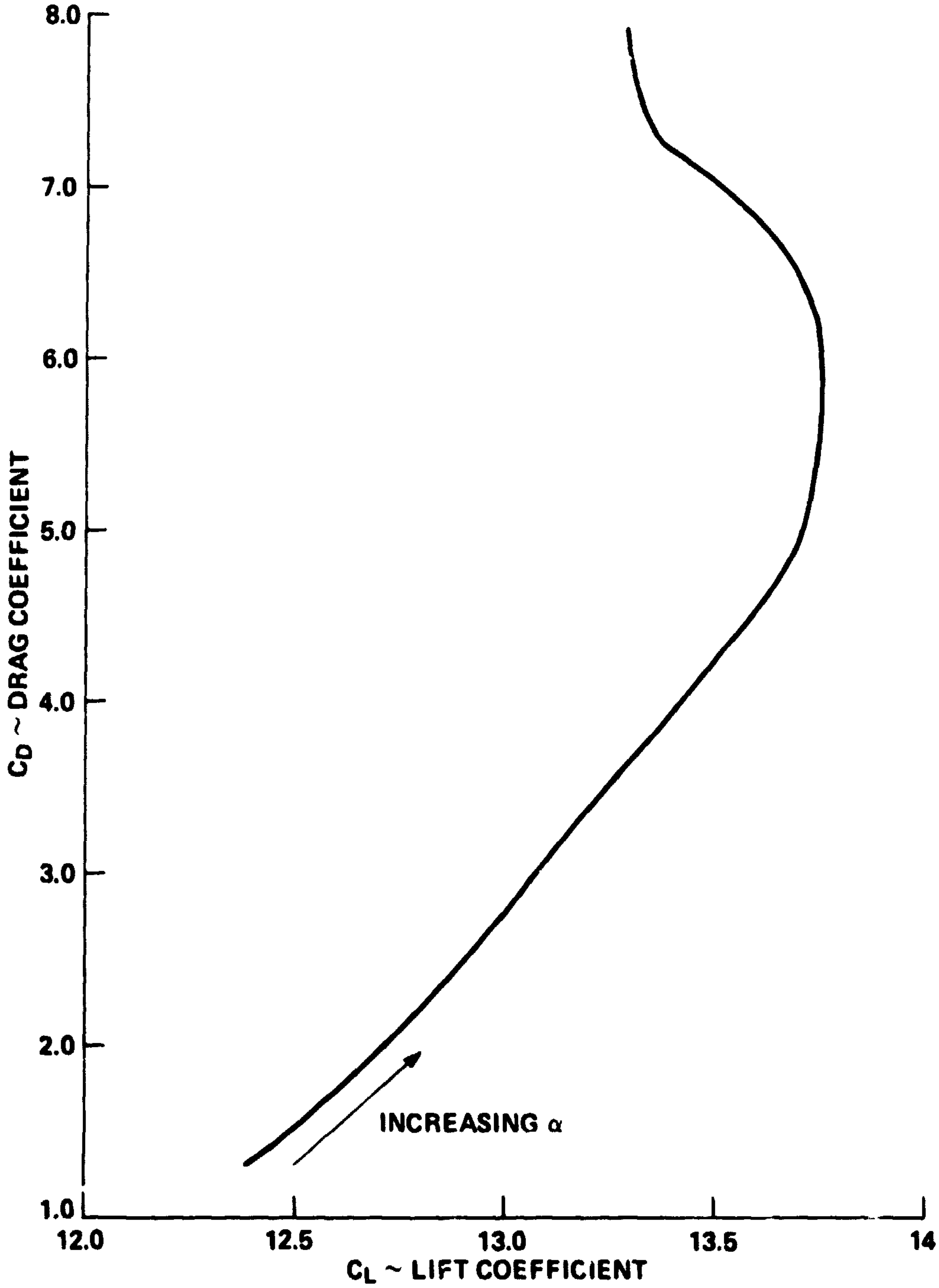

(f) $C_\mu = 6.0$

Figure 16.- Continued.

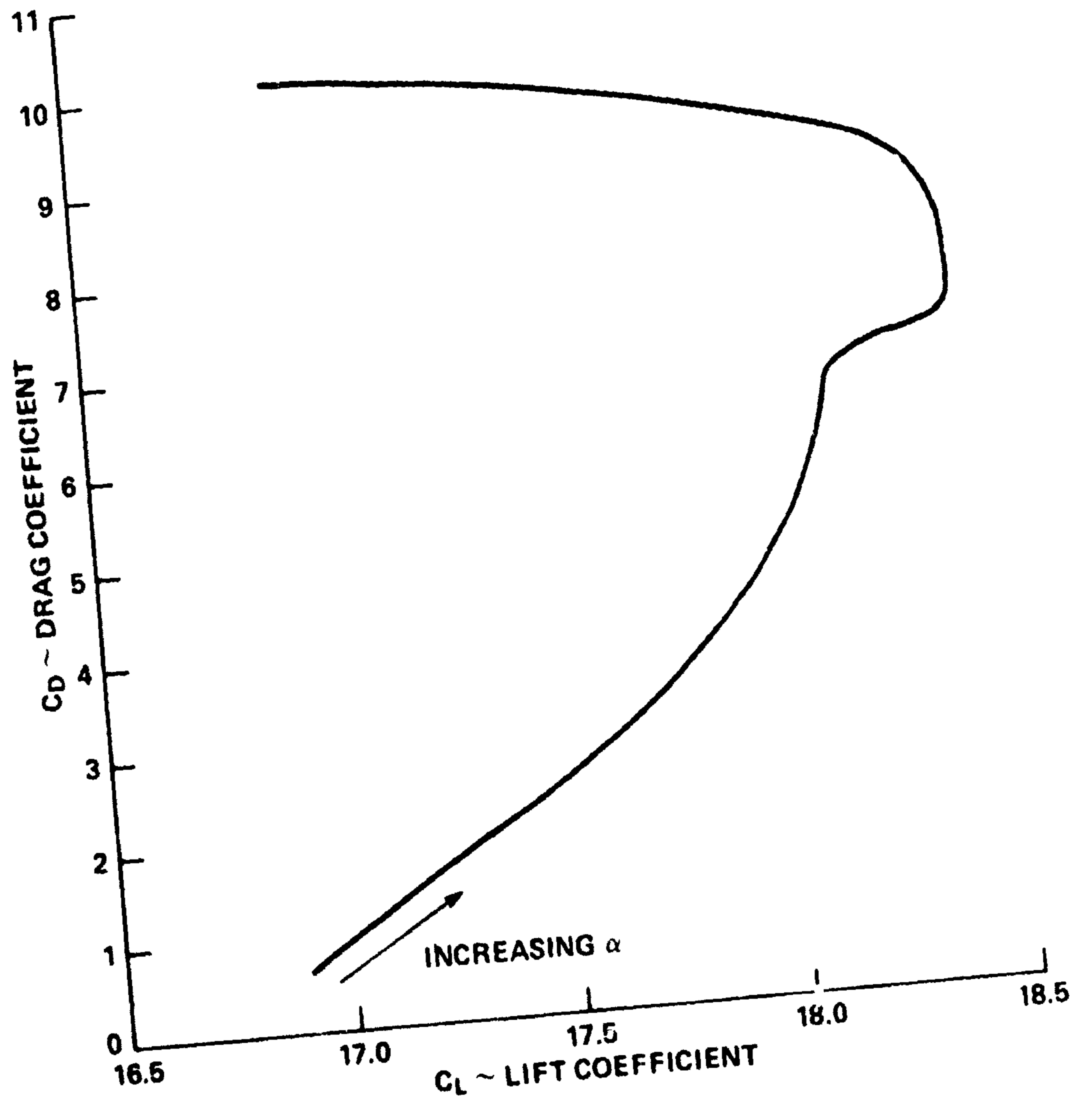

(g) C_μ = 10.0

Figure 16.- Concluded.

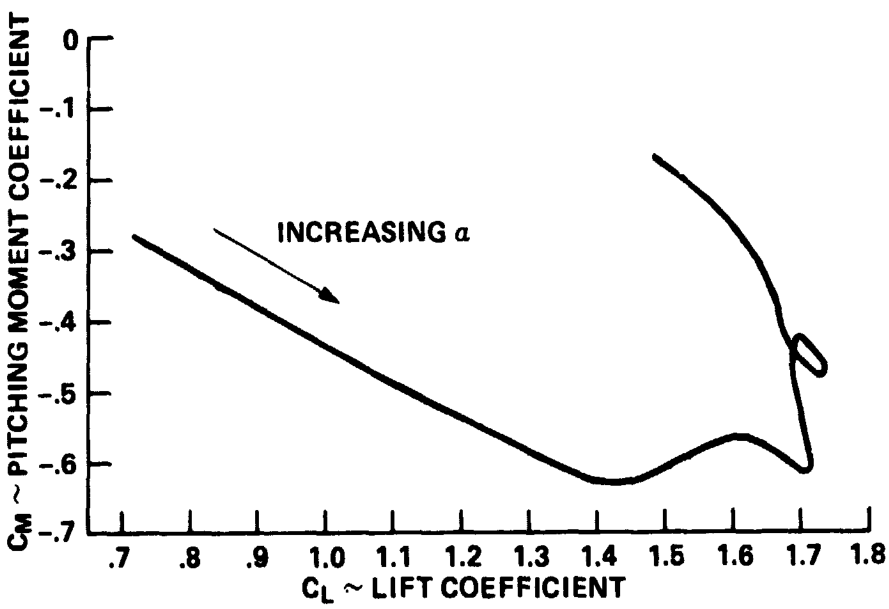

(a) $C_\mu = 0$

Figure 17.- Variation of pitching moment with lift for the straight-wing model with full-span leading-edge slats and full-span knee-blown flaps at various blowing rates.

ORIGINAL PAGE IS
OF POOR QUALITY

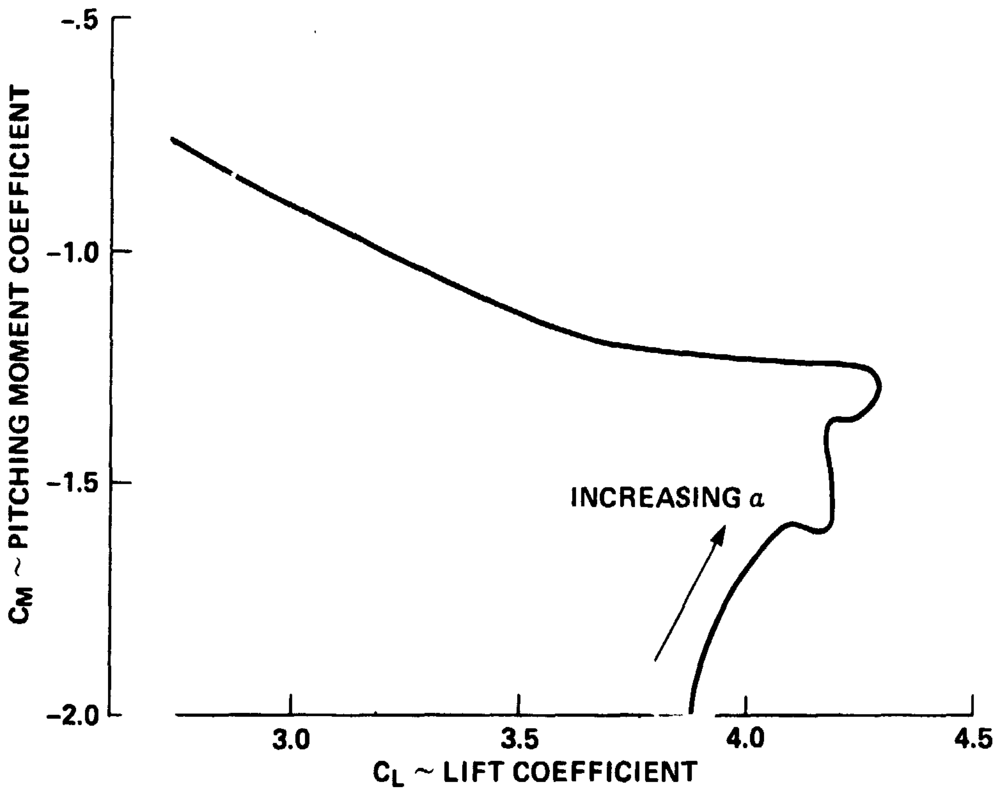

(b) C_μ = 0.4

Figure 17.- Continued.

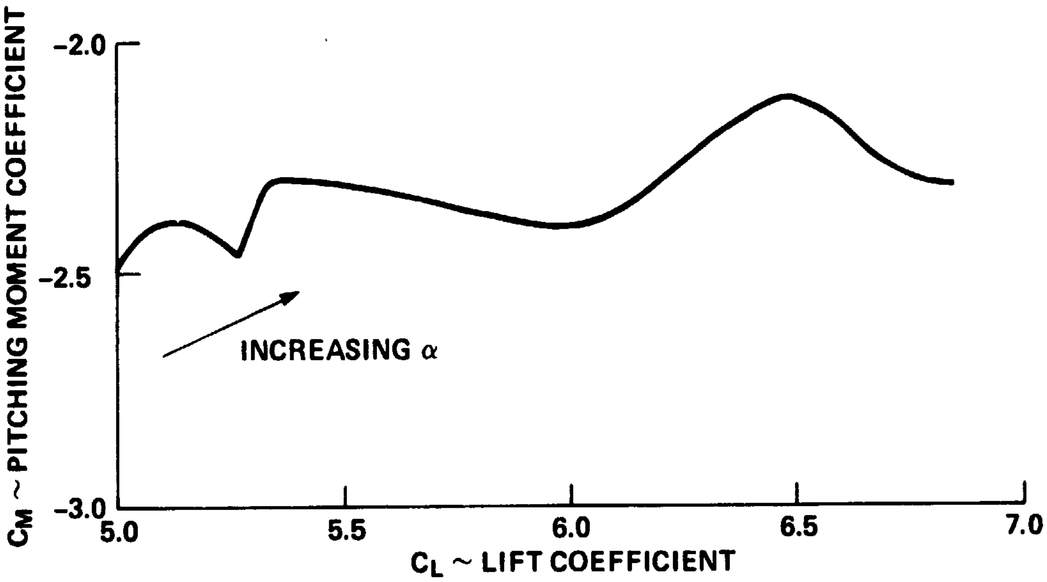

(c) $C_\mu = 1.0$

Figure 17.- Continued.

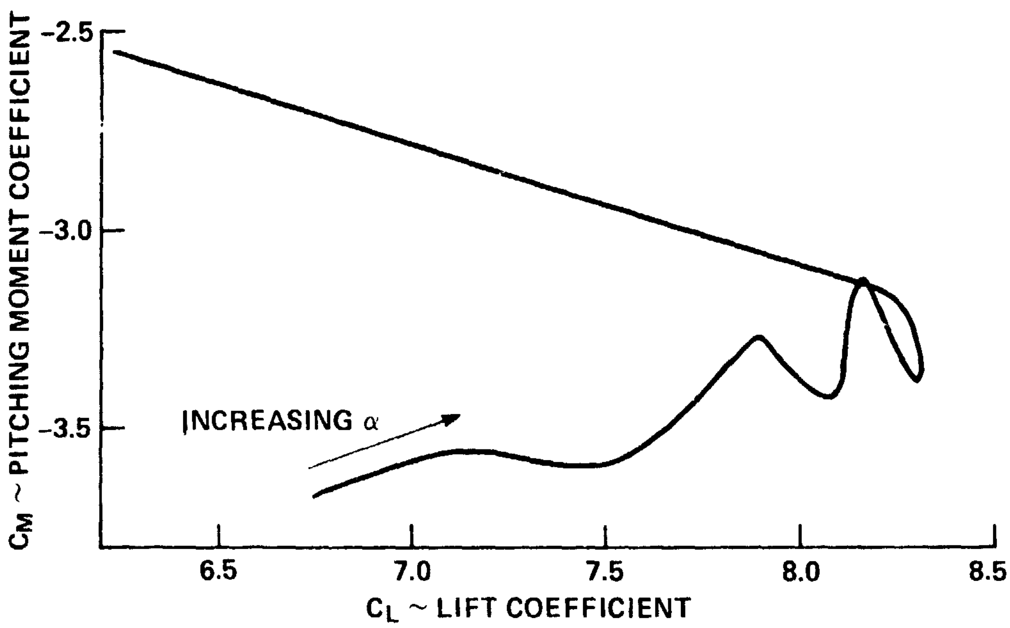

(d) $C_\mu = 2.0$

Figure 17.- Continued.

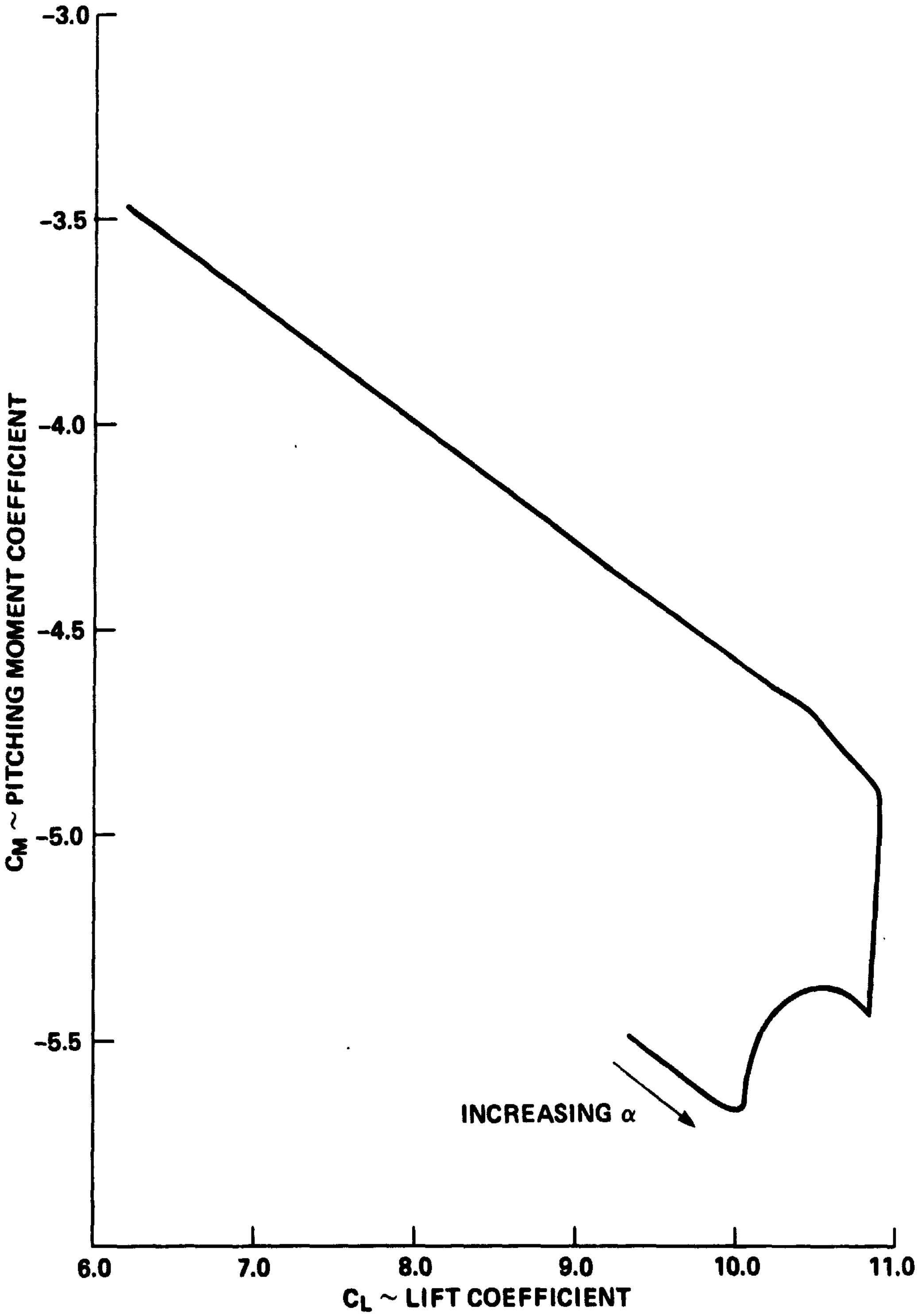

(e) $C_\mu = 4.0$

Figure 17.- Continued.

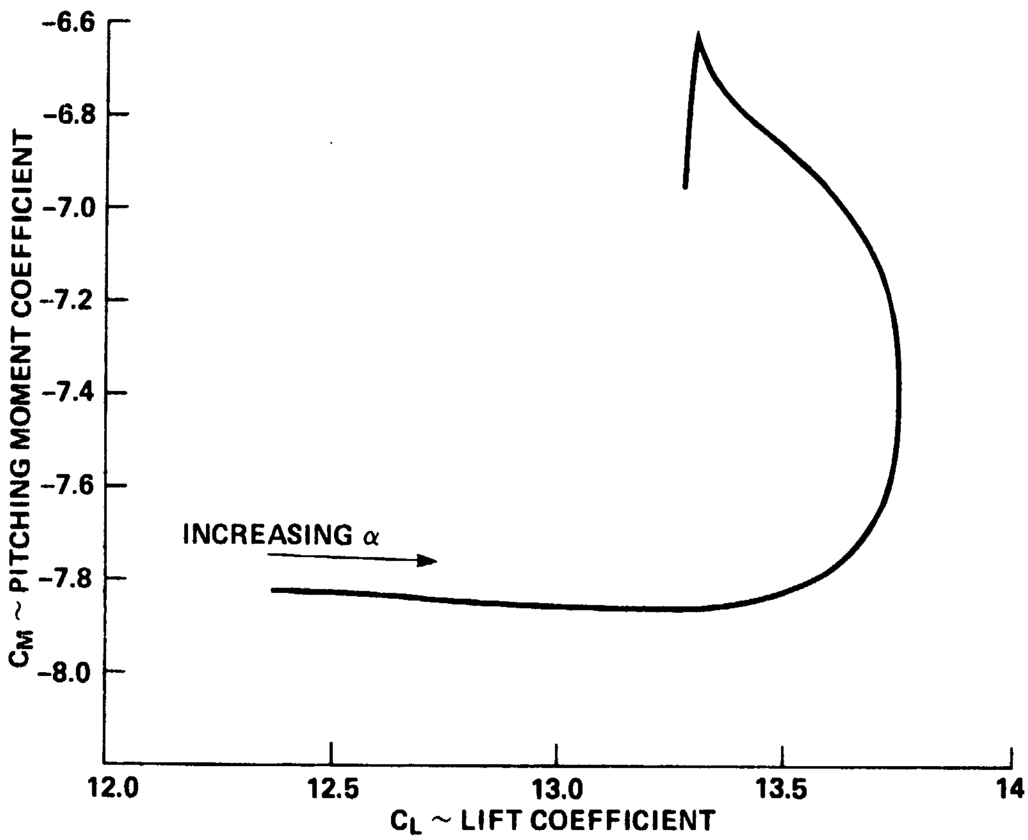

(f) $C_\mu = 6.0$

Figure 17.- Continued.

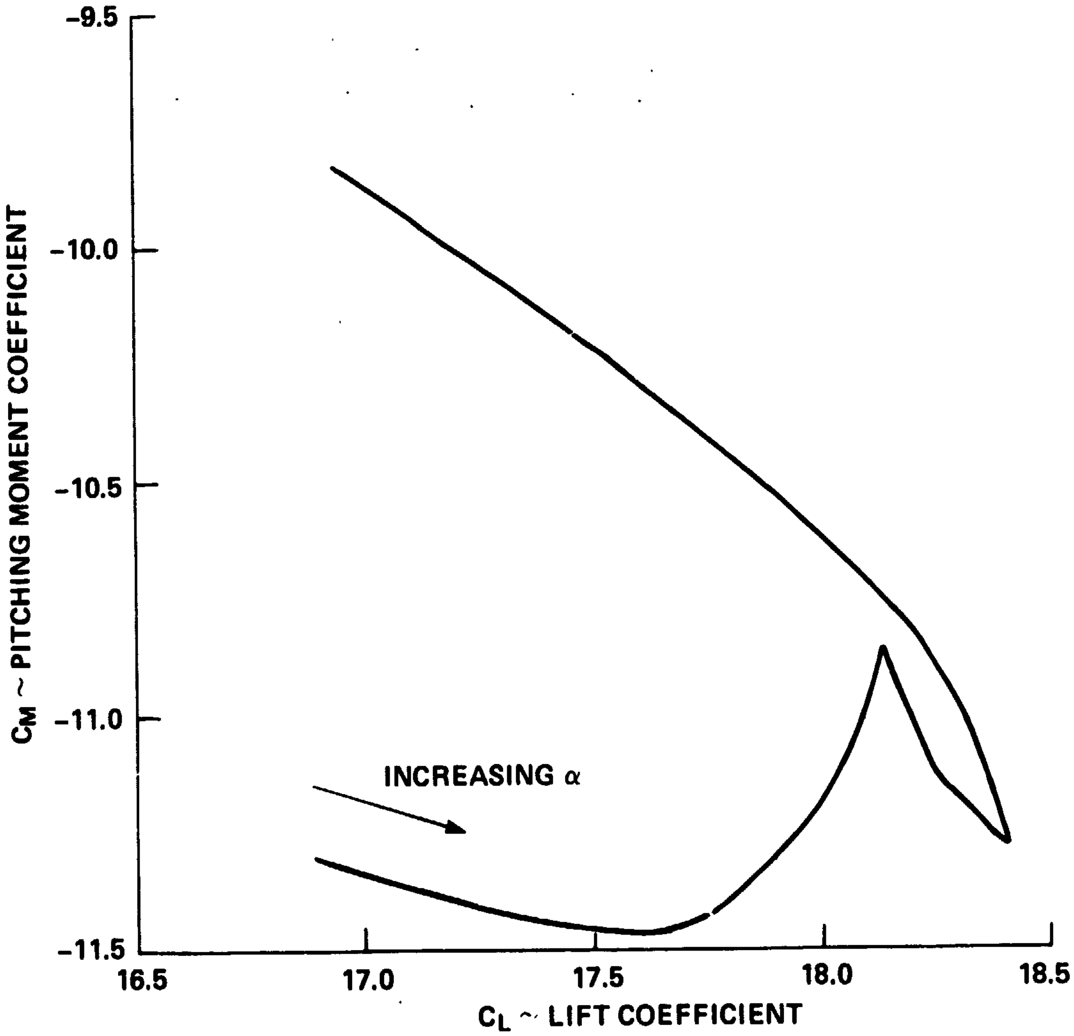

(g) $C_\mu = 10.0$

Figure 17.- Concluded.

ORIGINAL PAGE IS
OF POOR QUALITY

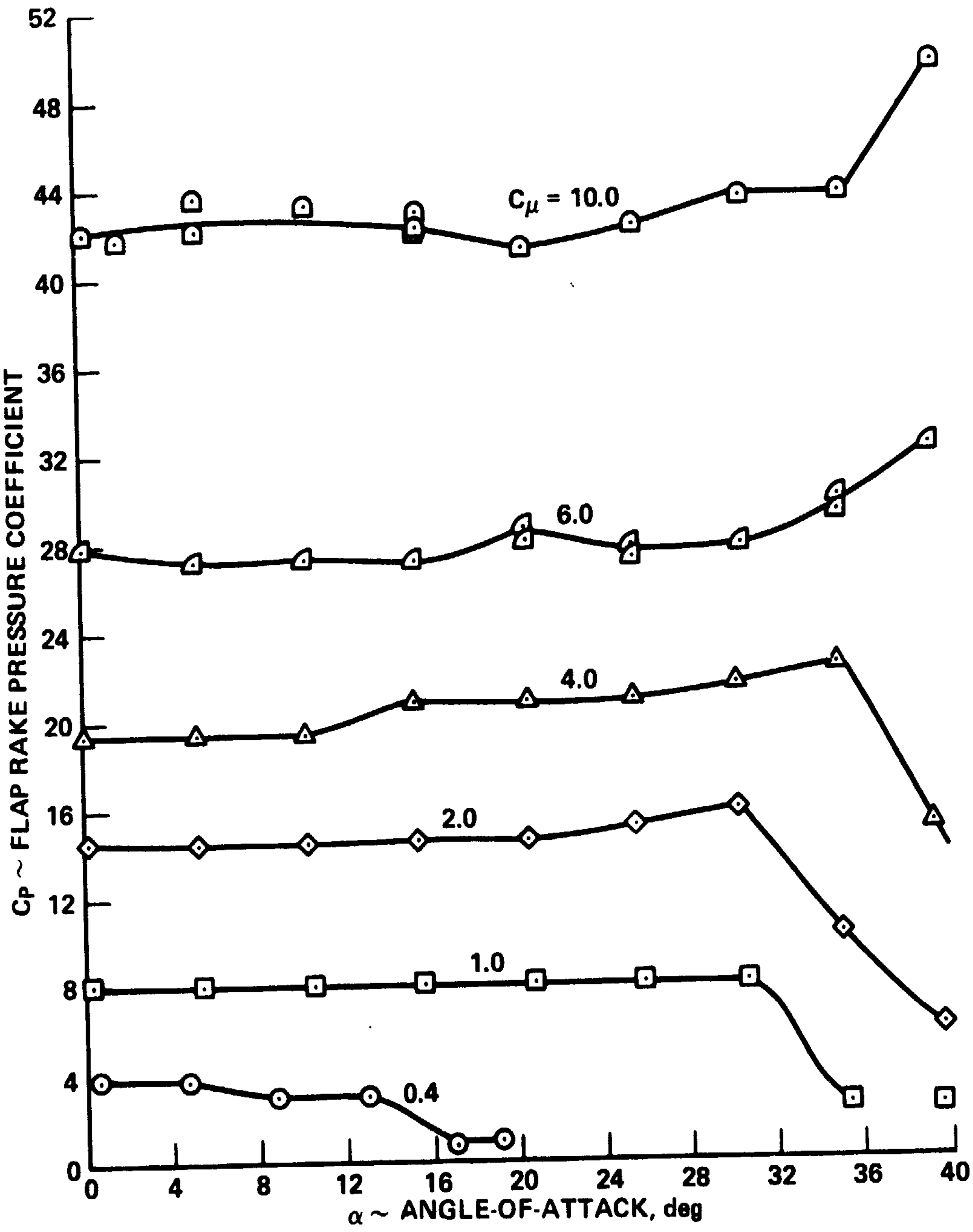

(a) Tube 1: 0.46 mm (0.018 in.) above flap upper surface.

Figure 18.- Variation of flap rake pressure coefficients with angle-of-attack for the straight-wing model with full-span leading-edge slats and full-span knee-blown flaps at various blowing rates.

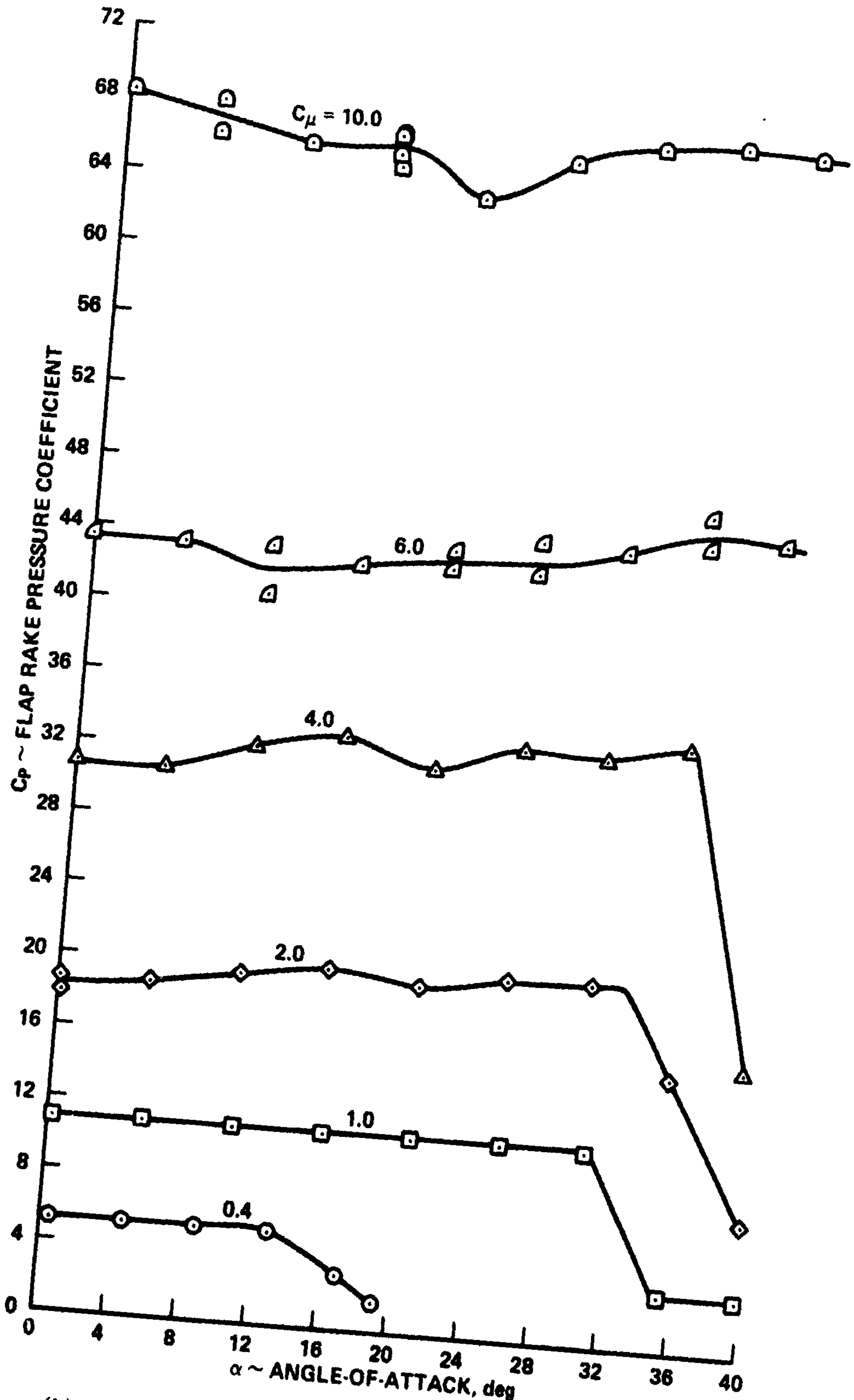

(b) Tube 2: 2.36 mm (0.093 in.) above flap upper surface.

Figure 18.- Continued.

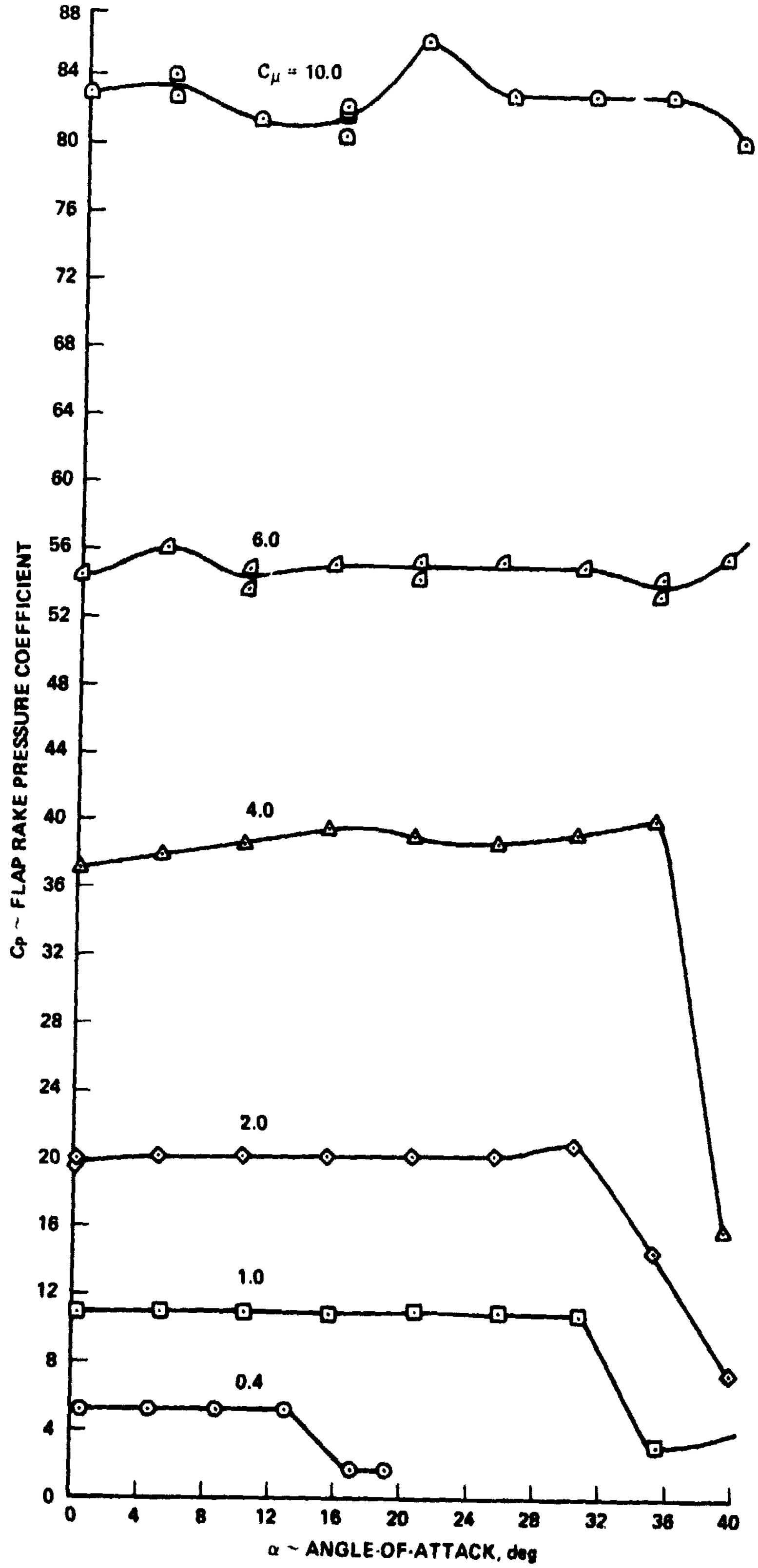

(c) Tube 3: 3.43 mm (0.135 in.) above flap upper surface

Figure 18.- Continued.

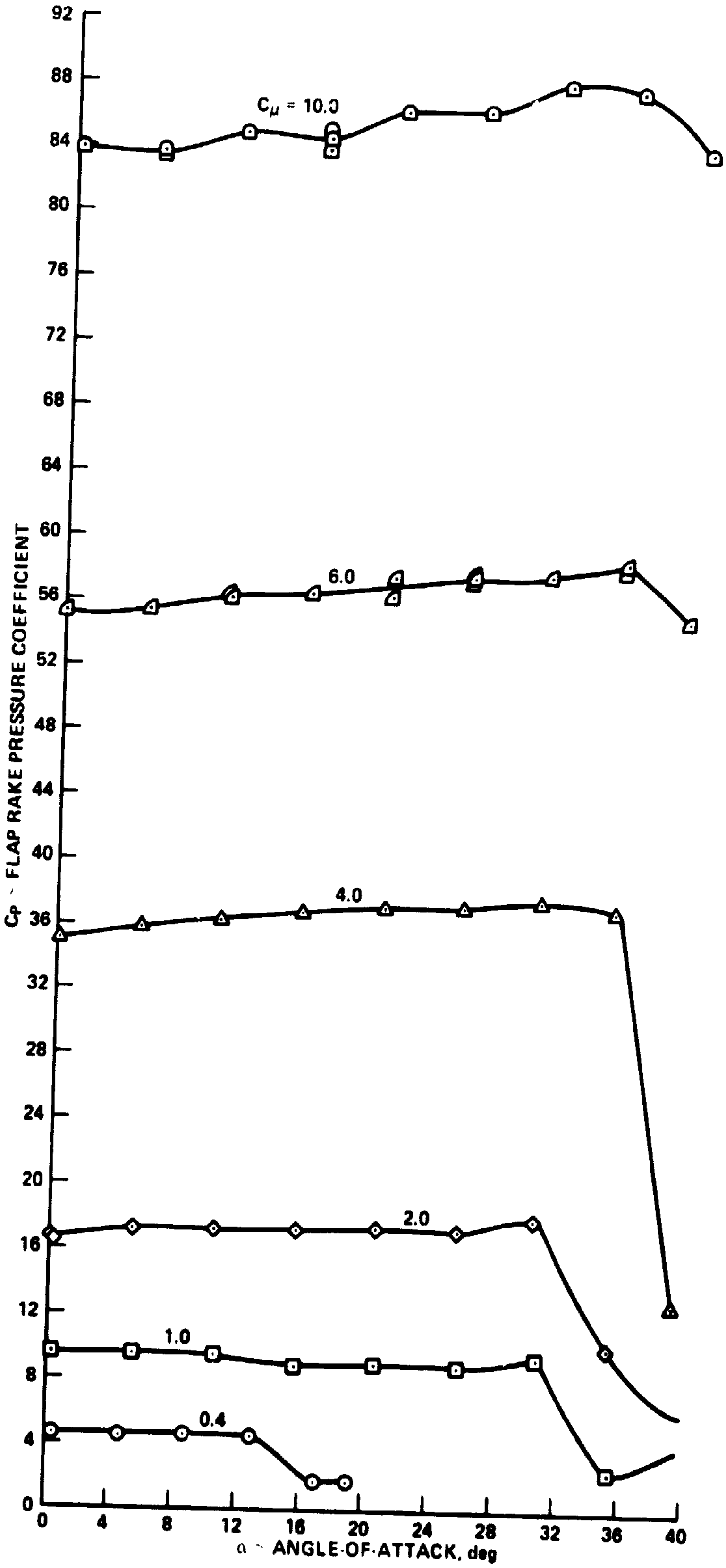

Tube ... .75 mm (0.187 in.) above flap upper surface.

Figure 18.- Continued.

ORIGINAL PAGE IS
OF POOR QUALITY

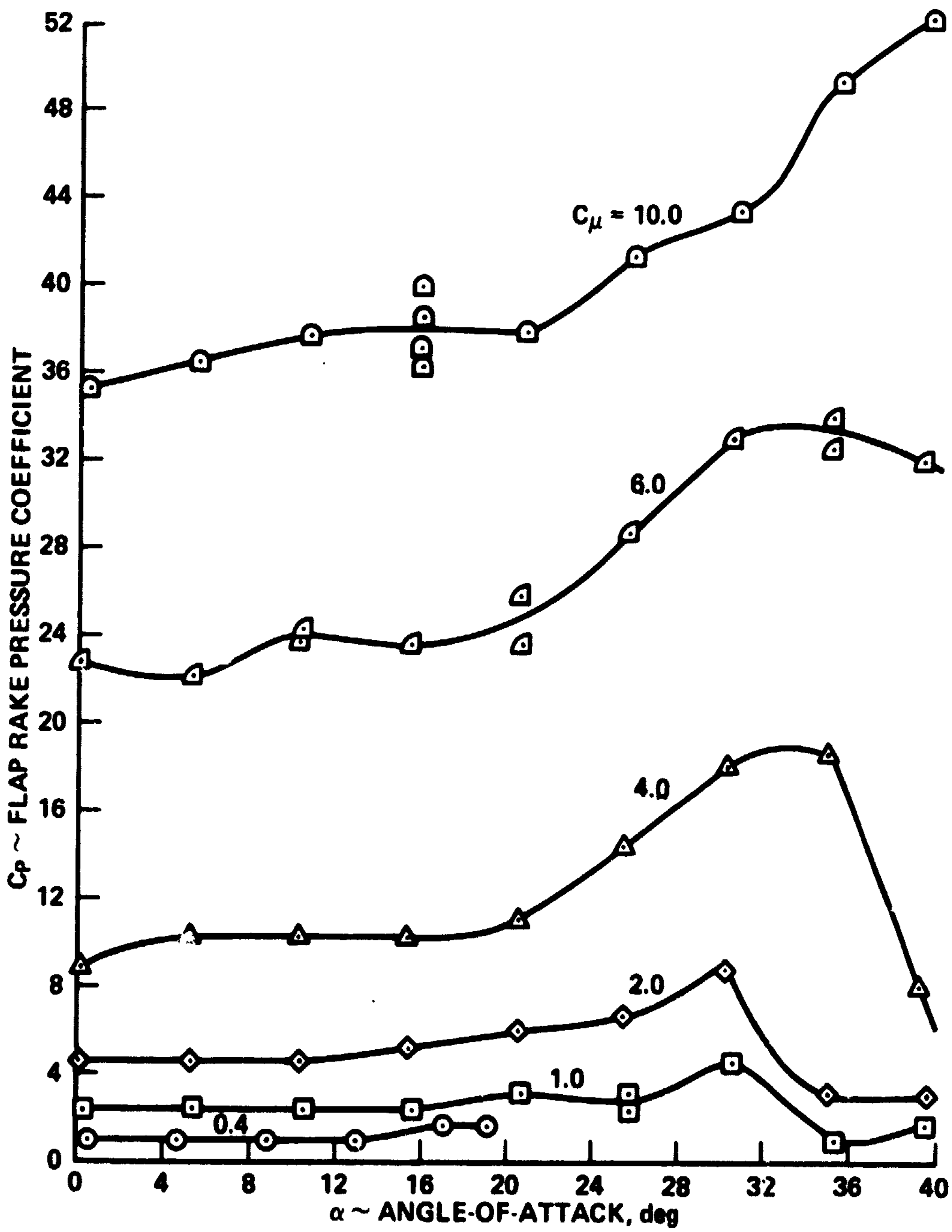

(e) Tube 5: 8.18 mm (0.322 in.) above flap upper surface.

Figure 18.- Continued.

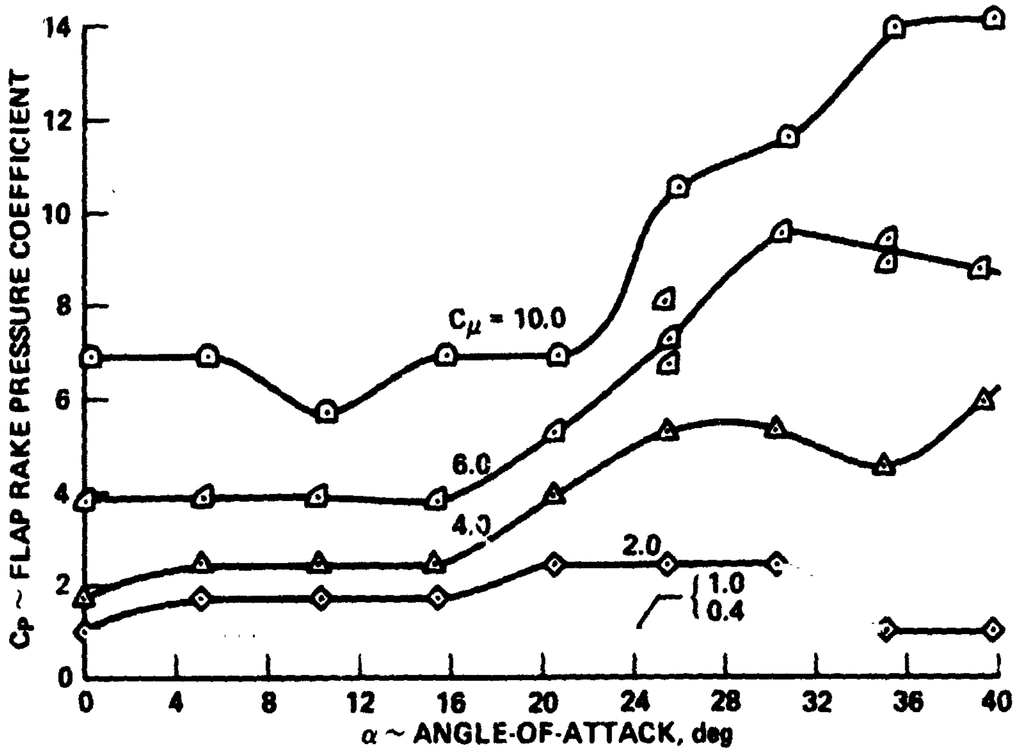

(i) Tube 6: 11.40 mm (0.449 in.) above flap upper surface

Figure 18.- Concluded.

ORIGINAL PAGE IS
OF POOR QUALITY

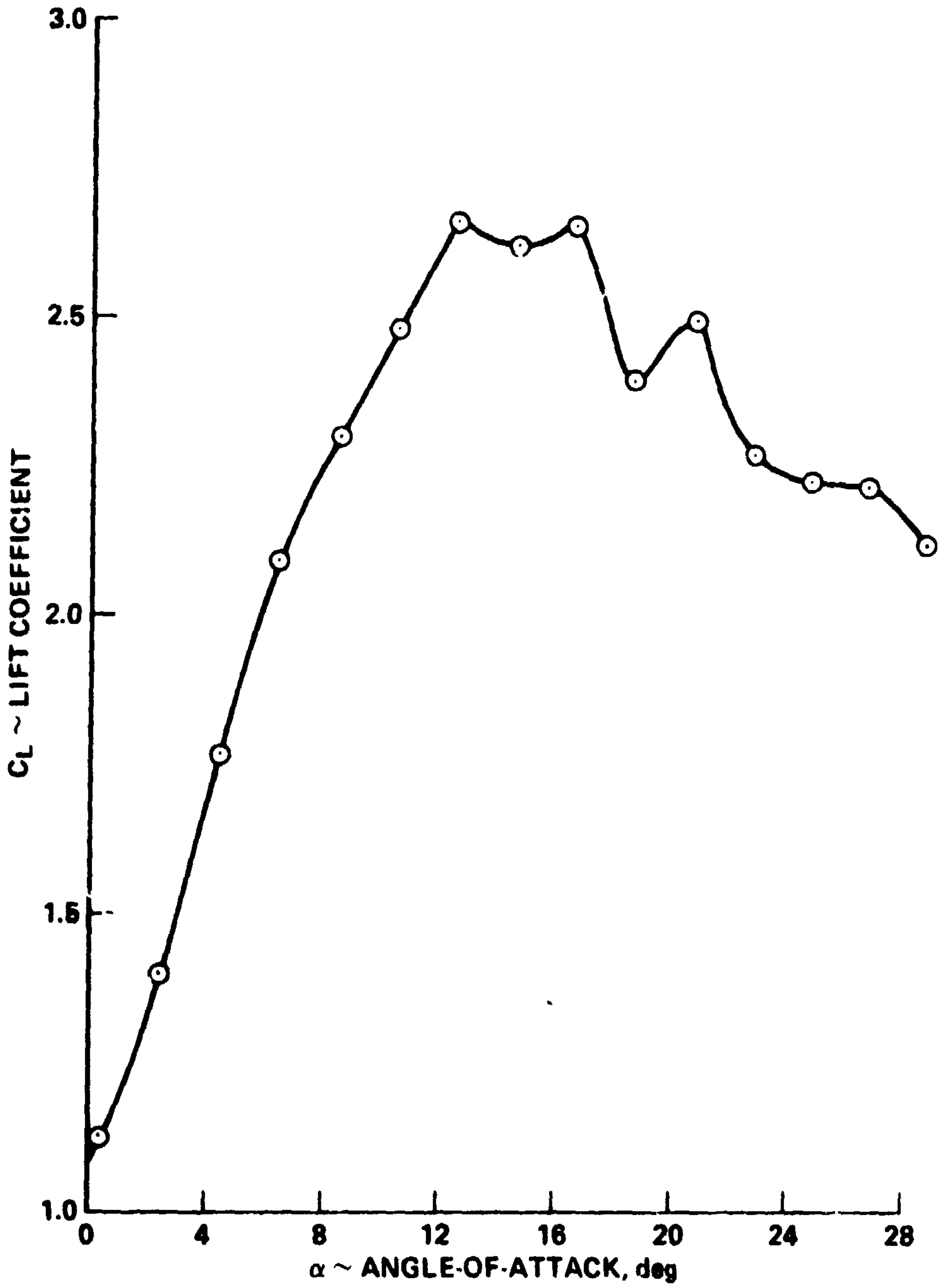

(a) $C_\mu = 0$

Figure 19.- Variation of lift with angle-of-attack fo. .he swept-wing model with full-span leading-edge slats and full-span knee-blown flaps at various blowing rates.

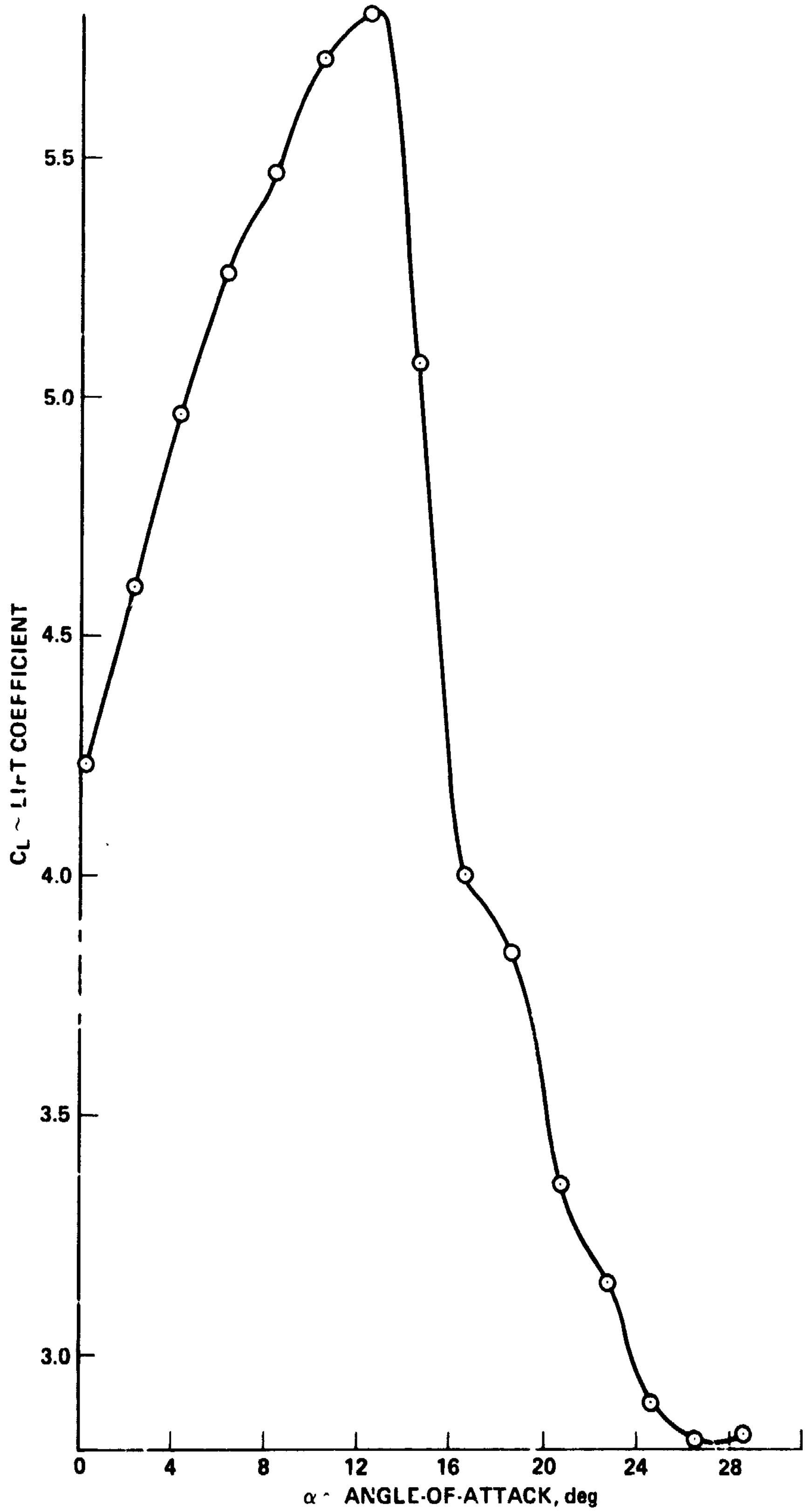

(b) C_μ = 0.4

Figure 19.- Continued.

(c) $C_\mu = 1.0$

Figure 19.- Continued.

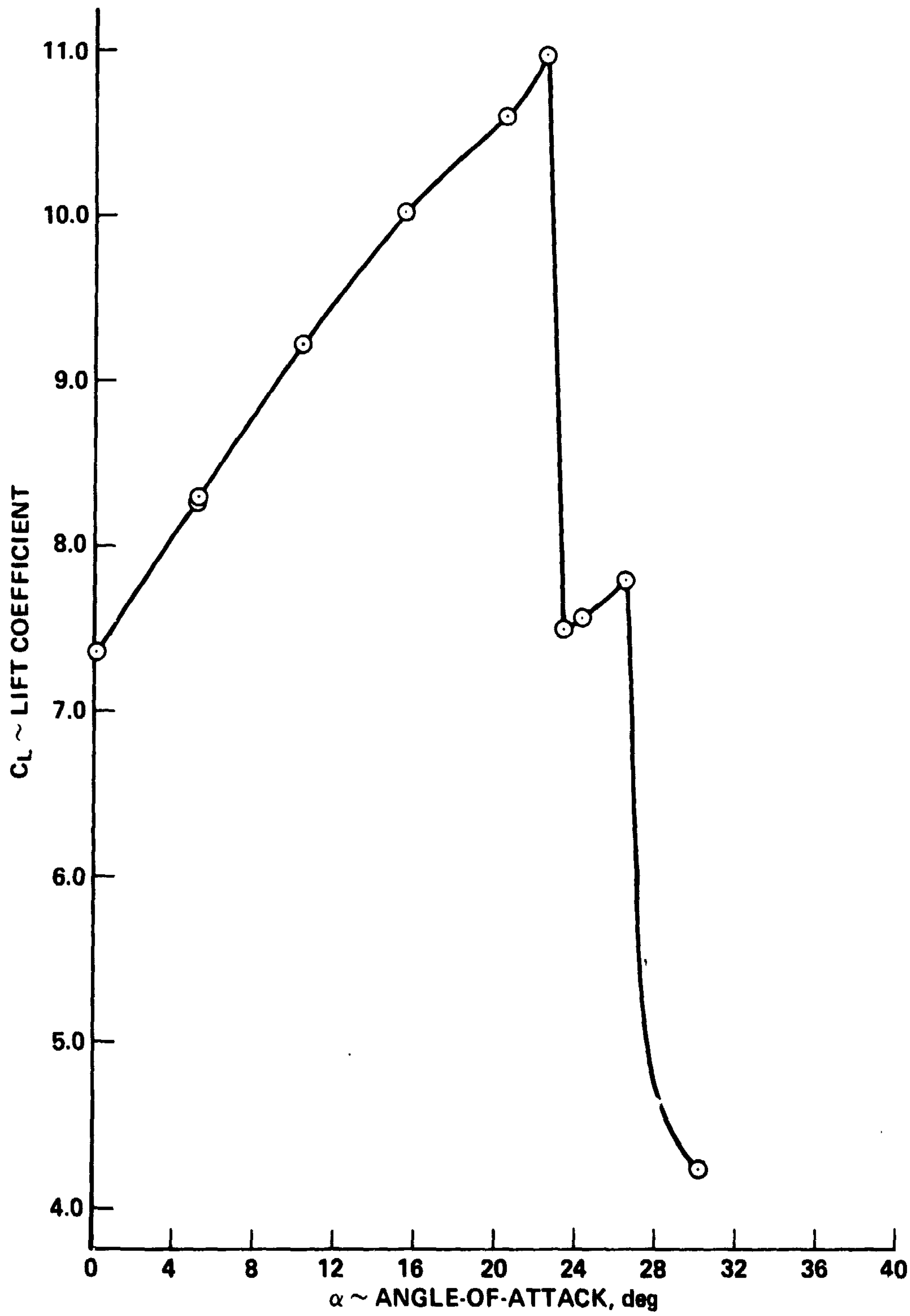

(d) $C_\mu = 2.0$

ORIGINAL PAGE IS
OF POOR QUALITY

Figure 19.- Continued.

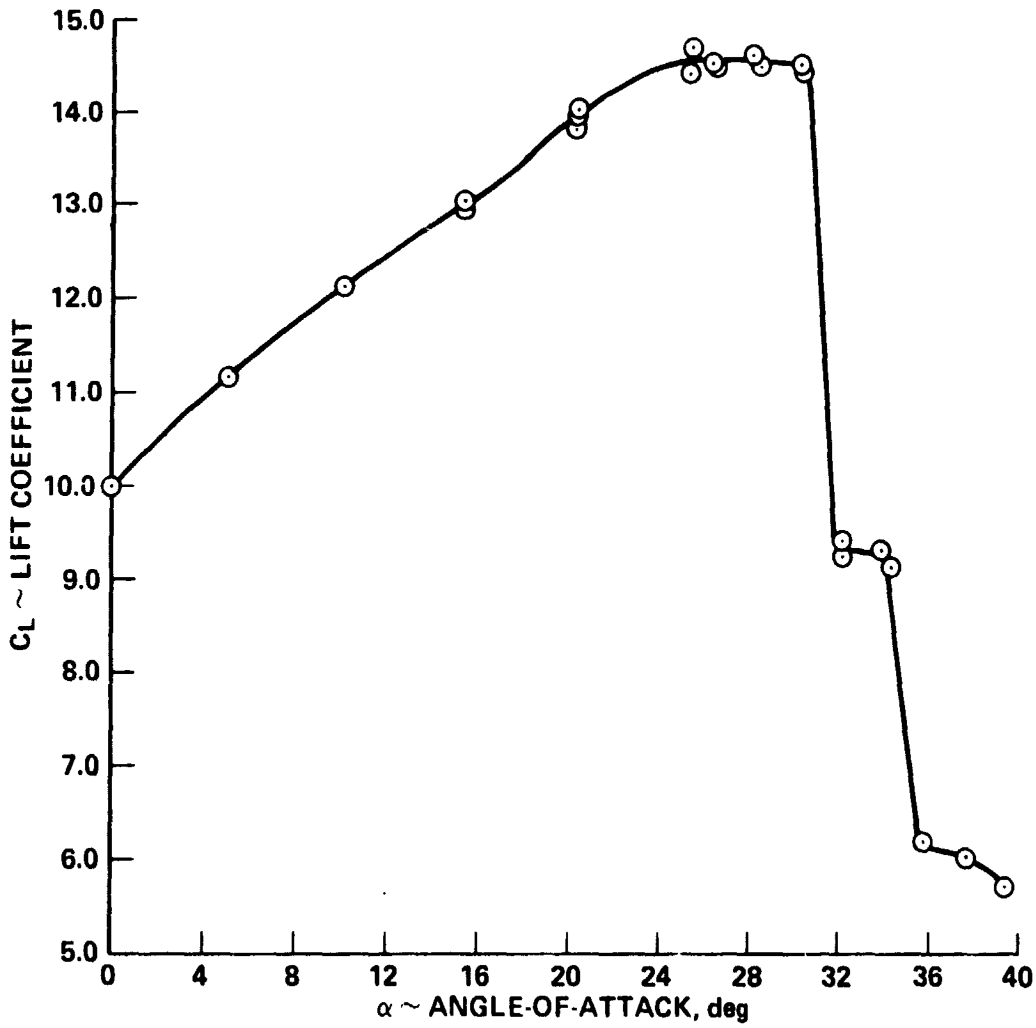

(e) $C_\mu = 4.0$

Figure 19.- Continued.

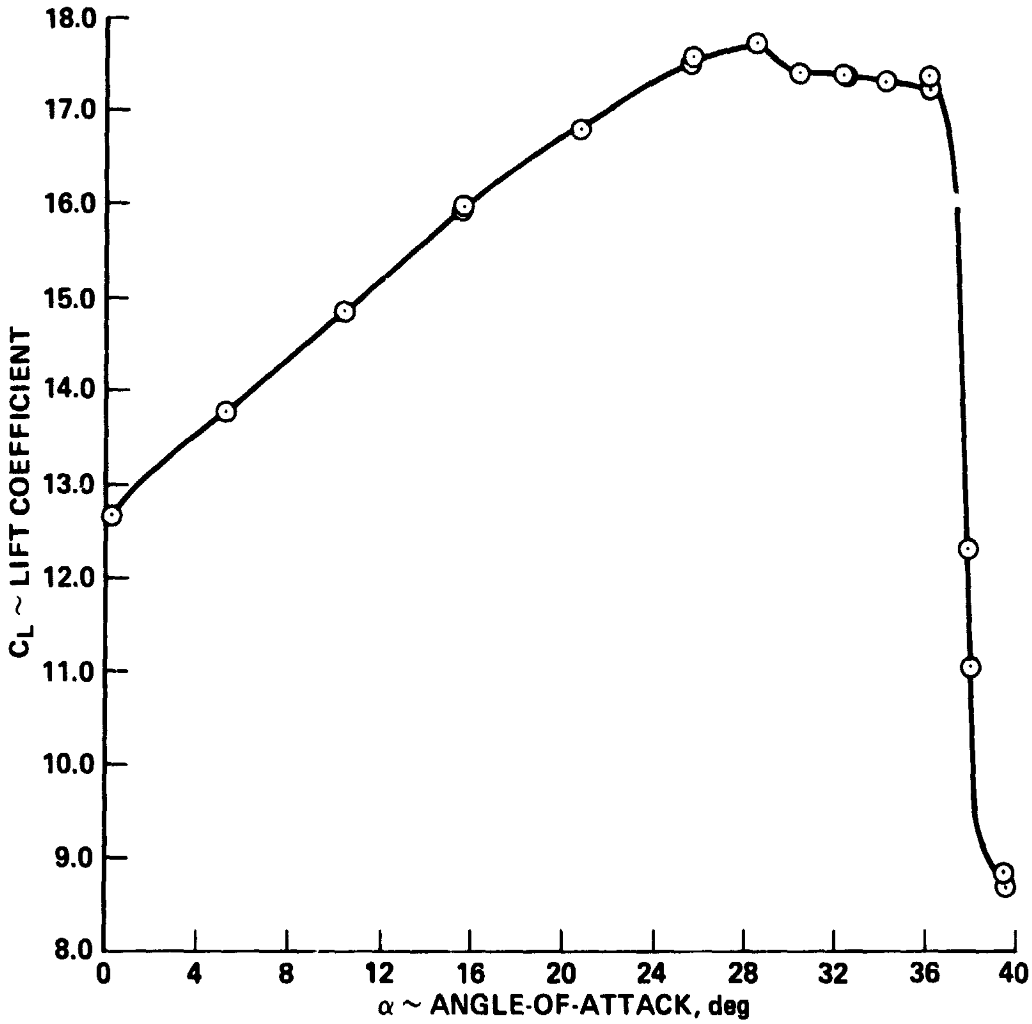

(f) $C_\mu = 6.0$

Figure 19.- Continued.

ORIGINAL PAGE IS
OF POOR QUALITY

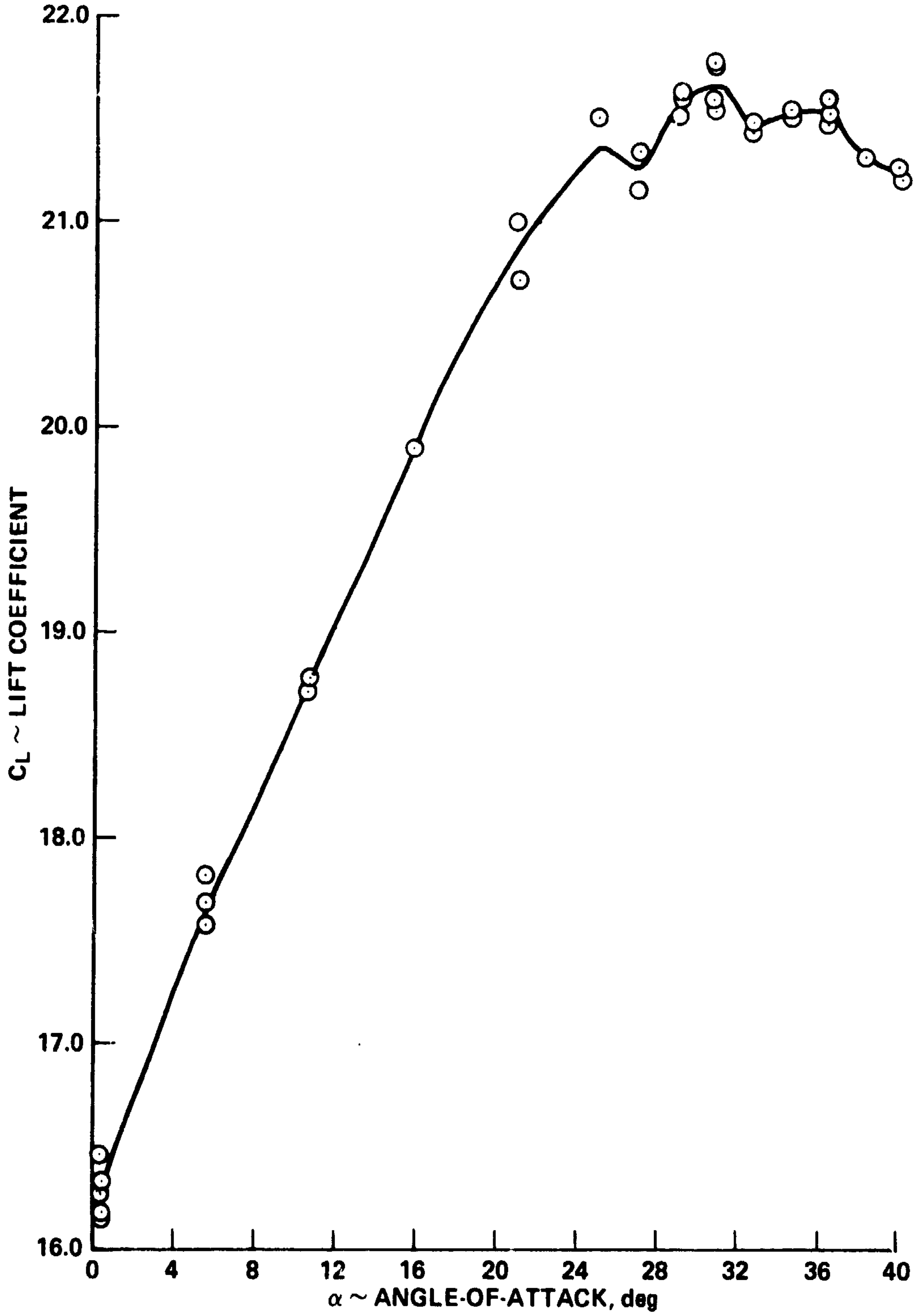

(g) C_μ = 10.0

Figure 19.- Concluded.

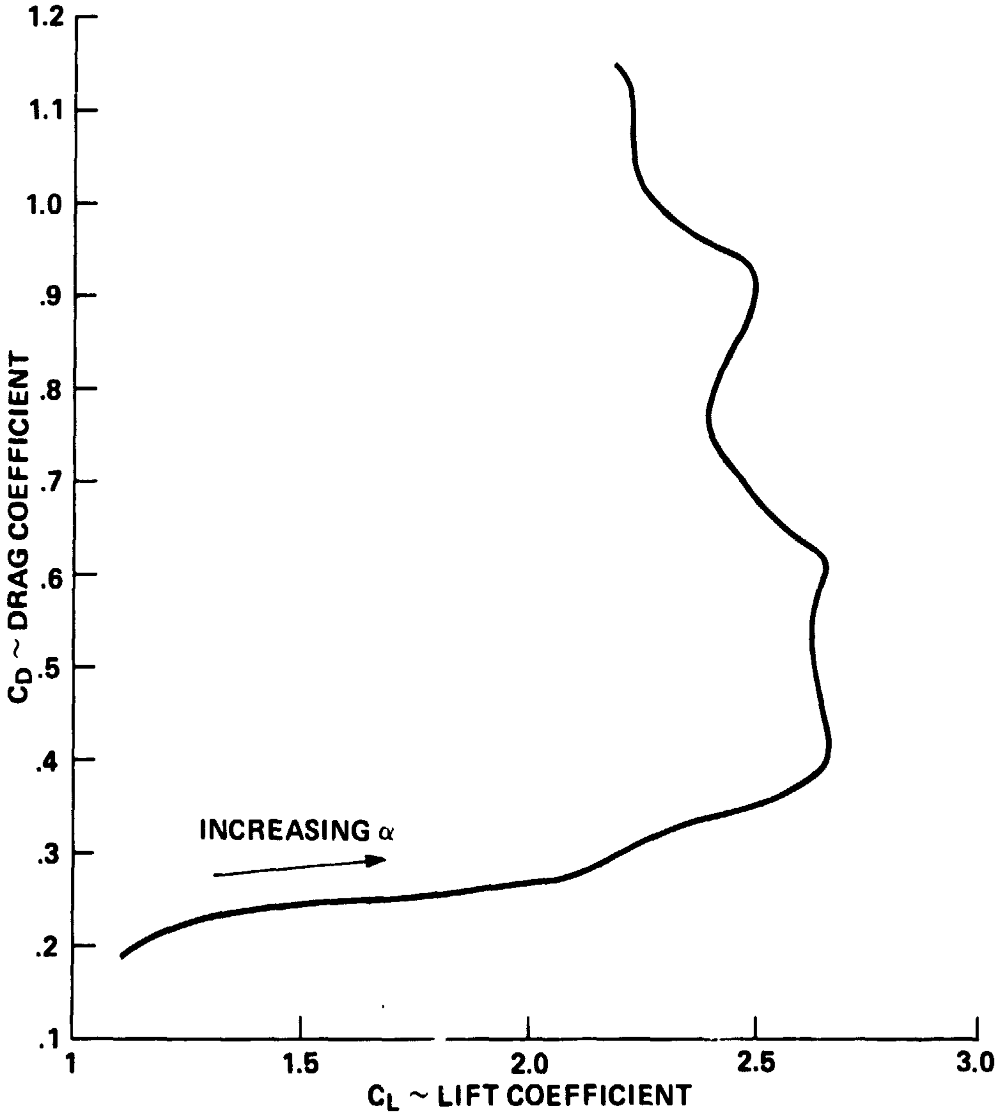

(a) $C_\mu = 0$

Figure 20.- Variation of drag with lift for the swept wing model with full-span leading-edge slats and full-span knee-blown flaps at various blowing rates.

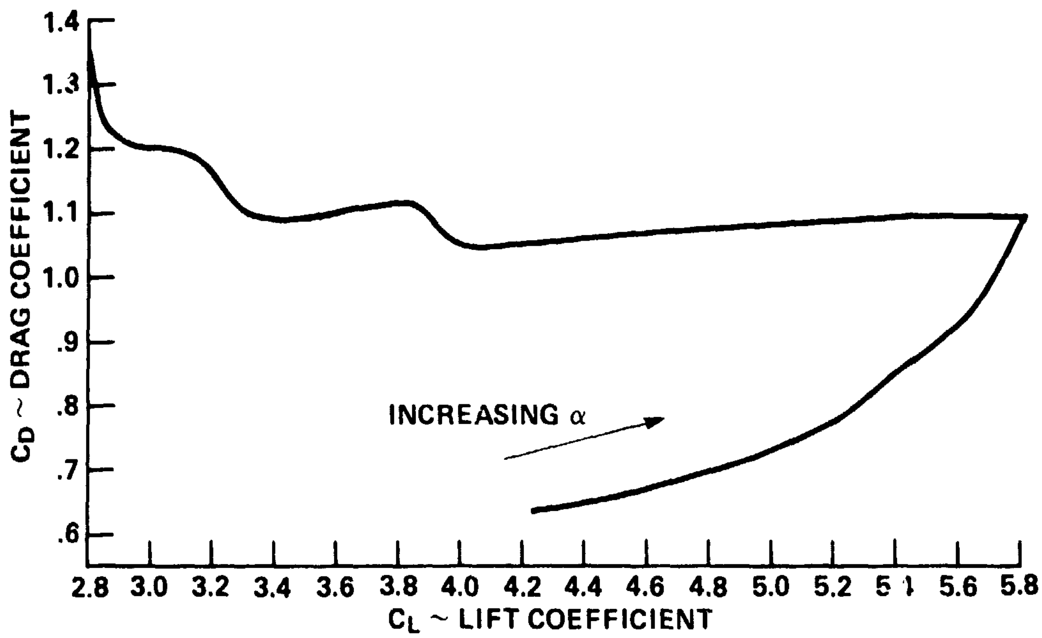

(b) $C_\mu = 0.4$

Figure 20.- Continued.

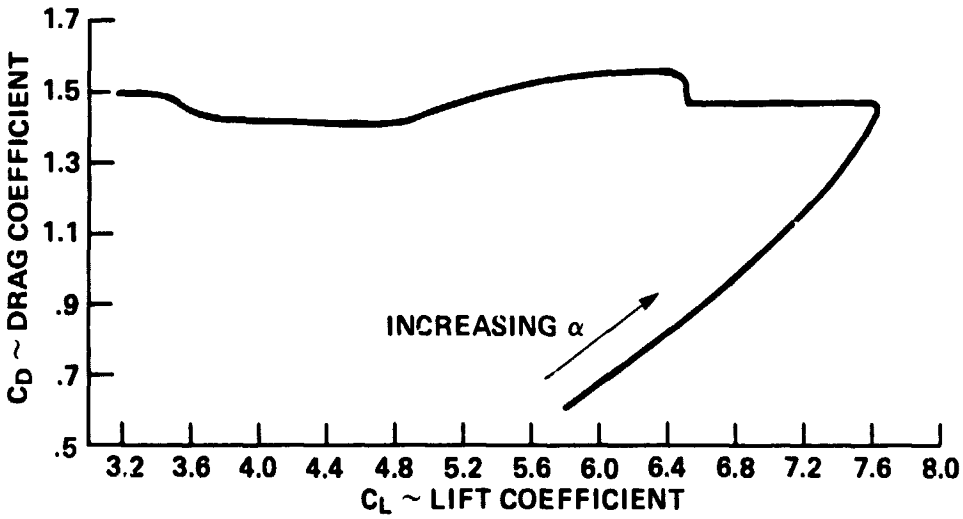

(c) $C_\mu = 1.0$

Figure 20.- Continued.

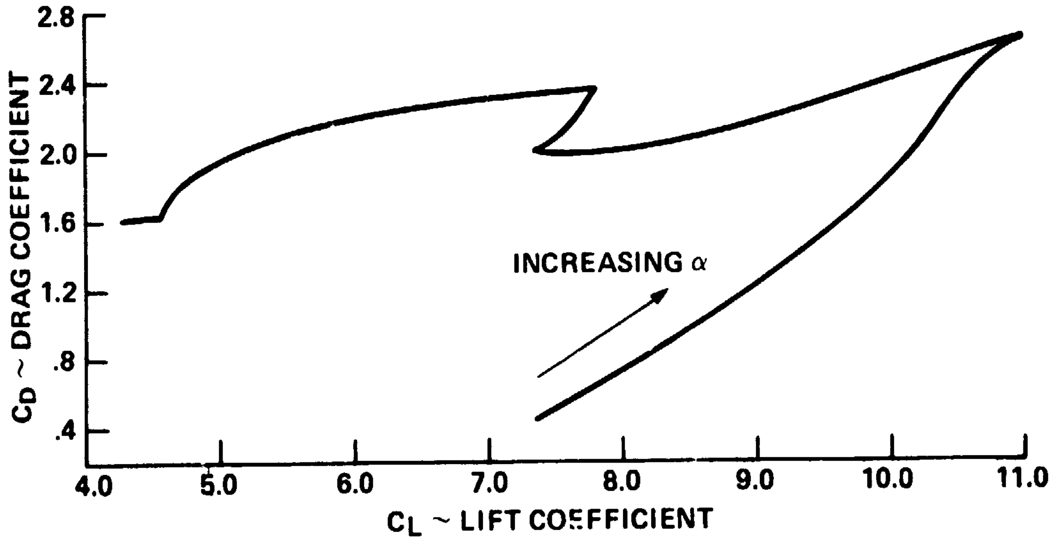

(d) $C_\mu = 2.0$

Figure 20.- Continued.

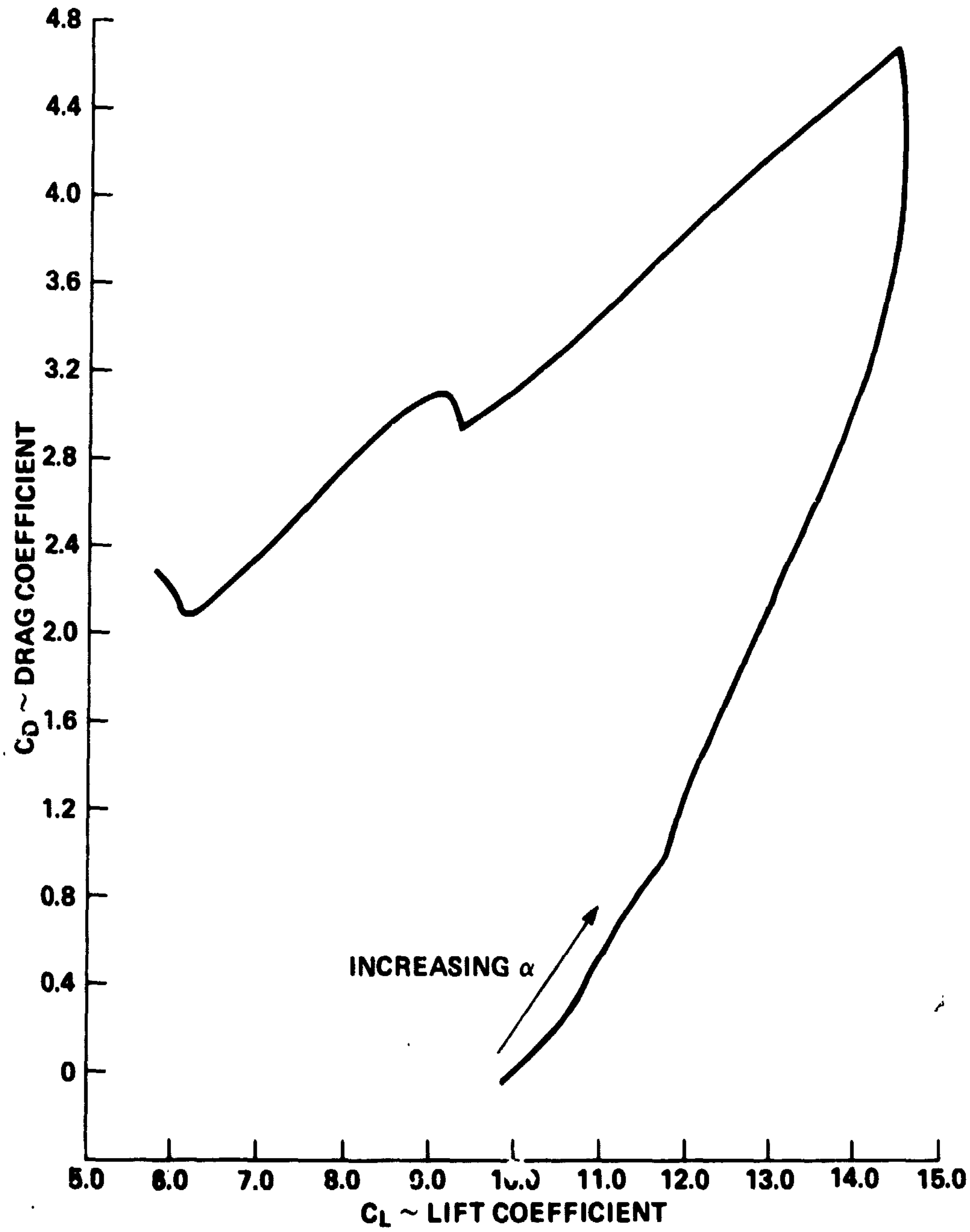

(e) $C_\mu = 4.0$

Figure 20.- Continued.

ORIGINAL PAGE IS
OF POOR QUALITY

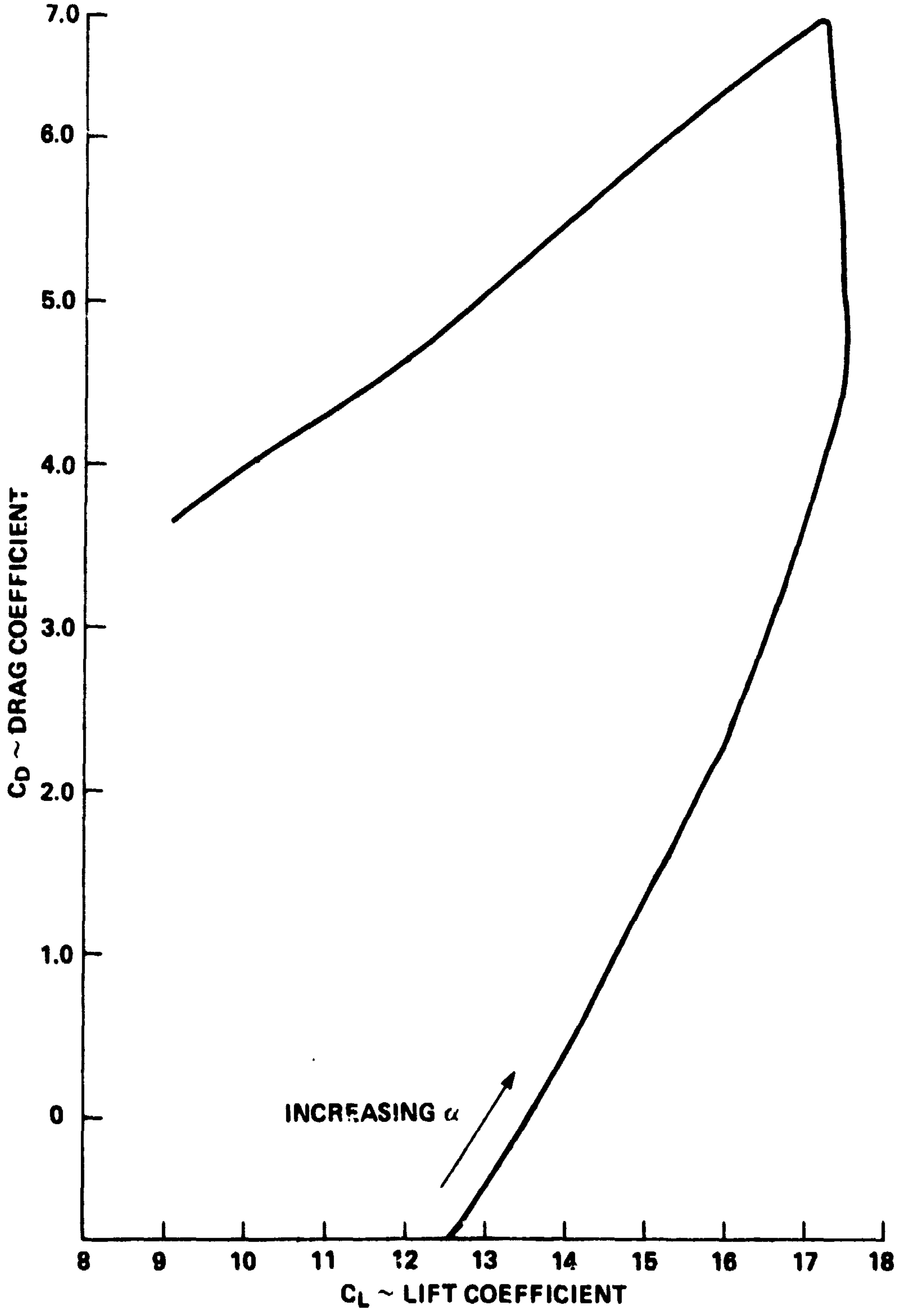

(f) C_μ = 6.0

Figure 20.- Continued.

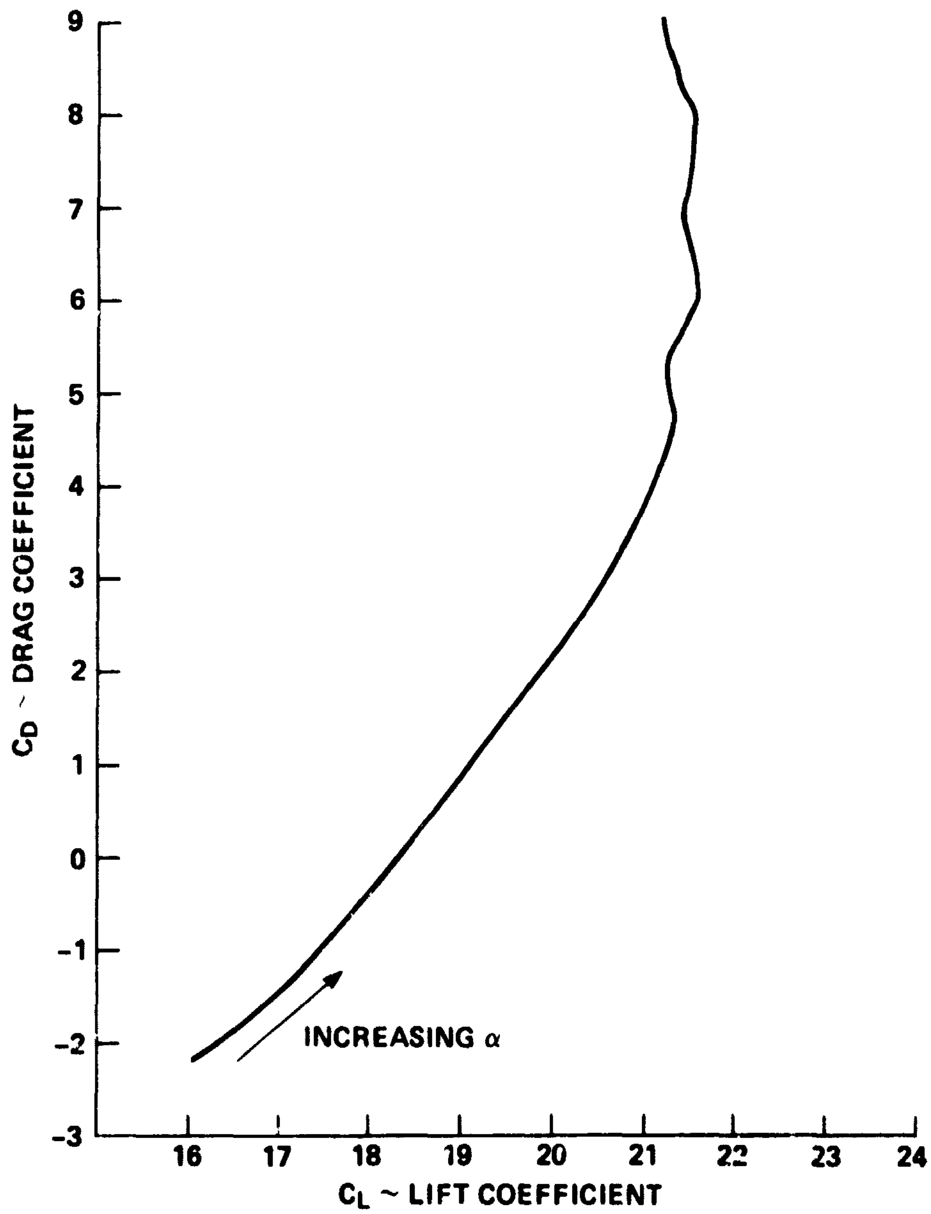

(g) C_μ = 10.0

Figure 20.- Concluded.

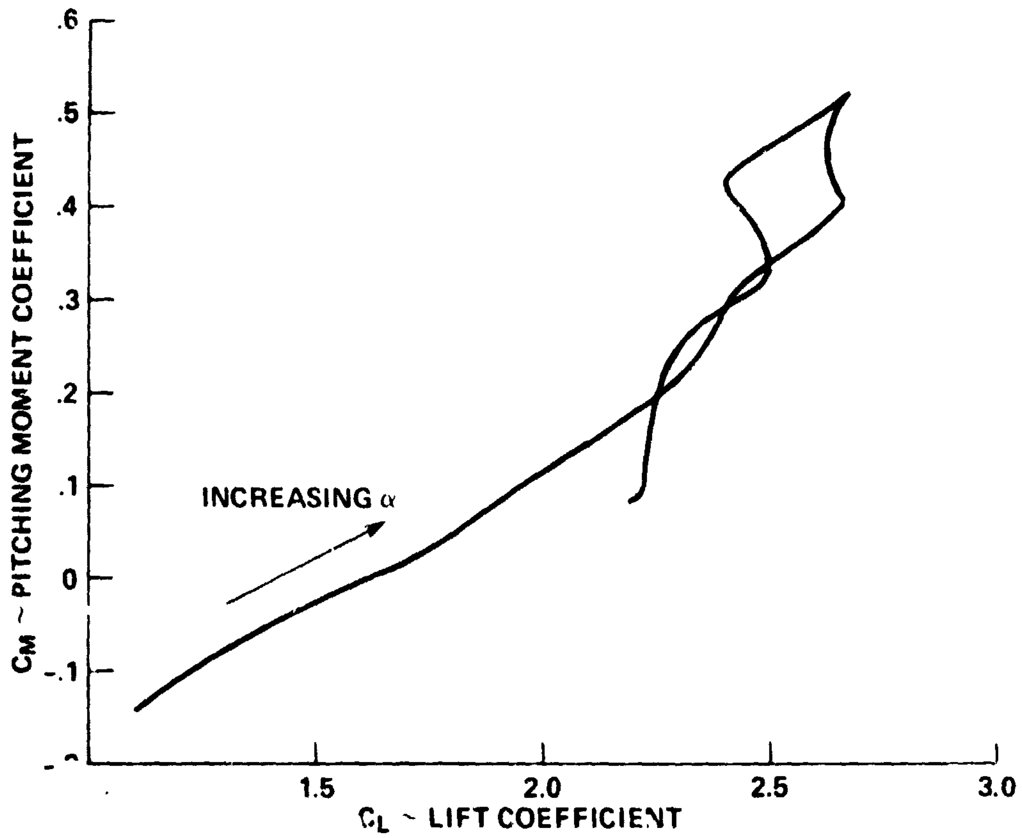

(a) C_μ = 0

Figure 21.- Variation of pitching moment with lift for the swept-wing model with full-span leading-edge slats and full-span knee-blown flaps at various blowing rates.

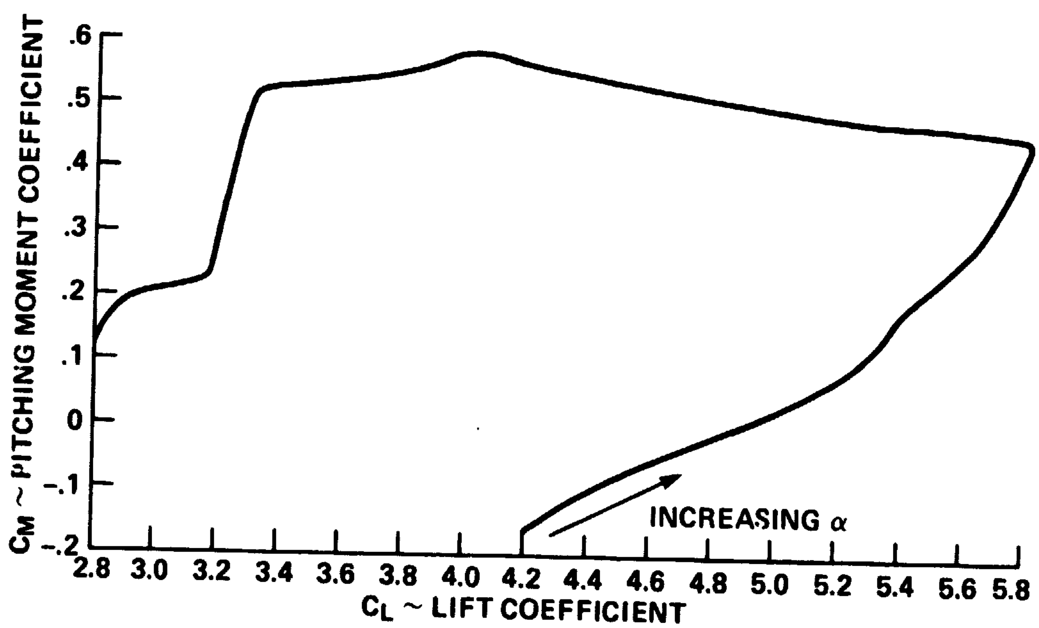

(b) $C_{\mu} = 0.4$

Figure 21.- Continued.

ORIGINAL PAGE IS
OF POOR QUALITY

C-2

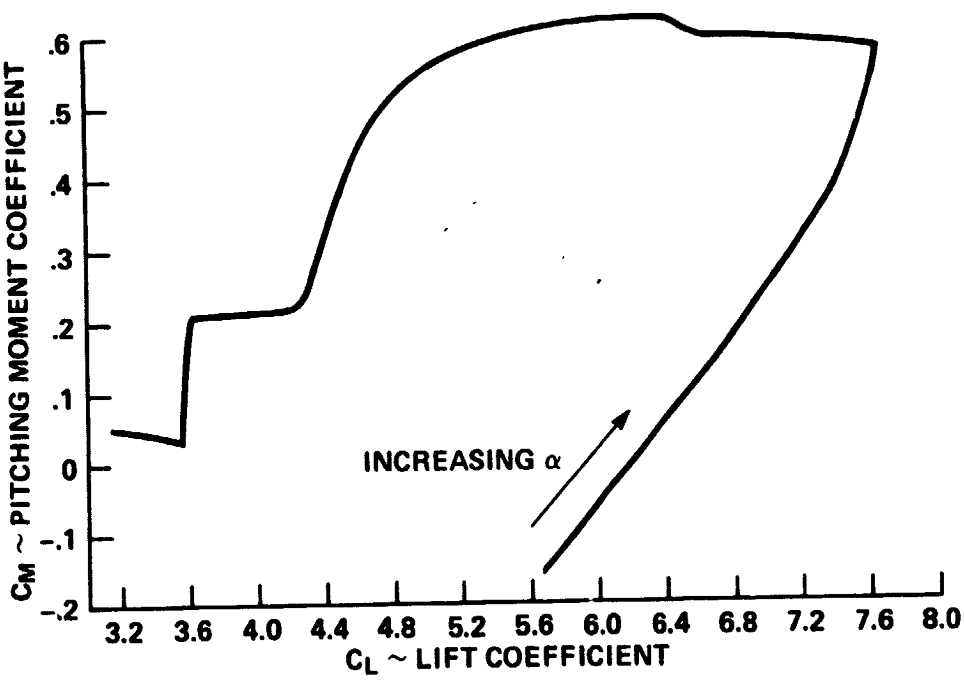

(c) $C_\mu = 1.0$

Figure 21.- Continued.

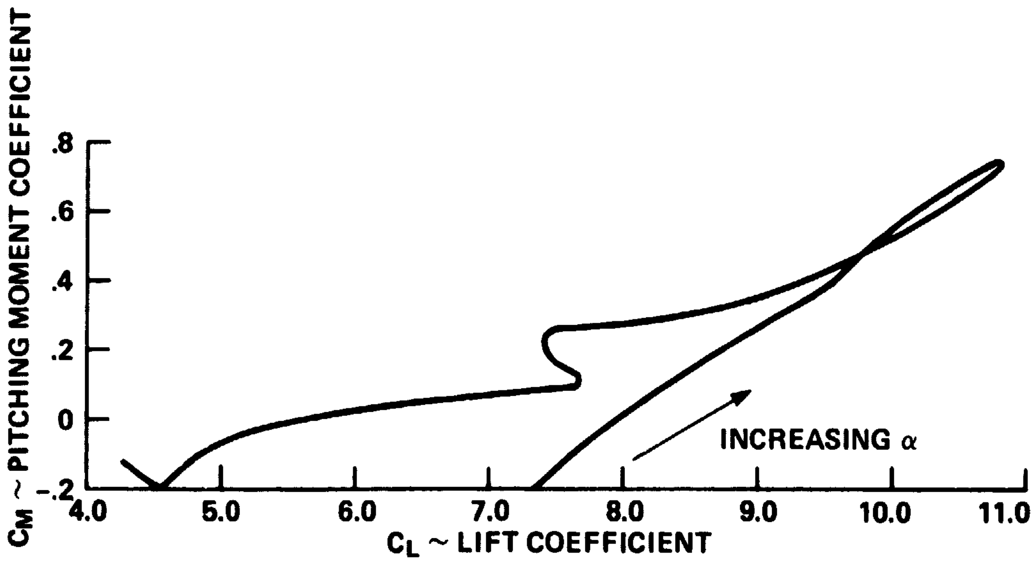

(d) C_μ = 2.0

Figure 21.- Continued.

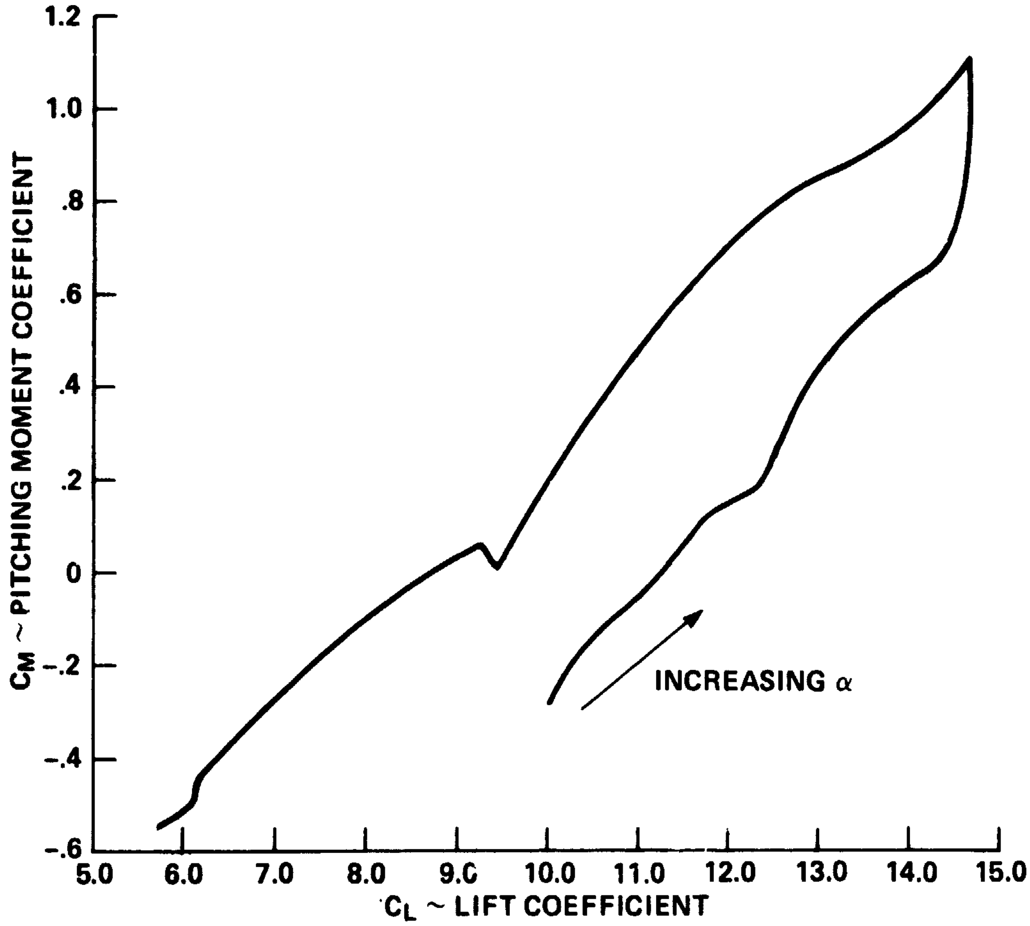

(e) $C_\mu = 4.0$

Figure 21.- Continued.

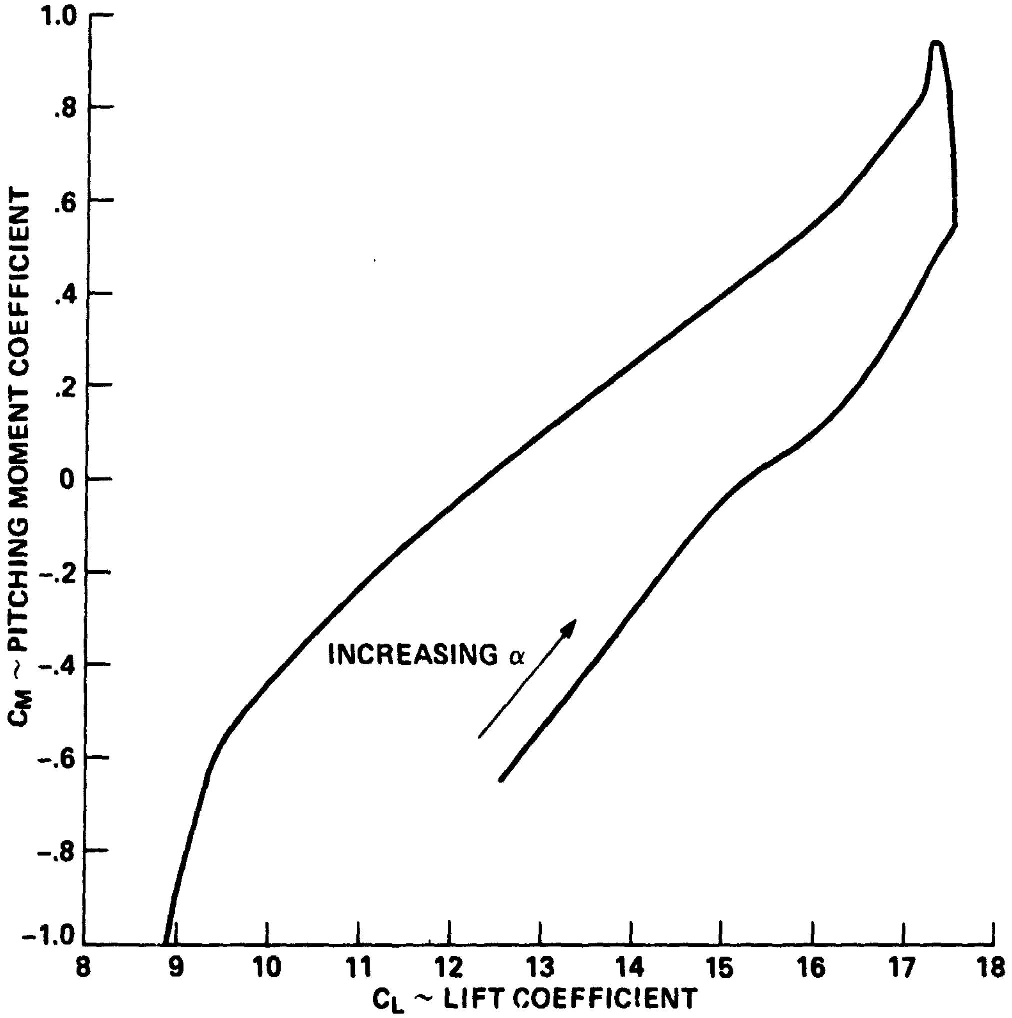

(f) $C_\mu = 6.0$

Figure 21.- Continued.

ORIGINAL PAGE IS
OF POOR QUALITY

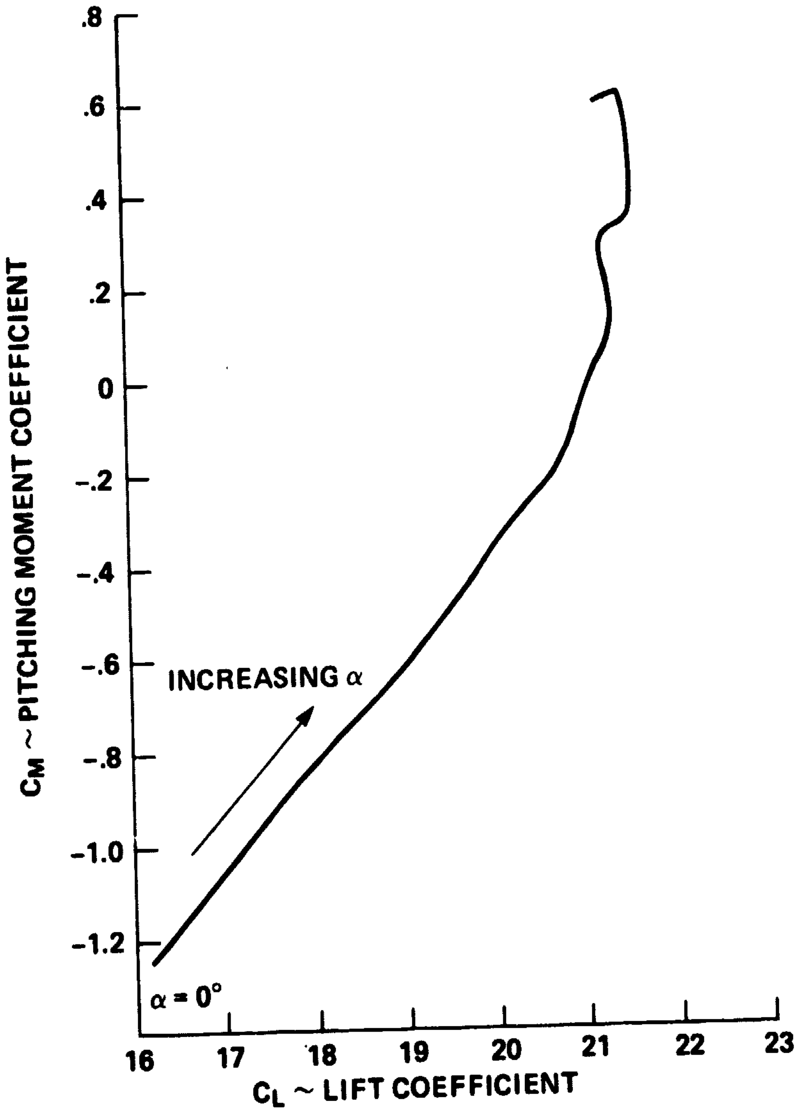

(g) C_μ = 10.0

Figure 21.- Concluded.

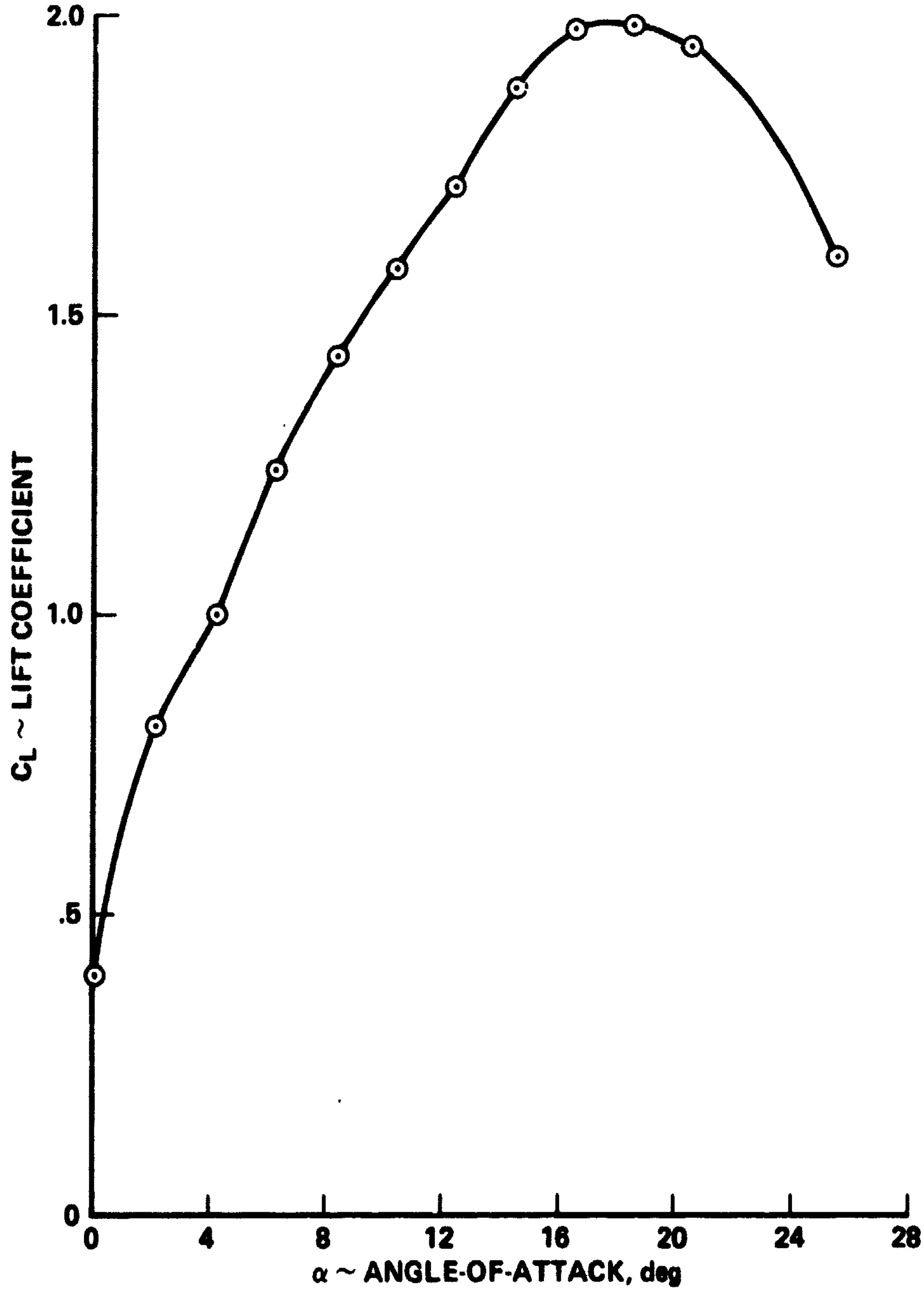

(a) $C_\mu = 0$

Figure 22.- Variation of lift with angle-of-attack for the swept-wing model with full-span leading-edge slats and partial-span knee-blown flaps at various blowing rates.

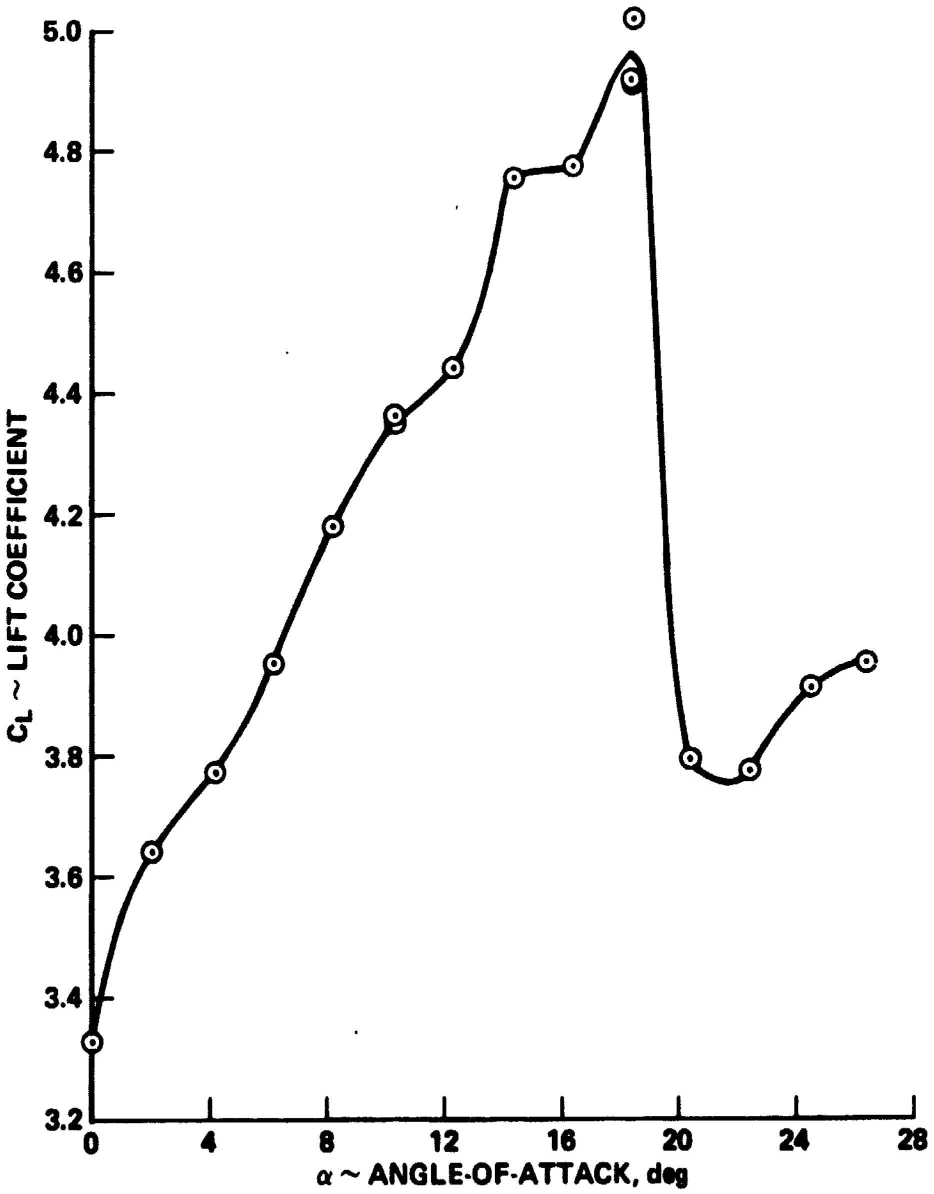

(b) $C_\mu = 0.4$

Figure 22.- Continued.

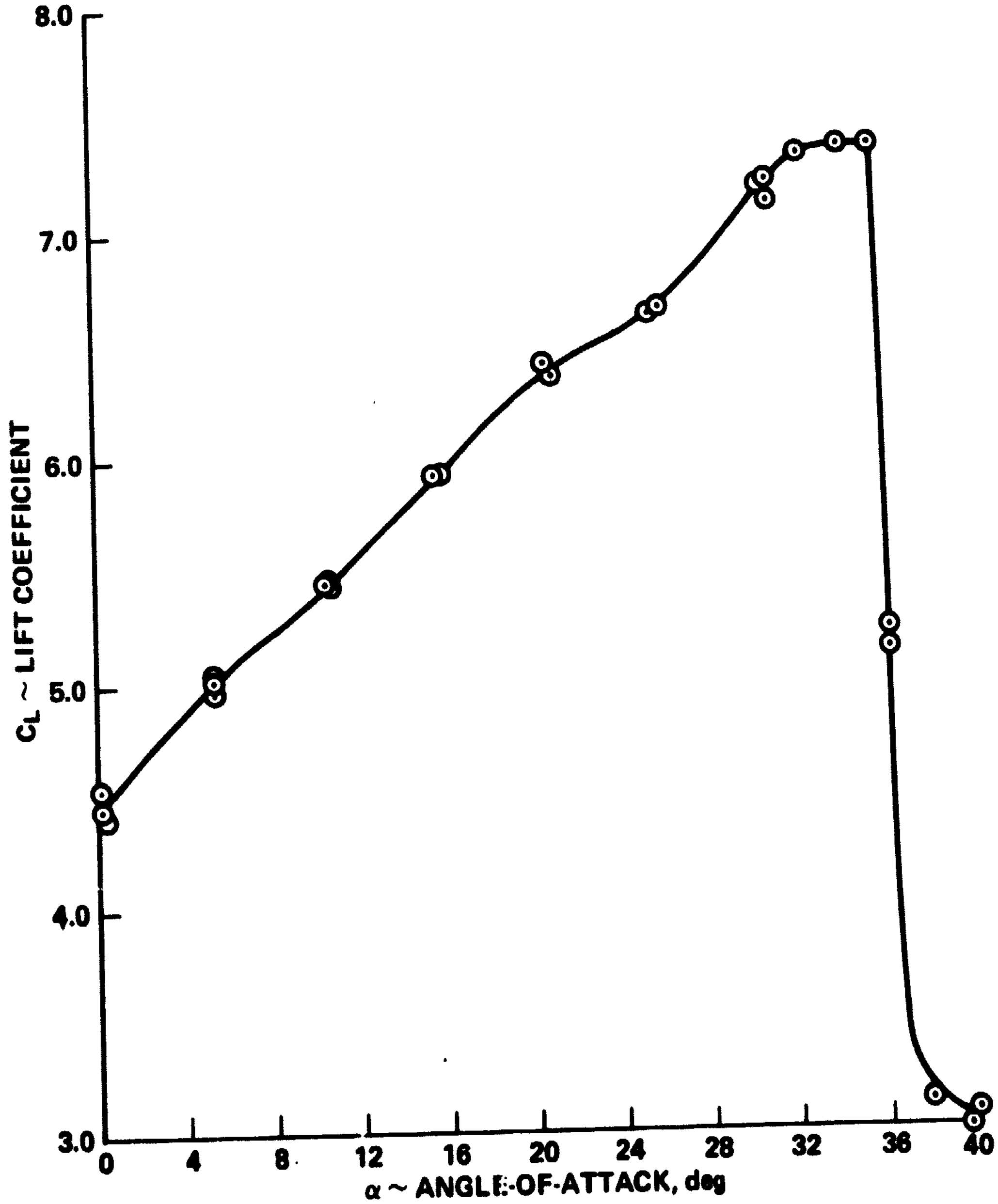

(c) C_μ = 1.0

Figure 22.- Continued.

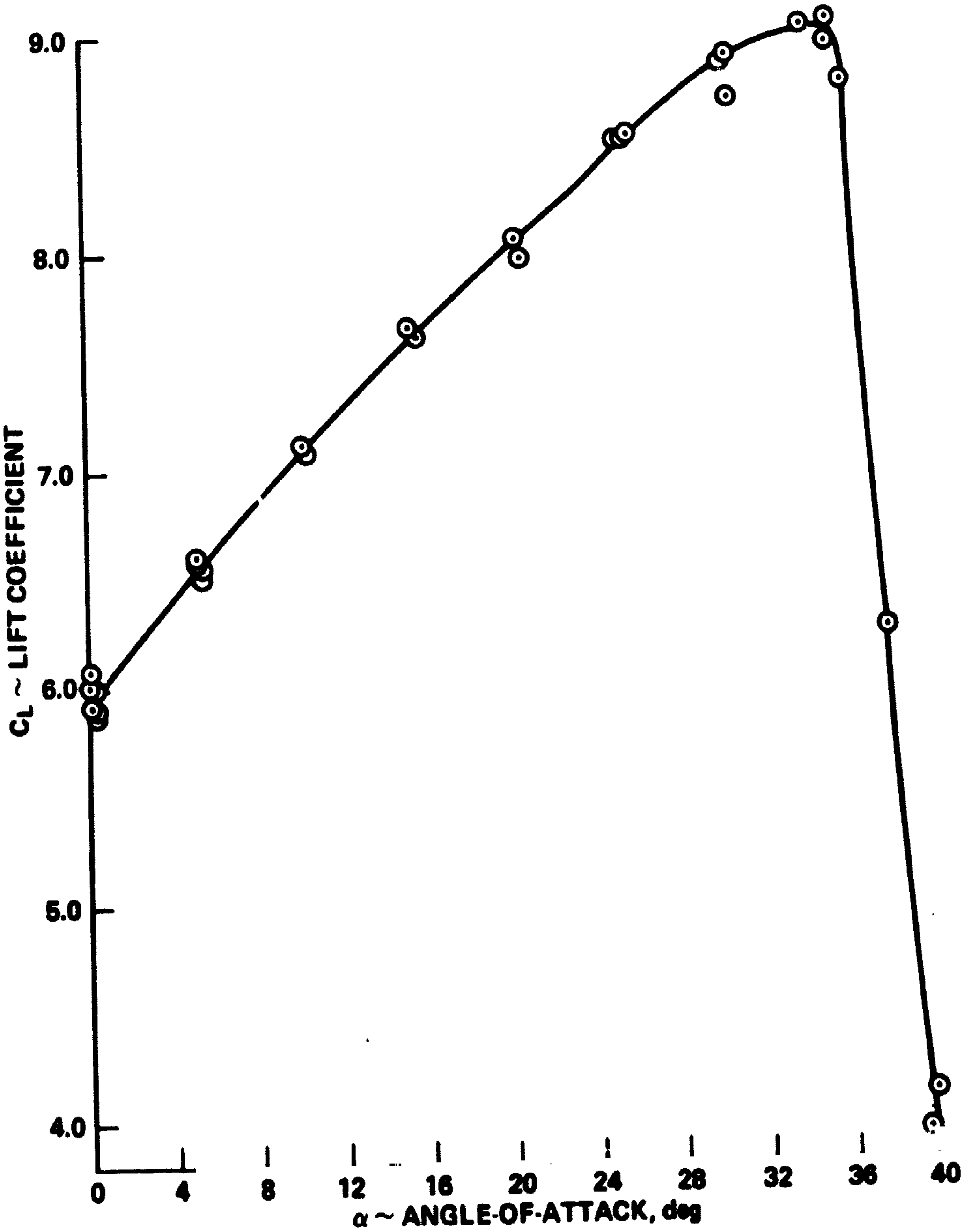

(d) $C_\mu = 2.0$

Figure 22.- Continued.

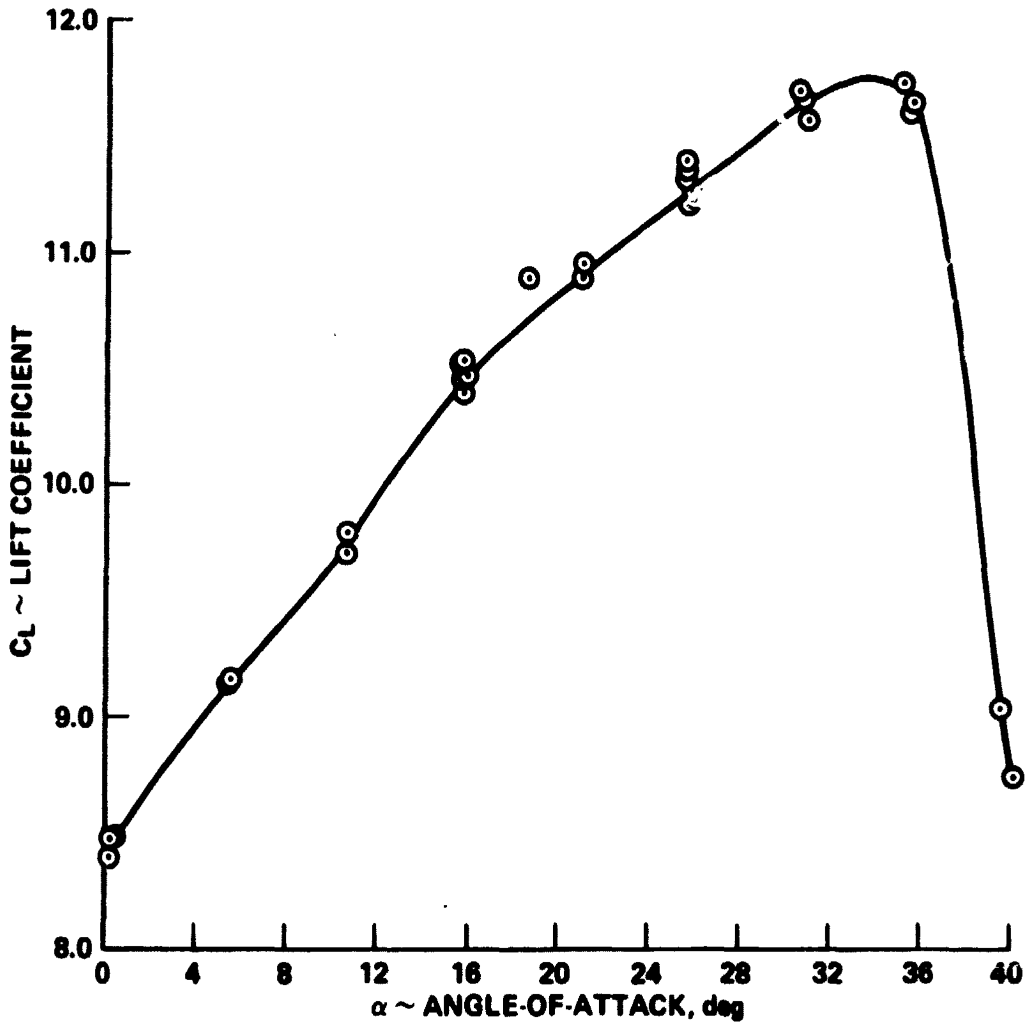

(e) $C_\mu = 4.0$

Figure 22.- Continued.

ORIGINAL PAGE IS OF POOR QUALITY

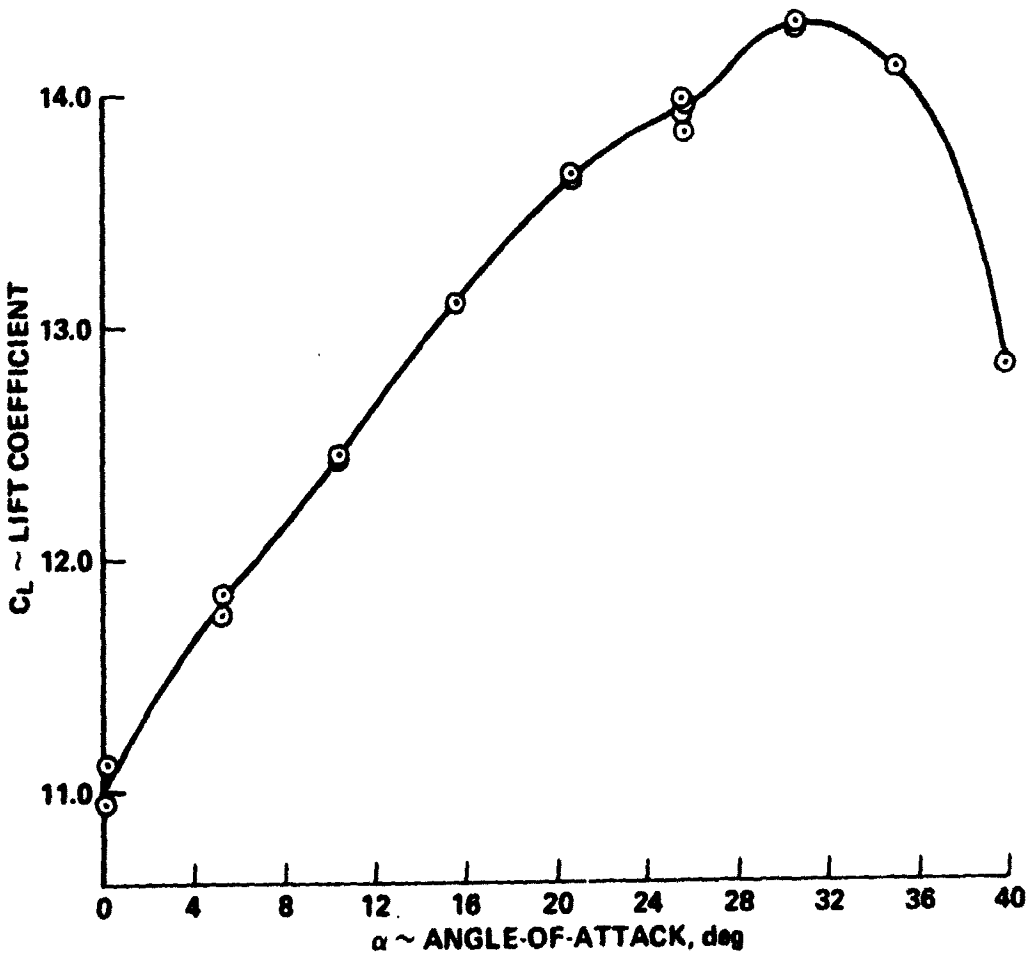

(f) $C_\mu = 6.0$

Figure 22.- Continued.

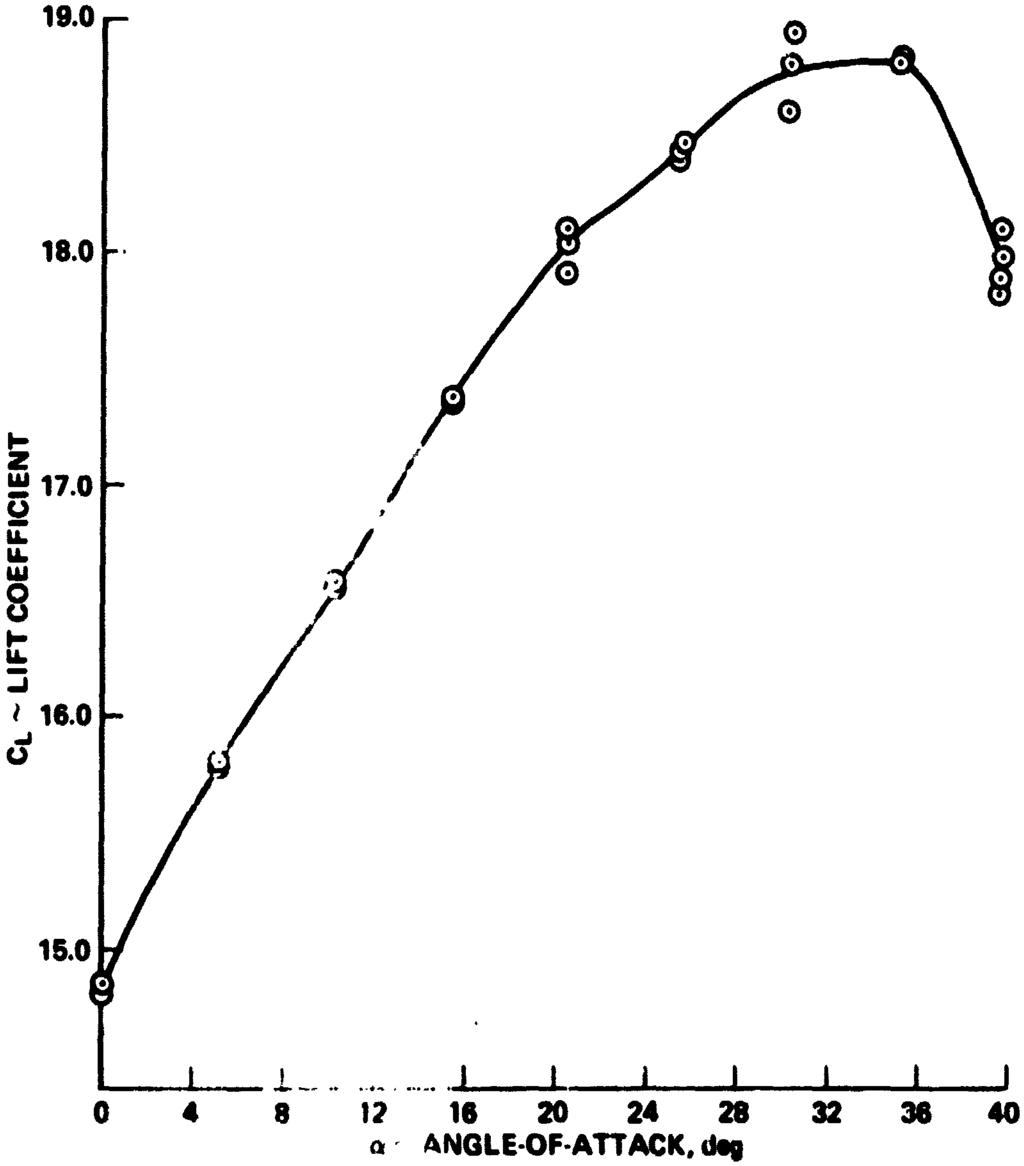

(g) $C_\mu = 10.0$

Figure 22.- Concluded.

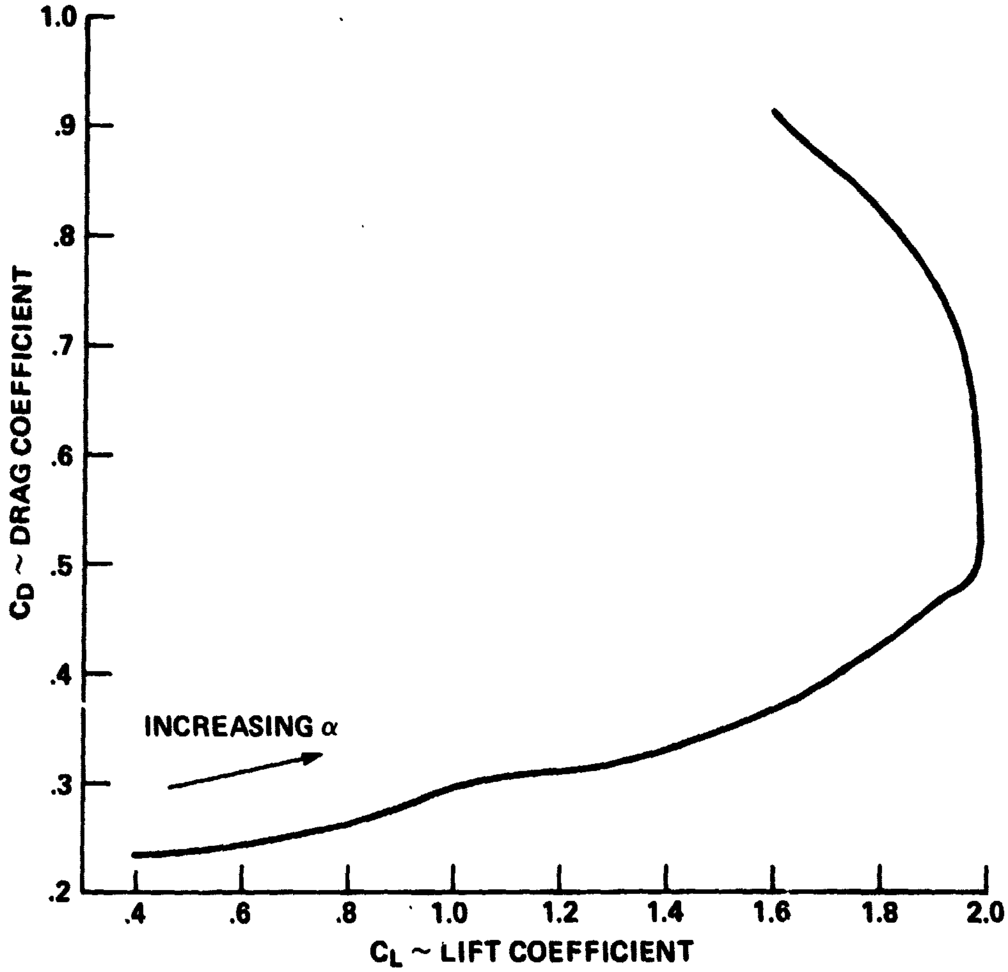

(a) $C_\mu = 0$

Figure 23.- Variation of drag with lift for the swept-wing model with full-span leading-edge slats and partial-span knee-blown flaps at various blowing rates.

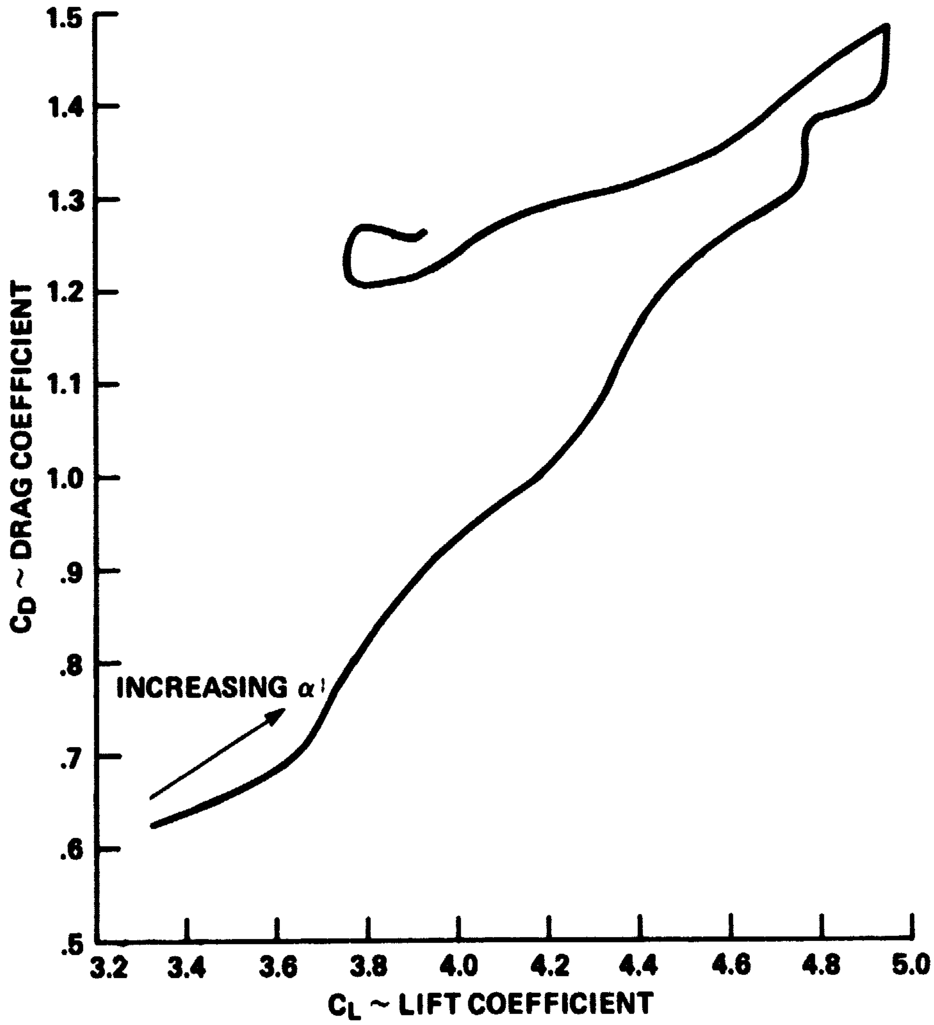

(b) $C_\mu = 0.4$

Figure 23.- Continued.

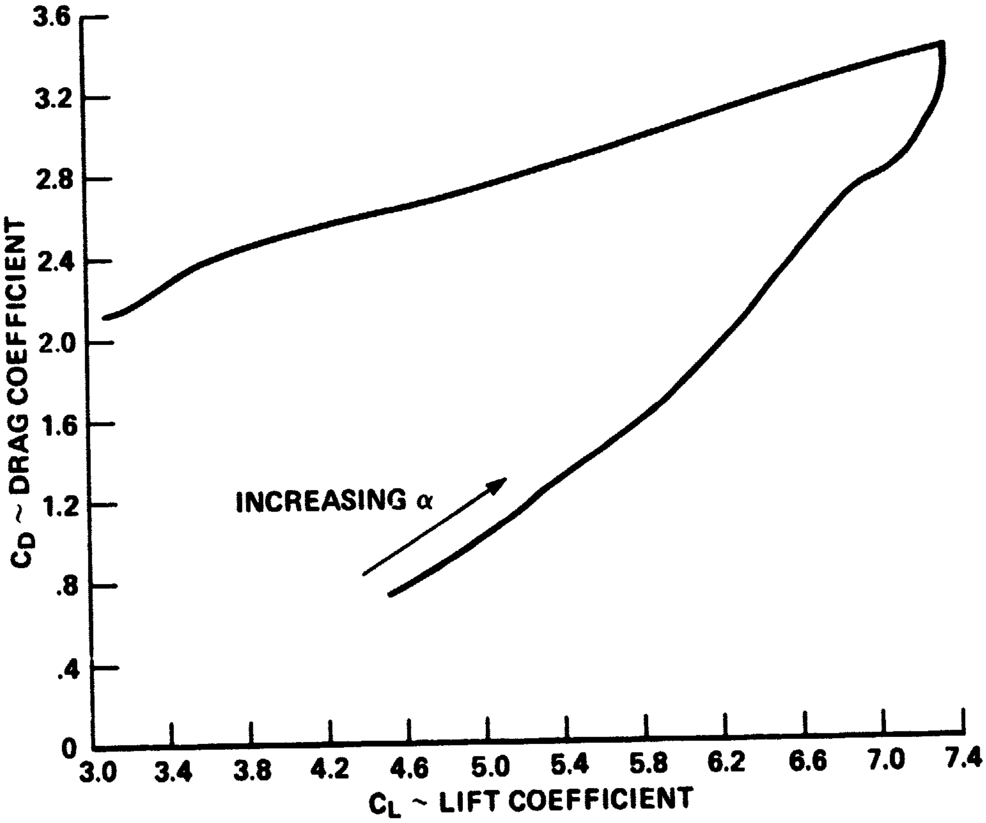

(c) $C_\mu = 1.0$

Figure 23.- Continued.

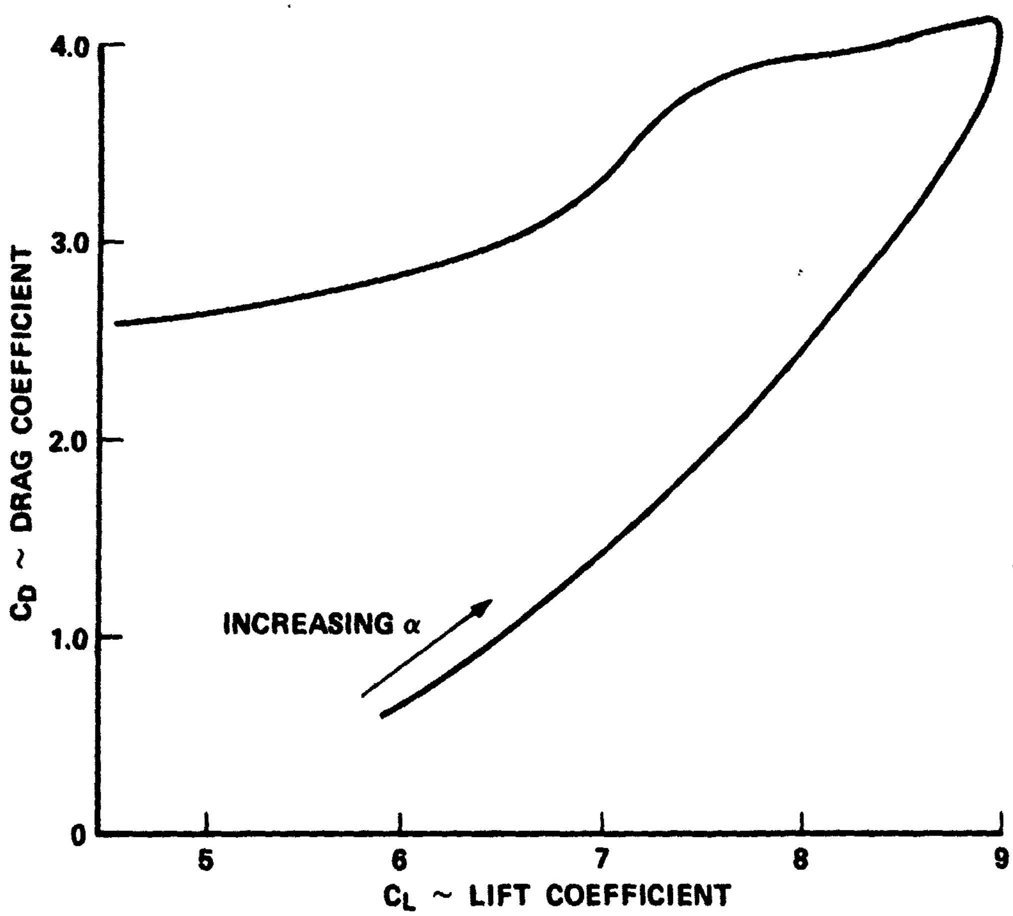

(d) $C_\mu = 2.0$

Figure 23.- Continued.

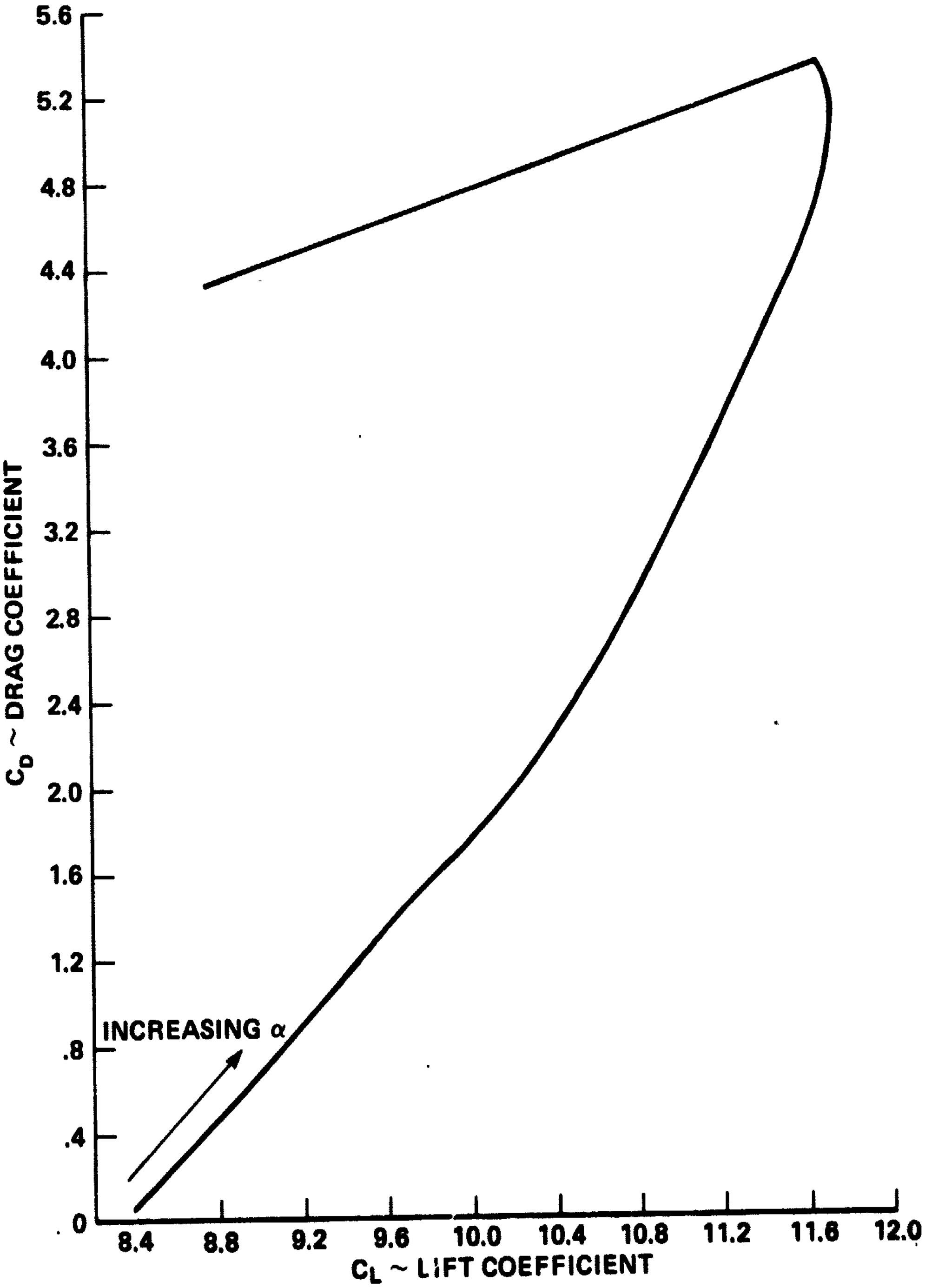

(e) $C_\mu = 4.0$

Figure 23.- Continued.

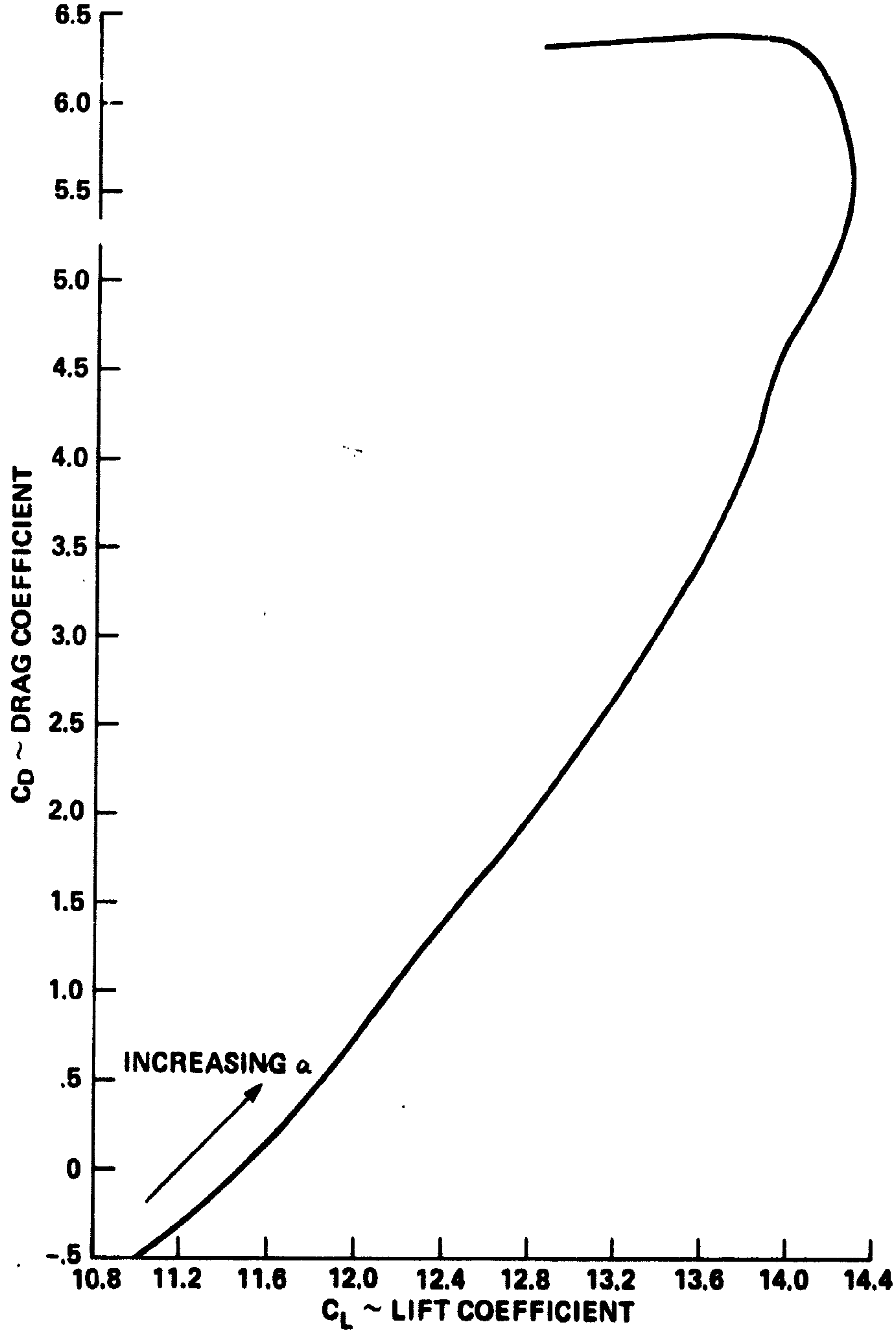

(f) $C_\mu = 6.0$

Figure 23.- Continued.

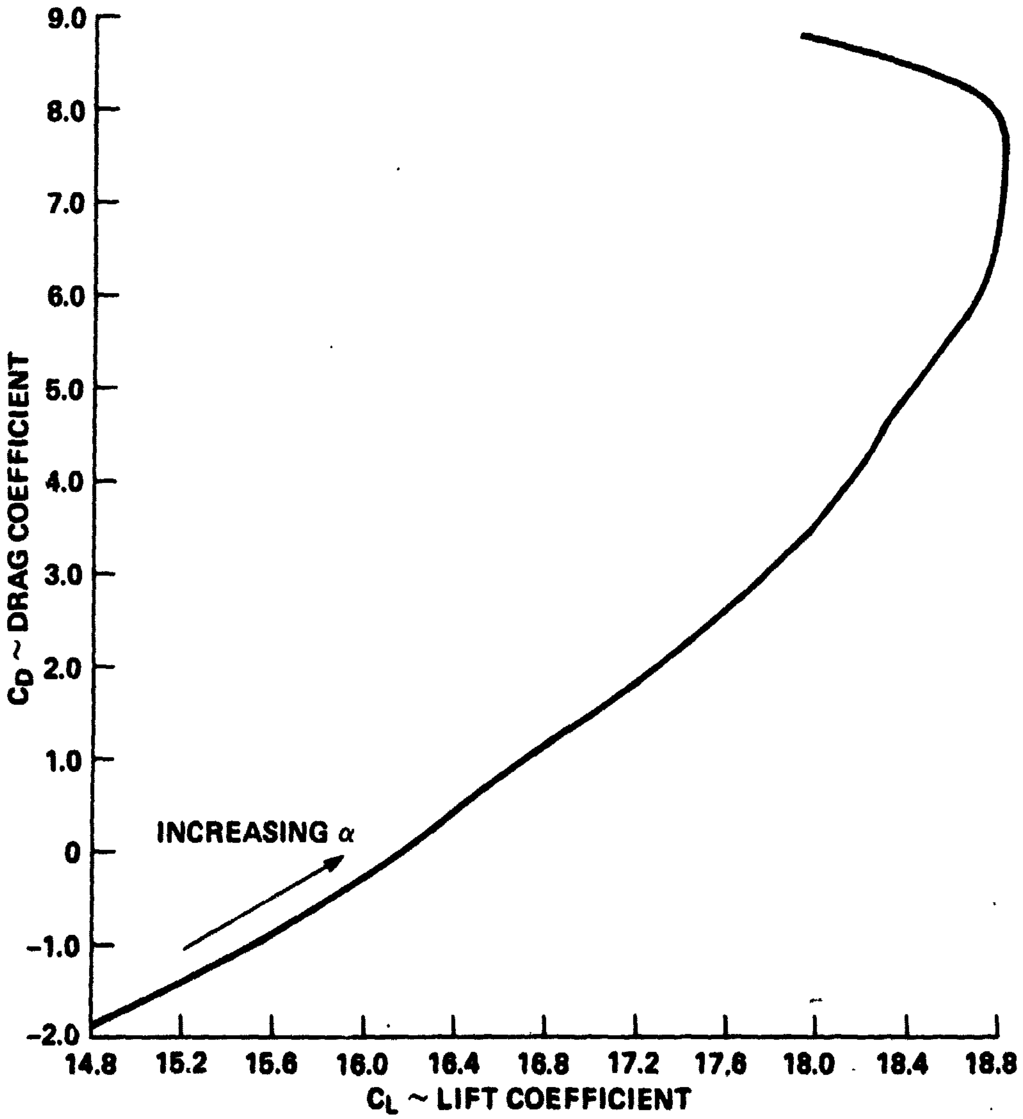

(g) $C_\mu = 10.0$

Figure 23.- Concluded.

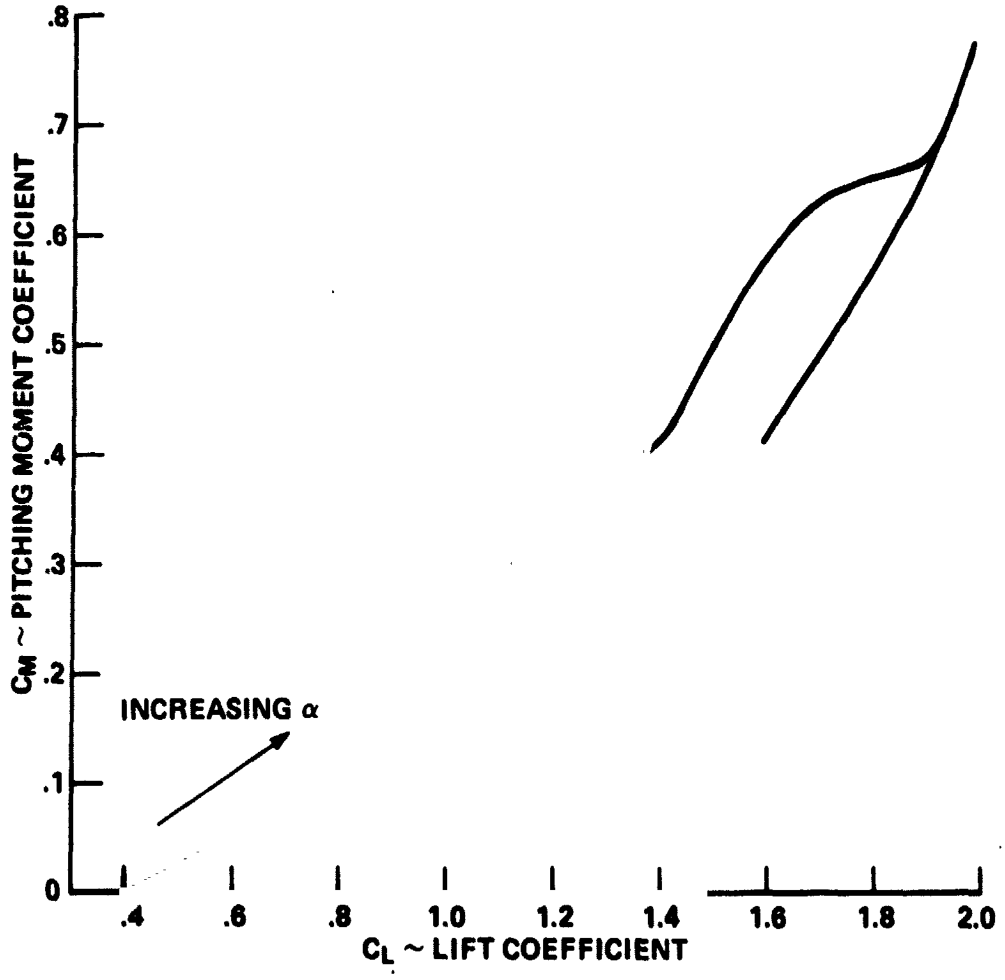

(a) $C_\mu = 0$

Figure 24.- Variation of pitching moment with lift for the swept-wing model with full-span leading-edge slats and partial-span knee-blown flaps at various blowing rates.

ORIGINAL PAGE IS
OF POOR QUALITY

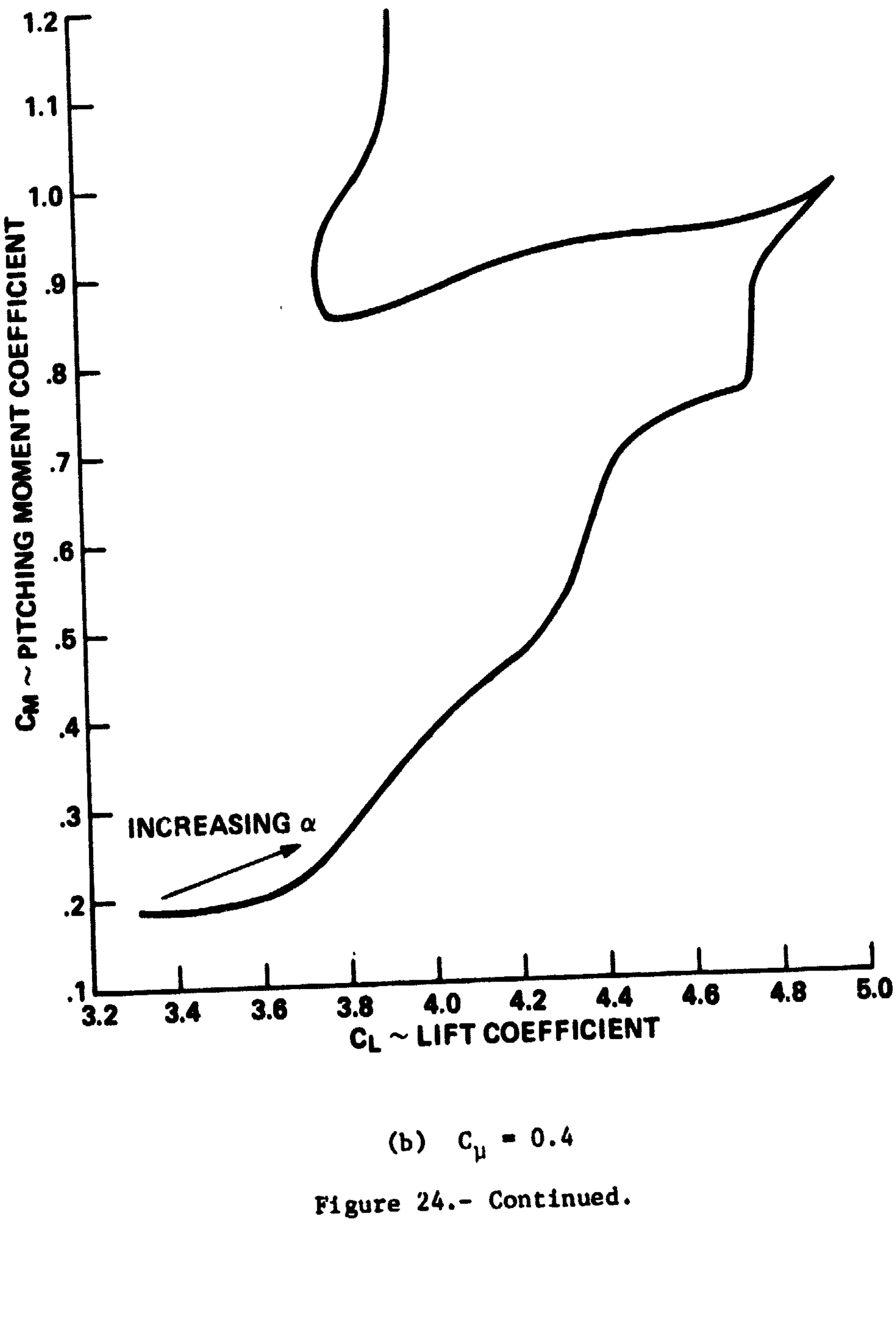

(b) $C_\mu = 0.4$

Figure 24.- Continued.

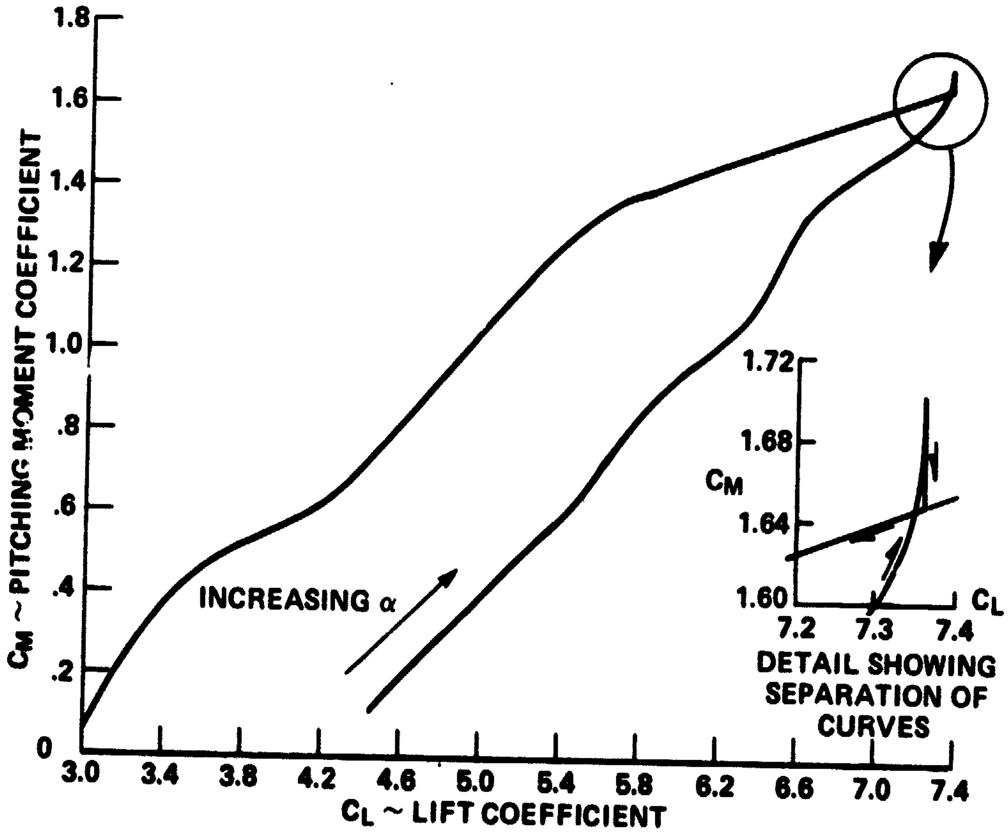

(c) $C_\mu = 1.0$

Figure 24.- Continued.

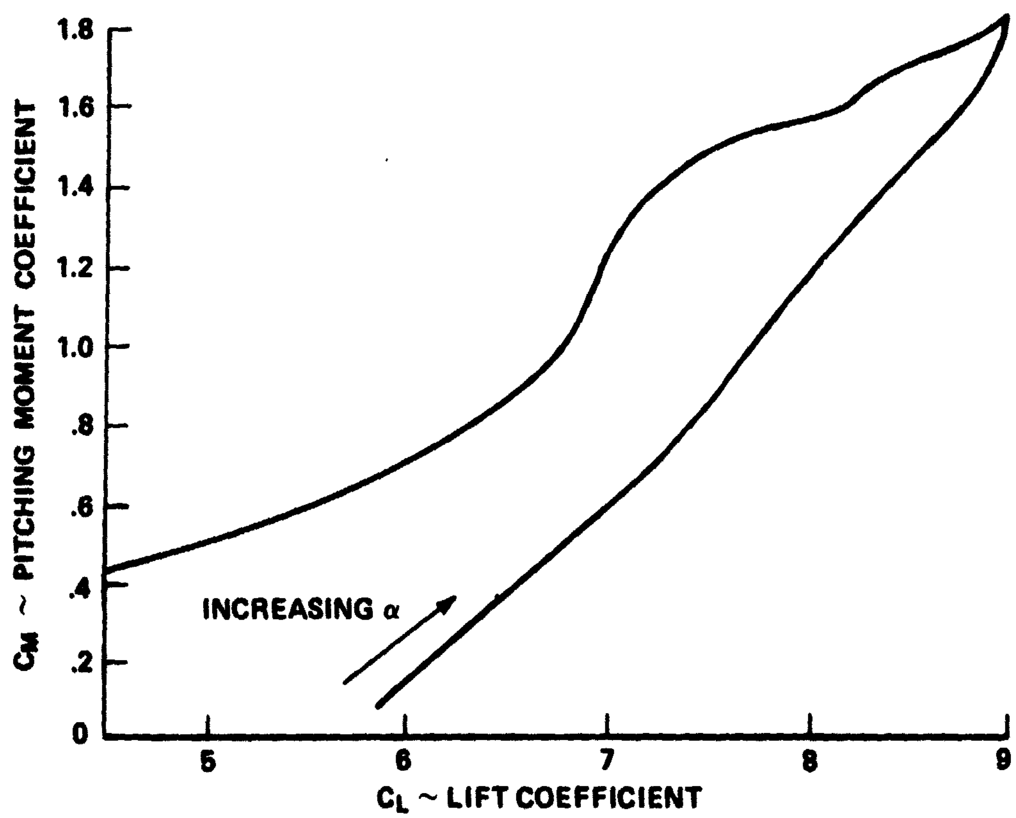

(d) $C_\mu = 2.0$

Figure 24.- Continued.

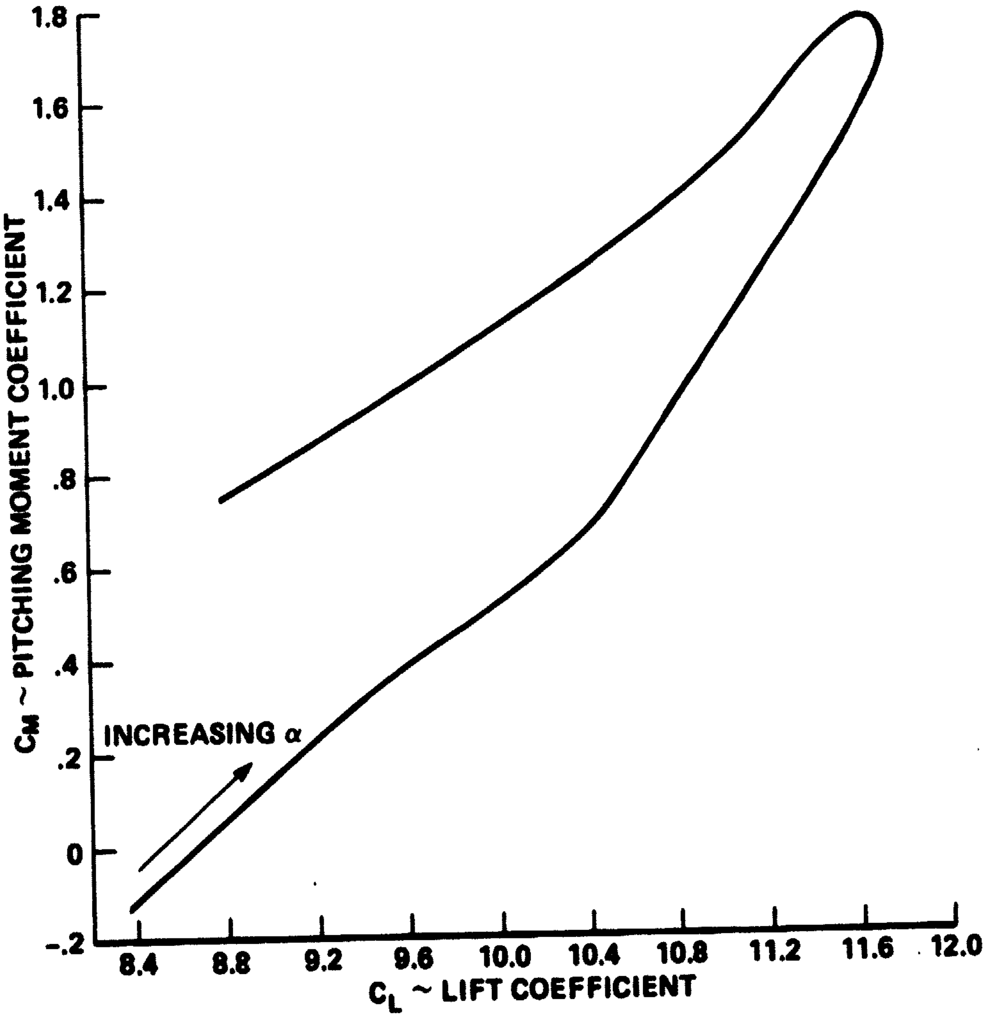

(e) $C_\mu = 4.0$

Figure 24.- Continued.

ORIGINAL PAGE IS
OF POOR QUALITY

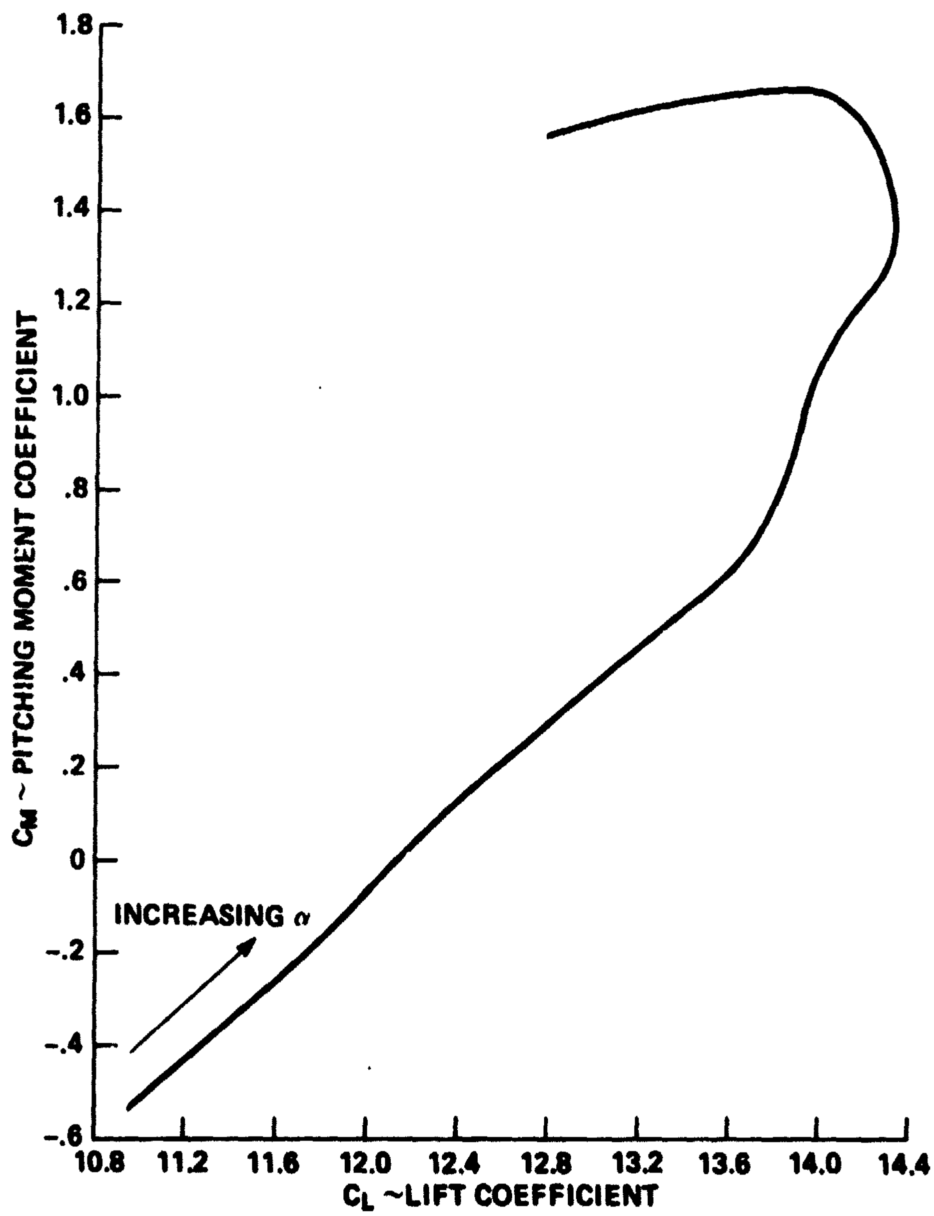

(f) $C_\mu = 6.0$

Figure 24.- Continued.

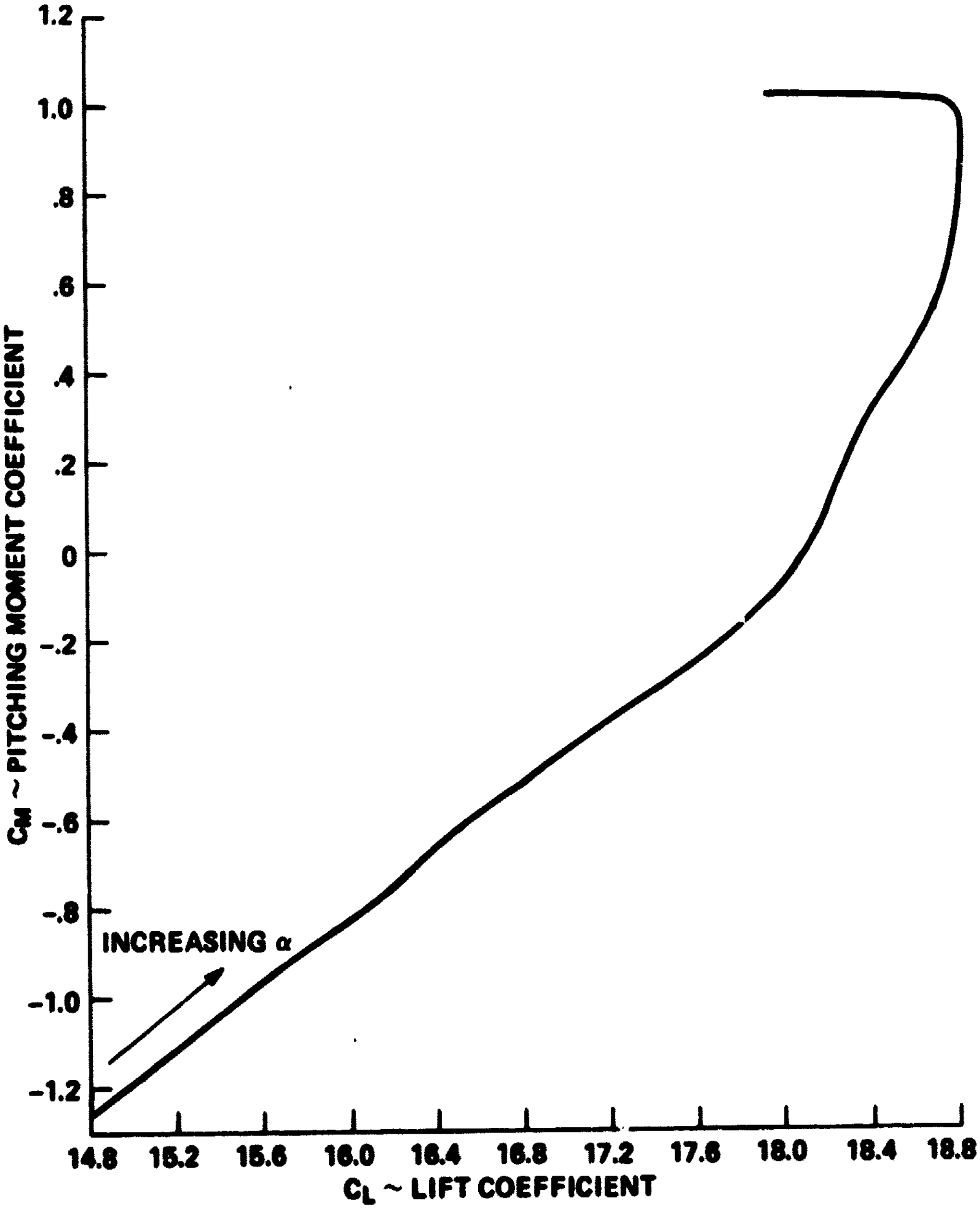

(g) C_μ = 10.0

Figure 24.- Concluded.

1. Report No.	2. Government Accession No.	3. Recipient's Catalog No.
NASA TM-78,427		

4. Title and Subtitle	5. Report Date
AERODYNAMIC CHARACTERISTICS OF A SMALL-SCALE STRAIGHT AND SWEPT-BACK WING WITH KNEE-BLOWN JET FLAPS	
	6. Performing Organization Code
7. Author(s) Gilbert G. Morehouse,* William T. Eckert,* and Robert A. Boles**	8. Performing Organization Report No. A-7161
	10. Work Unit No. 505-10-41
9. Performing Organization Name and Address *Ames Research Center, NASA, and Aeromechanics Lab., U.S. Army Aviation R&D Command, Ames Research Center Moffett Field, Calif. 94035 **Lockheed-Georgia Company, Marietta, Georgia 30063	11. Contract or Grant No.
	13. Type of Report and Period Covered Technical Memorandum
12. Sponsoring Agency Name and Address National Aeronautics and Space Administration Washington, D.C. 20546	14. Sponsoring Agency Code

15. Supplementary Notes

16. Abstract

Two sting-mounted, 50.8 cm (20 in.) span, knee-blown, jet-flap models were tested in a large (2.1- by 2.5-m (7- by 10-ft)) subsonic wind tunnel. A straight- and swept-wing model were tested with fixed flap deflection with various combinations of full-span leading-edge slats. The swept-wing model was also tested with wing tip extensions.

Data were taken at angles-of-attack between 0° and 40°, at dynamic pressures between 143.6 N/sq m (3 lb/sq ft) and 239.4 N/sq m (5 lb/sq ft), and at Reynolds numbers (based on wing chord) ranging from 100000 to 132000. Jet-flap momentum blowing coefficients up to 10 were used. Lift, drag, and pitching-moment coefficients, and exit flow profiles for the flap blowing are presented in graphical form without analysis.

17. Key Words (Suggested by Author(s))	18. Distribution Statement
Blown flap Jet flap Swept wing Straight wing	Unlimited STAR Category - 02

19. Security Classif. (of this report)	20. Security Classif. (of this page)	21. No. of Pages	22. Price*
Unclassified	Unclassified	124	$5.50

*For sale by the National Technical Information Service, Springfield, Virginia 22161